ADSORPTION AND SURFACE DIFFUSION IN MICROPOROUS MEDIA

by

RICHARD WILLIAM BAKER

A thesis submitted for the degree of
Doctor of Philosophy in the
University of London

July 1966

Chemistry Department,
Imperial College,
London, S.W.7.

ABSTRACT

Two plugs, one of graphon and the other of black pearls carbon blacks, were prepared. A study of the diffusion of argon and SF_6 through these plugs has been carried out over an extremely wide range of temperatures and surface coverages. The form of the plots of surface diffusion coefficient against coverage have been explained, as have the results of other workers.

A method of calculating the steady-state concentration at any point inside a porous medium has been developed and used with the method of Frisch (1957) to obtain a calculated value for the time lag. It has been shown that an extra term is necessary when applying the Frisch method to porous media to account for the blind pore character of these media.

It has also been shown that the efficiency of a surface for surface flow is very strongly dependent on the physical smoothness of the surface.

ACKNOWLEDGEMENTS

The author wishes to thank Professor R. M. Barrer and Mr R. Ash for their advice and encouragement during the course of this investigation. Thanks are also due to the technical staff for their assistance.

The execution of this work was made possible by the award of a grant from the Gas Council.

CONTENTS

1. THEORETICAL

1. The Steady State of Flow

(a) Gas-phase flow in single capillaries

The case of gas-phase flow in a single, cylindrical, infinite capillary will be treated in detail, since models based on cylindrical capillaries are often used as a basis of comparison for the more complex microporous systems which are encountered in practice.

A simple formulation of flow in infinite single cylindrical capillaries has been given by Weber (1954). He splits the flow into three components:

1) self diffusion J_1
2) conduction J_2 $\qquad J_T = J_1 + J_2 + J_3$
3) streamline flow J_3

where J_T is the total flux in moles per sec crossing the unit area of a plane at right angles to the concentration gradient. Splitting the total flux into these three components Weber showed that

the self-diffusion term $$J_1 = -\left(\frac{1}{1 + 2r/\lambda}\right)\frac{dC_g}{dx} K_\alpha$$

the conduction term $$J_2 = -\left(\frac{2r/\lambda}{1 + 2r/\lambda}\right)\frac{dC_g}{dx} K_\alpha$$

and the streamline flow term $$J_3 = -\left(\frac{3\pi . r}{64\ \lambda}\right)\frac{dC_g}{dx} K_\alpha$$

where r is the radius of the capillary, λ is the mean free path of the molecule at the concentration, C_g and K_α is a constant called the Knudsen permeability. Re-writing J_T in terms of permeabilities

where K, the over-all permeability, is defined as $K = \frac{J_T \cdot \ell}{C_g^o - C_g^\ell}$, and C_g^o is the gas concentration in moles/cm^3 at the plane x=0, and C_g^ℓ is the concentration in moles/cm^3 at the plane x=ℓ. It is necessary to make the condition $\overline{C} = \frac{C^o + C^\ell}{2} \gg C^o - C^\ell$ so that $\frac{dC_g}{dx}$ may be equated to $\frac{C^o - C^\ell}{\ell}$. We then obtain the expression

$$K = K_\alpha \left[\frac{3\pi}{64} r/\lambda + \pi/4 \left(\frac{2r/\lambda}{1 + 2r/\lambda}\right) + \left(\frac{1}{1 + 2r/\lambda}\right)\right] \qquad (1)$$

As $C_g \to \infty$ $r/\lambda \to \infty$ streamline flow is dominant and $K \to K_\alpha \frac{3\pi}{64} r/\lambda$.

As $C_g \to 0$ $r/\lambda \to 0$ self diffusion is dominant and $K \to K_\alpha$. The region where self diffusion is the only important term is called the Knudsen region, and this is the region in which much of the work with microporous media has been done. In this region K the permeability as already defined will be a constant for a given gas at a given temperature and independent of the values of C^o and C^ℓ. Constancy of K is not a rigorous test of the Knudsen region, however, since it may be that the other components of the flow are just large enough to cancel any change in the self-diffusion term and so keep K constant.

Another more general treatment is to express the flux in terms of a diffusion coefficient and a concentration gradient then, per unit cross-section normal to the direction of flow,

$$J_{T(t)} = -D \frac{\partial c}{\partial x} \qquad (2)$$

which for the transient state leads to the equation

$$\frac{\partial c}{\partial t} = \frac{\partial}{\partial x} D\left[\frac{\partial c}{\partial x}\right] \qquad (3)$$

These equations are called Fick's first and second laws respectively. When $J_{T(t)}$ is time invarient, the system is in a steady state and $\partial c/\partial t = 0$. $J_{T(t)}$ will then be written as J_T and the equation (3) can be put in terms of a complete differential:

$$J_T = -D \frac{dc}{dx} \tag{4}$$

In the Knudsen region the diffusion coefficient is a constant for a cylindrical infinite capillary, and following the treatment of Knudsen (1909) D can be shown to have the value

$$D = \frac{4r}{3}\left(\frac{2RT}{\pi M}\right)^{\frac{1}{2}} \left(\frac{2-f}{f}\right) \tag{5}$$

where M is the molecular weight of the diffusing gas. The term f is called the coefficient of specular reflection and is the fraction of the collisions with the container walls which are reflected diffusely. f is related to the time the molecule stays on the surface. This residence τ time is given by

$$\tau = \tau_0 e^{-\Delta E/RT}$$

where ΔE is the energy of adsorption. When ΔE is several times RT it has been shown on theoretical grounds that f approaches 1. Since this is nearly always the case, then to a good approximation we may put equation 5 as

$$D = \frac{4r}{3}\left(\frac{2RT}{\pi M}\right)^{\frac{1}{2}} \tag{6}$$

From equations (6) and (4) for an equal concentration gradient and the same capillary in the Knudsen region we obtain for two different gases the important result

$$\frac{J_{T_1}}{J_{T_2}} = \left(\frac{T_1}{T_2}\,\frac{M_2}{M_1}\right)^{\frac{1}{2}} \tag{7}$$

(b) Gas-phase flow in microporous media

A microporous medium is made in the laboratory by taking a powder, often of a very high surface area, and compressing it into a plug. The medium will then generally consist of innumerable small capillaries whose shape and cross-sectional area will vary widely, depending on the surface area of the powder and the degree of

compression. The capillaries will usually have a very irregular shape and be randomly orientated. The problem of predicting gas-phase flow is thus very difficult. Early workers using microporous media attempted to explain their results by assuming various models for the pore structure and then deriving equations for these hypothetical systems, and linking these models to real porous media by means of various constants.

The simplest of these models regards the pore system as equivalent to a series of identical capillaries, parallel to the line of flow. Consider a medium of porosity ϵ: that is, the fraction of void space in the porous medium is ϵ, and $1-\epsilon$ is the fraction of the solid phase. Then for 1 cm^3 of porous medium made up on the cylindrical capillary model, $\epsilon = n\pi r^2$ where n is the number of capillaries/unit area of cross-section. Putting A as the surface area/cm^3 of porous medium, then the ratio of volume to area/cm^3 is

$$\frac{\epsilon}{A} = \frac{n\pi r^2}{n2\pi r} = \frac{r}{2} \qquad (8)$$

Hence it is possible to derive the radius of the capillaries based on this model from ϵ and A. This radius can then be substituted into the Weber treatment to obtain an idea of the type of gas-phase flow present. This treatment is a crude approximation to the real situation in microporous media and can give only a very approximate guide to the behaviour to be expected in such a medium. A number of attempts have been made to improve the cylindrical capillary model, notably by Carman (1950), and Pollard and Present (1948). None of the treatments based on models has been very successful in predicting gas-phase flow in microporous media, and when surface flow is present the problems are of course even greater.

(c) Surface flow

In order to simplify the treatment, equations will be derived only for the Knudsen region of flow. They can be readily

extended to cover slip flow, but this tends to mask the physical significance of many of the results.

In the Knudsen region the equation (7) holds for a single cylindrical capillary, and it is still thought to be correct for microporous media. For the gases helium, hydrogen and neon this is generally so but with many other gases, depending on the porous medium, it appears that the flux is too large when compared with the theoretical value calculated from the helium flux using equation (7). This additional flux is now known to be due to an extra flow partly on the surface and brought into existence by the presence of mobile adsorbed films in a concentration gradient. Thus J_T, the total flux, can be split into two components:

J_s, the surface flux in moles per cm^2 per sec ;

and J_g, the gas-phase flux in moles per cm^2 per sec.

The magnitude of J_s depends very much on the gas flowing and the porous medium as discussed later. Suffice it to say that J_s is strongly dependent on the amount of adsorption which takes place on the surface and hence on the temperature dependence of the adsorption. Thus J_s tends to increase with increasing molecular weight of the gas diffusing and, for dilute films, to decrease with increasing temperature. This is in direct contrast to J_g so that the presence of a surface flow is generally easily detected. Since $J_T = J_s + J_g$, Fick's equation must be rewritten, per unit cross-section normal to x, as

$$J_T = -D_g \frac{dC_g}{dx} - D_s \frac{dC_s}{dx} \qquad (9)$$

where J_T is the total flux per unit cross-section in moles/cm^2/sec normal to the concentration gradient, and where C_s and C_g are the total number of moles/cm^3 of porous medium on the surface and in the gas phase respectively. D_g and D_s are called the gas and the surface diffusion coefficients respectively.

2. Theories and Results of Surface Diffusion

(a) Treatment of Carman

The work of Carman and Raal (1950, 1951) and of Carman and Malherbe (1951) was among the first to show the large, and at that time, unexpected dependence of D_s on the surface coverage. Using Carbolac (area approx. 960 sq.m/g) and Linde silica (area 300 sq.m/g), they found that their surface diffusion coefficient for SO_2, CO_2, and CF_2Cl_2 rose steeply with increasing surface concentration until a slight maximum was reached at approximately a monolayer after which it stayed fairly constant up to the region of capillary condensation when it rose again rapidly. It was already known that surface diffusion was an activated process (Wicke, 1941) and so Carman (1951) explained his results by saying that the first molecules would occupy the sites with the highest adsorption energies. At higher surface concentrations sites with lower adsorption energies would be occupied and hence these molecules would be more mobile than those first adsorbed. Therefore D_s should rise with increasing surface concentration reaching a maximum value at about the monolayer and then remaining fairly steady until capillary condensation sets in.

Applying this theory to a homogeneous surface, it would appear that D_s should be practically independent of surface concentration since the site energies are all of the same value. Such a surface was studied by Haul (1958) who found that a very large maximum in D_s was reached at approximately a monolayer coverage. The size and sharpness of this peak was much larger than anything found before and was explained by Haul by invoking entropy considerations. In effect what Carman had said was that

$$D_s = D_0 e^{-\Delta E^*/RT} \qquad (10($$

where ΔE^* was the Arrhenius energy of activation which varied with coverage. Haul said that equation (10) should be re-written

$$D_S = D_0 e^{-\Delta H^*/RT} e^{\Delta S^*/R} \qquad (11)$$

where ΔH^* is the enthalpy of activation, and ΔS^* is the entropy of activation. As evidence for the concentration dependence of ΔS^* he pointed to the molar and differential entropies of adsorption found in the results of Singleton and Halsey (1954), Hill, Emmett and Joyner (1951) and others on homogeneous surfaces, which are markedly concentration dependent. In using the theories of Carman and Haul it must be remembered that while ΔH^* and ΔS^* for the activation process may be linked with the ΔH and ΔS for adsorption, they are not the same and it is not possible to relate the two except in a very qualitative manner.

On the Haul and Carman treatments, D_S is fixed for any surface and gas and should be independent of the type of gas-phase flow since the energies and entropies of the active sites should be independent of gas-phase flow. In addition, when experiments are performed with different plugs made of the same material but compressed to different porosities, it has been observed (Haul 1954, Carman and Raal 1954, and Barrer and Strachan 1955) that the surface diffusion coefficient is markedly different. Since the adsorption isotherms are not markedly different, these quite marked differences in the diffusion coefficient cannot be explained by the Carman-Haul theory. Also ΔS^* sometimes has unreasonably large values.

We can see, therefore, that the Carman-Haul treatment is of limited use. It is able to give only a qualitative idea at the very best of the form of the relation between adsorbate concentration and surface diffusion coefficient and is unable to explain the effect of changing porosity.

(b) The treatment of Babbit

Babbit (1950) postulated, by analogy with the flow of heat and electricity, that for surface diffusion it is possible to write the equation

$$\frac{d\Phi}{dx} = A_{(x)}$$

where $A_{(x)}$ is the resistive force, and Φ is the surface pressure, defined in the thermodynamic treatment of Gibbs as (definition of C'_s, C'_g, page 11)

$$\Phi = RT\int_0^{C'_g} \frac{1}{\Sigma} d\ell n\, C'_g \qquad (13)$$

Also Σ is the area occupied per mole of adsorbate, that is

$$\Sigma = 1./C'_s \qquad (14)$$

we may then write

$$\Phi = \int_0^{C'_g} C'_s\, d\ell n\, C'_g \cdot RT \qquad (15)$$

Babbi t also postulated that this resistive force could be written

$$A_{(x)} = -C_R.u. \qquad (16)$$

where C_R is the coefficient of resistance per mole and is independent of the surface concentration, u is the average resultant velocity of the molecules crossing the surface of the solid. We may therefore write equation (12) as

$$\frac{d\Phi}{dx} = -C_R.u. \qquad (17)$$

By using the various adsorption equations for mobile monolayers, ideal localized monolayers (the Langmuir isotherm), and also the B.E.T. equations, Babbit was able to derive the product $C'_s.u$, that is the surface flux per cm^2, in terms of the adsorption isotherm. Since these equations of adsorption often only approximate to the true situation (see later section on the adsorption results) the resultant equations for the flux $(C'_s.u)$ in terms of C'_g are of little more than academic interest.

Gilliland, Baddour and Russel (1958) obtained a more useful equation for the general case, which can be applied to any

isotherm. From equation (15) we can obtain on differentiating with respect to C'_g the equation

$$\frac{d\Phi}{dC'_g} = \frac{C'_s}{C'_g} \cdot RT \tag{18}$$

If we now substitute this in equation (17) we obtain

$$-C_R u = \frac{C'_s}{C'_g} \frac{dC'_g}{dx} \cdot RT \tag{19}$$

since u is the velocity of the molecules crossing the surface we must include a tortuosity factor to transform u into the average velocity (u_p) of the molecules crossing a plane,

$$u_p = u/k \tag{20}$$

On substituting this, and multiplying both sides of the equation (19) by C'_s we arrive at the equation

$$u_p C'_s = \frac{C_R}{k} \frac{C'^2_s}{C'_g} \frac{dC'_g}{dx} \cdot RT \tag{21}$$

$u_p . C'_s$ is the surface flux per cm^2 crossing a plane at right angles to the concentration gradient, and so on integration of both sides from 0 to ℓ and C'^0_g to 0 we arrive at the final equation

$$J_s . \ell = \frac{C_R}{k} \int_0^{C'^0_g} \frac{C'^2_s}{C'_g} dC'_g \cdot RT \tag{22}$$

This equation contains only one variable parameter, and can be used to derive J_s from the adsorption isotherm. The equation has been found by some workers to fit their results reasonably well.

It may be remarked that equation (15) is easily linked with Fick's first law equation (2) as shown below. From equation (19) and equation (2) we may write

$$RT \cdot \frac{C_R}{k} \frac{C'^2_s}{C'_g} \frac{dC'_g}{dx} = D_s \frac{dC_s}{dx} \tag{23}$$

hence

$$C_R = D_s.k \frac{C_g'}{C_s'^2} \frac{dC_s}{dC_g'} \cdot RT \qquad (24)$$

The theoretical basis for equation (12) and hence the rest of this treatment is, however, open to doubt. Babbit (1950) derived equation (12) empirically on analogy with the flow of heat and electricity, but from simple irreversible thermodynamics (Denbigh 1951) it can be shown that the analogous equation to flow of heat and electricity is

$$u.C_R = -\frac{d\mu_s}{dx} \cdot L \qquad (25)$$

where μ_s is the chemical potential of the adsorbed phase.

These criticisms do not detract from the empirical use of equation (22) as a correlation of the surface flow and the isotherm. In practise it is more readily applicable than the Carman/Haul treatment.

(c) Treatment of Barrer

A simplified account of Barrer's treatment will be given here together with some extensions of it. In his treatment (Barrer 1963) the total flux was still split into two components J_s and J_g. He suggested that inside the porous media there were two effects taking place:

i) Blockage, which was the effect on the gas-phase flow due to the physical presence of the adsorbed molecules. He characterised this by the term S which he defined as being equal to the fraction of the pores occupied by the surface phase.

ii) He also postulated that the fraction of the total flux which was travelling on the surface might not be the same at all points along the plug and that there might be a gradual change in the ratio J_s/J_g on going from the high surface concentration end of the plug to the low surface concentration end.

(i) Notation

Expressing Fick's law in its general form, for the steady state when D_T is a function of concentration only, then

$$J_T = -D_T \frac{dC}{dx} \tag{4}$$

where J_T is the flux in moles per sec crossing unit area of a plane at right angles to the concentration gradient, D_T is the total diffusion coefficient and has units cm^2 per sec and C is the total concentration in moles per cm^3 of porous medium. Splitting J_T into two components, J_g and J_s, one has $J_T = J_s + J_g$ where J_s is the fraction of the total flux due to the presence of the mobile surface phase flux, and where J_g is the fraction of the total flux due to molecules in the gas phase. One then writes equation (4) as

$$J_T = -D_s \frac{dC_s}{dx} - D_g \frac{dC_g}{dx} \tag{9}$$

where

$$J_s = -D_s \frac{dC_s}{dx} \quad \text{and} \quad J_g = -D_g \frac{dC_g}{dx} \tag{26,27}$$

C_s and C_g are the concentrations in moles per cm^3 of porous media on the surface and in the gas phase respectively. Then if S is the average fraction of the pores which are occupied by the adsorbed phase, and ϵ is the porosity, $S\epsilon$, is the volume of sorbed phase per cm^3 of porous medium. If C_g' is the number of moles per cm^3 of gas phase, then

$$(1 - S)\epsilon\, C_g' = C_g \tag{28}$$

For an ideal gas

$$P_g = RT\, C_g' \tag{29}$$

where P_g is the pressure of the gas phase and R is the gas constant. If C_s' is put equal to the measured surface excess in moles per cm^2 of surface, and A is the area of the surface per cm^3 of the porous medium, then

$$C_s = AC_s' + S\epsilon C_g' \tag{30}$$

the $S\epsilon C_g'$ term is present because C_s' is only a surface excess, thus

$$C = C_s + C_g = (1-S)\epsilon C_g' + AC_s' + S\epsilon C_g'$$
$$= \epsilon C_g' + AC_s' \qquad (31)$$

Since ϵ, C_g' and the product AC_s' are measured quantities this means that C can be defined exactly but that C_s and C_g can only be defined by including the blockage term S over which there may be some doubt. When it is necessary to define a function at a particular position along a plug of length ℓ this will be done by using superscripts. Thus C^0 is the concentration at the plane x=0. When it is necessary to refer to a particular experiment this will be shown by the use of an asterisk as shown; thus C^{0*} is the concentration at the plane x=0 where C^0 has a fixed value. The flux for a particular experiment will be shown as follows: $\left[J_T\right]_{C^\ell}^{C^0}$ will denote the flux when the concentration at the plane x=0 is C^0 and the concentration at the plane x=ℓ is C^ℓ. Similarly $\left[J_T\right]_{C^\ell}^{C^x}$ is the flux which would be obtained if the concentration at the plane x=0 were C^x and the concentration at the plane x=ℓ were C^ℓ. When the concentration at the plane x=ℓ is 0 then the symbol C^ℓ will be omitted.

(ii) Equations of diffusion

We may start from the equation

$$J_T = -D_T . dC/dx \qquad (4)$$

Then for a particular experiment

$$C^0 = C^{0*} \quad ; \quad C^\ell = C^{\ell*}$$

$$J_T = \left[J_T\right]_{C^{\ell*}}^{C^{0*}}$$

and at any point along the plug let C be C^{x*}. Then integrating (4) from 0 to ℓ and C^{0*} to $C^{\ell*}$ we arrive at

$$\left[J_T\right]_{C^{\ell*}}^{C^{0*}} \cdot \ell = \int_{C^{\ell*}}^{C^{0*}} D_T \cdot dC \tag{32}$$

and also integrating (4) from 0 to x and C^{0*} to C^{x*} we arrive at

$$\left[J_T\right]_{C^{\ell*}}^{C^{0*}} \cdot x = \int_{C^{x*}}^{C^{0*}} D_T \cdot dC \tag{33}$$

So that, from (32) and (33) we obtain

$$\frac{x}{\ell} = \frac{\int_{C^{x*}}^{C^{0*}} D_T dC}{\int_{C^{\ell*}}^{C^{0*}} D_T dC} \tag{34}$$

which in the special case $C^{\ell*}=0$ reduces to

$$\frac{x}{\ell} = \frac{\int_{C^{x*}}^{C^{0*}} D_T dC}{\int_{0}^{C^{0*}} D_T dC} \tag{35}$$

This expression was derived by Barrer(1941), and from it, if the concentration dependence of D_T on C is known from the experimental results, it is possible on integration to obtain the concentration profile of C against x along the plug for any particular experiment with C^0 equal to C^{0*}. Equation (35) is quite rigorous but has the disadvantage that D_T is not a primary measured quantity for most experimental techniques so that expressing its dependence on C may be subject to error which will in turn lead to error in the concentration profile. In the experimental method of Barrer which will be discussed later it is possible to express the concentration profile in terms of a directly measured quantity.

In the method of Barrer, C^{ℓ} is always very much less than C^0 and in fact can be put as 0. C^0 in Barrer's method is varied and a graph of J_T against C^0 obtained (with $C^{\ell}=0$). We may write equation (33) in the form

$$x\left[J_T\right]^{C^{0*}} = \int_{C^{x*}}^{C^{0*}} D_T dC$$

$$= \int_0^{C^{0*}} D_T dC - \int_0^{C^{x*}} D_T dC \qquad (36)$$

which gives

$$x\left[J_T\right]^{C^{0*}} = \left\{\left[J_T\right]^{C^{0*}} - \left[J_T\right]^{C^{x*}}\right\}\ell \qquad (37)$$

where $\left[J_T\right]^{C^{x*}}$ is the flux corresponding to an experiment when the concentration at the plane x=0 is equal to C^{x*} and at the plane $x=\ell$ is equal to 0. Hence we may write equation (37) as

$$\frac{x}{\ell} = \frac{\left[J_T\right]^{C^{0*}} - \left[J_T\right]^{C^{x*}}}{\left[J_T\right]^{C^{0*}}} \qquad (38)$$

These results are expressed graphically in the diagram overleaf. We see that equation (38) in fact enables us to obtain the concentration profile directly from a plot of J_T against C^0. All that it is necessary to do is to change the J_T axis so that instead of reading from 0 to $\left[J_T\right]^{C^{0*}}$ it reads from ℓ to 0.

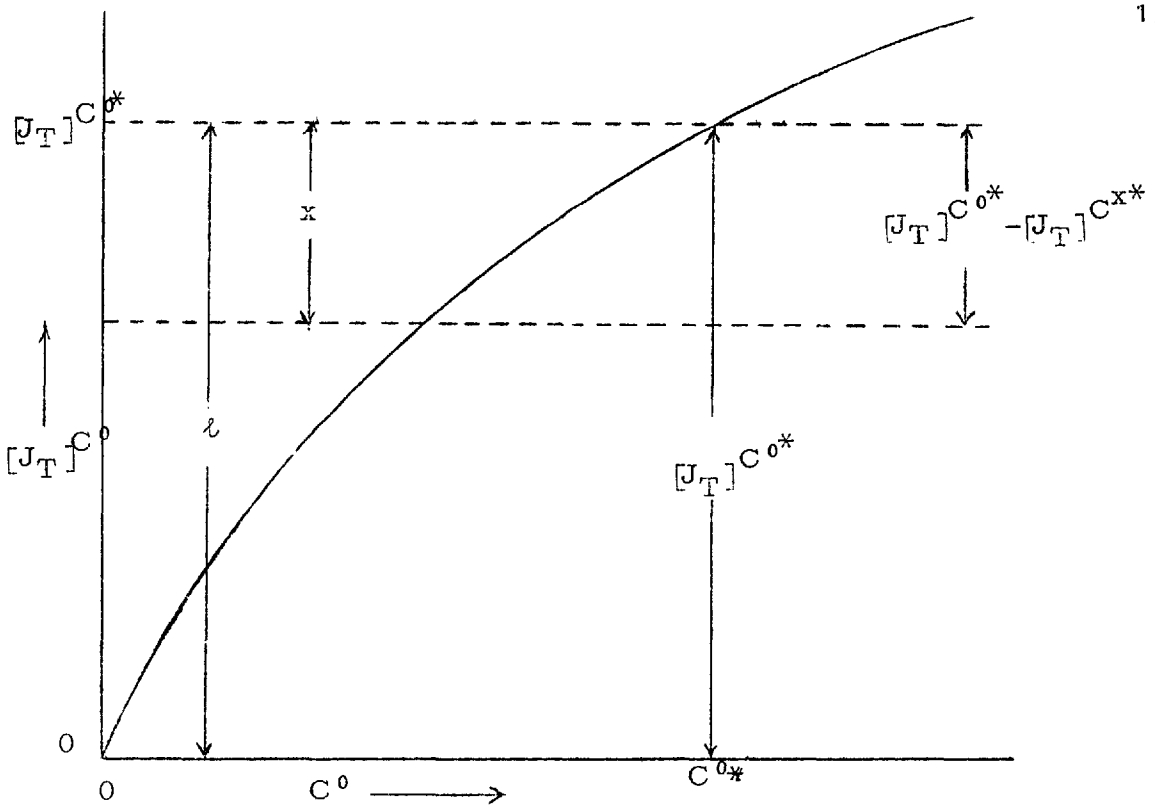

We are, therefore, able to obtain the concentration profile along the plug with as much accuracy as the primary experimental results.

Another equally important result can be derived starting from equation (4) as before. With the boundary condition $C^{\ell} = 0$, integration gives

$$\left[J_T\right]^{C^0} \ell = \int_0^{C^0} D_T . dC \tag{39}$$

On differentiating w.r.t. C^0 the above expression becomes

$$\left(\frac{dJ_T}{dC^0}\right)_{C^0=C} . \ell = \left[D_T\right]_C \tag{40}$$

Now for a particular experiment

$$C^0 = C^{0*} \quad ; \quad J_T = \left[J_T\right]^{C^{0*}}$$

equation (21) becomes

$$\left[J_T\right]^{C^{0*}} = -D_T \frac{dC}{dx} \tag{41}$$

and at some point along the plug at the plane x and concentration C^{x*} one obtains from (29)

$$\left[J_T\right]^{C^{0*}} = -\left[D_T\right]_{C^{x*}} \left(\frac{dC}{dx}\right)_{C=C^{x*}} \tag{42}$$

Substituting from equation (40) we obtain

$$-\left(\frac{dJ_T}{dC^0}\right)_{C^0=C} \frac{\ell}{\left[J_T\right]^{C^{0*}}} = \left(\frac{dx}{dC}\right)_{C^x=C} \tag{43}$$

If in the proofs of equation (43) and (38), instead of starting from the equation (4)

$$J_T = -D_T \frac{dC}{dx}$$

we had started from the equation

$$J_T = -B_T \frac{dC'_g}{dx}$$

where

$$B_T = D_T \frac{dC}{dC'_g}$$

we would have arrived at equations equivalent to equations (43) and (38) of the form

$$\left[\frac{dJ_T}{dC'^0_g}\right]_{C'^0_g=C'^{0x}_g} = -\frac{\left[J_T\right]^{C'^{0*}_g}}{\ell} \left[\frac{dx}{dC'_g}\right]_{C'_g=C'^x_g} \tag{44}$$

and

$$\frac{x}{\ell} = \frac{\left[J_T\right]^{C^{0*}_g} - \left[J_T\right]^{C'^{x*}_g}}{\left[J_T\right]^{C'^{0*}_g}} \tag{45}$$

Thus from a graph of J_T against C_g^{10} we could obtain the concentration profile of $C_g^!$ against x in exactly the same manner as for the concentration profile of J_T against C. Similarly for C_s, $C_s^!$ or C_g we can obtain equations of the type (44) and (45) and a concentration profile in the steady state as outlined in the method above.

The only assumptions made in these two derivations are firstly that the sorbate-free medium is isotropic, i.e. that in the steady state the diffusion coefficient may be a function of concentration but not of x, and secondly, that the results obtained from a static adsorption experiment may be applied to the porous medium when flow is taking place.

3. Experimental Methods of Determining J_s, J_g and D_s

(a) The method of Barrer and his co-workers

In this method the concentration of the ingoing side of the porous plug is kept at a constant value C^0. The rate of rise of concentration at the outgoing side is used to determine the flux J_T. Whilst the outgoing side concentration is finite and large enough to be measured, it is small compared to the size of C^0 and to a good approximation it may be equated to zero in the diffusion equation.

Then from equation (4) we obtain

$$\frac{1}{\ell}\int_0^{C^0} D_T.dC = J_T$$

and differentiating w.r.t. C^0 we obtain

$$\left(\frac{dJ_T}{dC^0}\right)_{C^0=C} = \left[D_T\right]_C \Big/ \ell \qquad (46)$$

so that the slope of the experimental curve J_T against $C^0(C^{\ell}=0)$ gives D_T. To obtain D_s and D_g in equations (26), (27) is not so easy since we then have to make assumptions about flux interconversion and blockage. If, however, $J_s \gg J_g$ and $C_s \approx C$ these assumptions are not necessary and to a good approximation $D_T = D_s$ so that D_s is easily obtained. This equality is reasonable for most of our work in the region of high surface coverage.

(b) Carman's differential pressure method

In this experimental method the concentration difference $C^0 - C^{\ell} = \Delta C$ is made so small that to a good approximation dC/dx is a constant throughout the plug and so can be replaced by the term $-\Delta C/\ell$. Thus, making this assumption in equation (4) we obtain

$$\left[J_T\right]_{C^{\ell}}^{C^0} = D_T \frac{\Delta C}{\ell}$$

We can therefore obtain D_T corresponding to the mean concentration from one experiment. As a test for the validity of the substitution $-\Delta C/\ell = dC/dx$, Carman (1950) assumed that it was true so long as the adsorption isotherm could be assumed linear in the range C^{ℓ} to C^0.

In a Carman type experiment we can write

$$\left[J_T\right]_{C^{\ell}}^{C^0} \cdot \ell = \int_{C^{\ell}}^{C^0} D_T \cdot dC$$

and since permeability is defined as

$$= \frac{\left[J_T\right]_{C^{\ell}}^{C^0} \cdot \ell}{C_g'^{0} - C_g'^{\ell}} \qquad (47)$$

we arrive at the equation

$$K = \frac{\int_{C^{\ell}}^{C^{0}} D_T . dC}{C_g'^{0} - C_g'^{\ell}} \tag{48}$$

since in a Carman type experiment $C_g'^{0} - C_g'^{\ell}$ is made so small that D_T does not change in the concentration range used then

$$K_C = D_T \frac{\Delta C}{\Delta C_g'} = \frac{d[J_T]^{C^0} . \ell}{dC_g'} \tag{49}$$

In a Barrer type experiment ($C^{\ell}=0$) the permeability is given by the equation

$$k_B = \frac{\int_{o}^{C^{0}} D_T . dC}{C_g'^{0}} = \frac{[J_T]^{C^0} . \ell}{C_g'^{0}} \tag{50}$$

We see therefore that the two permeabilities are only equal when D_T is independent of concentration. In graphical terms the Carman permeability is equal to the slope of the curve below, whilst the Barrer permeability is given by the angle subtended from the origin in the graph below.

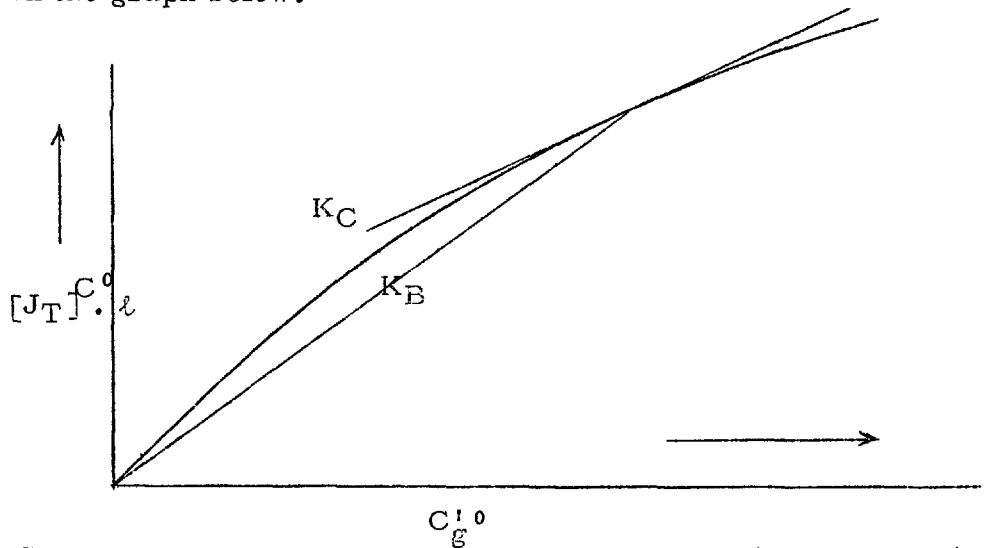

Confusion can arise over this point when comparing the experimental permeabilities obtained by different workers using different methods.

In the Carman treatment we see that if $\Delta C'_g$ is made too large then the resulting permeability will not be the permeability at the concentration $\bar{C}'_g$ but some mean permeability. It is essential therefore to make $\Delta C'_g$ as small as possible so that to a good approximation the Carman permeability does equal the slope of the J_T against C'^0_g curve as shown in the diagram. Some workers appear not to have done this, and their results are open to question on this point.

(c) Sorption/desorption method

In this method the rate of uptake of sorbent in an initially evacuated sample is used to derive a diffusion coefficient. This method is especially used for the study of polymer diffusion and a detailed analysis of the somewhat difficult treatment of the results is given by Crank (1956). A special modification by Haul for microporous media is given below.

(d) Haul's method

A very sensitive balance is constructed, on one arm of which a plug is suspended, the whole apparatus being placed in a thermostat bath. The gas is let in and by measuring the rate of diffusion into the plug, it is possible to derive the surface diffusion coefficient. The diffusion coefficient will not, however, be a steady-state one and this may lead to difficulties in interpretation. The calculations involved in this method tend to be complex (Haul 1952).

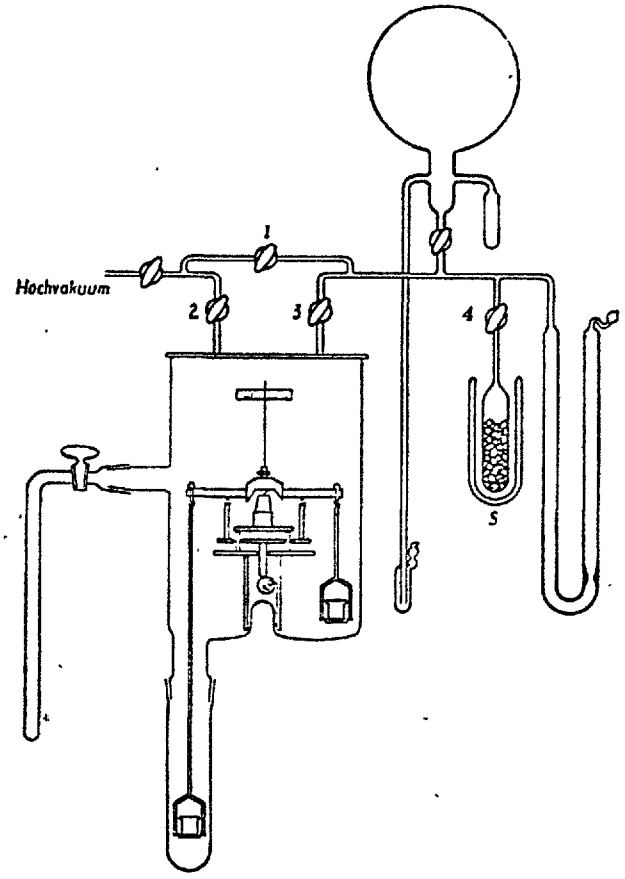

Abb. 1. Versuchsanordnung (schematisch).

(c) The early time method

Barrer and Chio (1965) and Meares (1965) both used for polymer diffusion what is called the "early time" method. This is a method of obtaining information about the diffusion coefficient in the transient period of flow. It can be shown that for small time t and a membrane of thickness l

$$\ln\left[t^{\frac{1}{2}} \cdot c\right] = \ln\left[\frac{2A_c C^0}{V}\left(\frac{D}{\pi}\right)^{\frac{1}{2}}\right] - l^2/4D.t$$

where q is the flux in moles per sec through the outgoing face of the membrane. A_c is the cross-sectional area of the membrane, and V is the volume into which the gas diffuses, and C^0 its concentration in moles just within the surface of entry to the membrane. D is a diffusion coefficient. By plotting $[\ln t^{\frac{1}{2}}.q]$ against $1/t$ we obtain a line of slope $-\ell^2/4D$.

In the proof of this equation (Rogers, Buritz, Alpert, 1954) it was assumed that D was independent of time and of concentration. In the general case therefore when D is a function of time and of concentration the equation is useful in giving the limiting slope as $t \to o$. This particular method has not yet been used for microporous media since diffusion coefficients which are only concentration dependent are found by easier methods. It now appears that in microporous media the diffusion coefficient may be time dependent as well (see later section) in which case this method will be useful.

4. Time lag in diffusion

In the experimental method of Barrer, it is possible to measure as well as the steady-state flux, which is characteristic of the steady-state diffusion coefficient, a quantity called the time lag which is characteristic of the transient state.

Consider an experiment where $C_{(x,t)}$ denotes the concentration in moles per cm^3. of porous medium at a point x and at time t. Then for an experiment which has the boundary conditions

$$C_{(x,0)} = 0 \quad \text{for} \quad x > 0$$
$$C_{(0,t)} = C^0 \quad \text{for} \quad t > 0$$
$$C_{(\ell,t)} = 0 \quad \text{for} \quad t > 0$$

a plot of the total quantity of diffusant appearing at the outgoing side against time will have the form shown in the figure below.

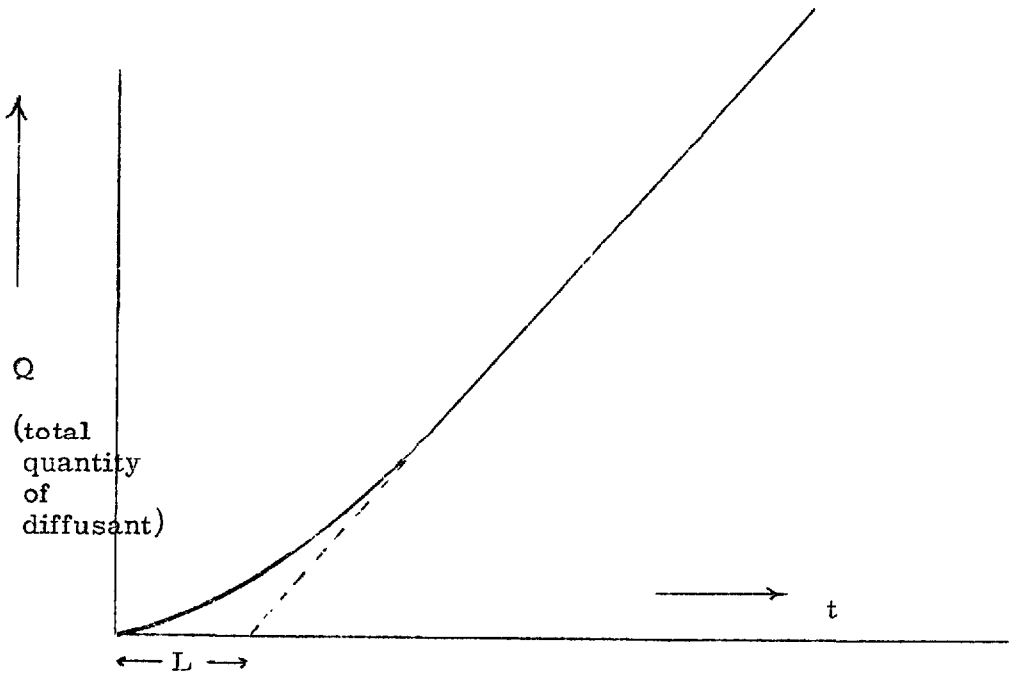

The time interval given by extrapolating the steady-state slope back to the time axis is called the time lag and is denoted by L. The starting point of all investigations into the time lag is Fick's second law, equation (3). It states that at any point x and time t

$$\frac{\partial C}{\partial t} = \frac{\partial}{\partial x}\left[D \frac{\partial C}{\partial x}\right] \qquad (3)$$

This is the most general form and D the diffusion coefficient can be an independent function of time, distance and concentration. In principle, by solving the diffusion equation (3) it is possible to find the time lag L. In practise it is not possible to solve equations of this type except for the most simple cases when D is a simple function of C. Examples of these cases are:

(i) if D is a constant independent of C then (Daynes 1920)

$$L = \frac{\ell^2}{6D} \quad ; \qquad (51)$$

(ii) if D has a concentration dependence of the form $D_{(c)} = D_0(1+bc)$. Then it has been shown for small b (Aitken and Barrer 1955) that

$$L = \frac{\ell^2}{6D}\left(\frac{1+\frac{1}{2}bC^0}{1+\frac{1}{2}bC^0}\right) \tag{52}$$

In 1957 H.L.Frisch derived the equation:

$$L = \frac{\int_0^{\ell} xC_{(x)}\,dx}{\int_0^{C^{0*}} DdC} \tag{53}$$

This extremely important result has found a wide use because with its assistance the time lag for a wide range of concentration dependent diffusion coefficients can be calculated. The method of previous workers (Ash, Barrer and Pope 1963, P.Meares 1958) has been to use equation (35) which together with equation (53) was shown by Frisch (1957) to lead to the equation below:

$$L = \frac{\ell^2 \int_0^{C^{0*}} CD_{(c)} \int_C^{C^{0*}} D_{(c)}dCdC}{\left(\int_0^{C^{0*}} D_{(c)}dC\right)^3} \tag{54}$$

For successful use of this equation it is necessary to know the concentration dependence of $D_{(c)}$ over the complete range of concentration 0 to C^{0*}. This restricts its applicability since in the method of Barrer which is used to measure the time lag, $D_{(c)}$ is obtained by taking slopes of an experimental curve (equation 46). In many cases it is also experimentally difficult to obtain the diffusion coefficient at low concentrations, so that the concentration dependence of D may require a sizeable and doubtful extrapolation. For these reasons equation (54) has not been very successful when applied to the experimental results in micropore systems.

Use of the concentration profile to calculate time lags

In the Frisch expression (53) the denominator is equal to $[J_T]^{C^{0*}}_{0}\ell$ from equation (39), whilst the numerator is the integral from 0 to ℓ of the product of x and the concentration at x. Equation (35) which was derived earlier allows the concentration C'_g at any point x in the steady state to be easily found. From this concentration profile and the adsorption isotherm it is then possible to obtain the profile for the total concentration C against x. Hence xC against x is easily calculated and can then be integrated graphically. The advantage of this method of calculating L is immediately apparent: firstly it uses the primary experimental results and eliminates the need to use the diffusion coefficient. Secondly, the region in which the experimental results are least accurate or even non-existent, i.e. those at low concentrations, has very little effect on the actual calculation since in the graphical integration of the xC against x curve the area under the curve at small values of C is small compared to the final result.

It may be that D as well as being a function of concentration is also a function of time. In this case the original Frisch expression must be modified to the form below (Frisch 1962(a)):

$$L = \frac{\int_0^{\ell} xC_{(x)}dx - \int_0^{t_\infty}\int_0^{C^{0*}}\left[D_{(ct)} - D_{(c)}\right]dc.dt}{\int_0^{C^{0*}} D_{(c)}.dC} \qquad (55)$$

In equation (55) $D_{(c)}$ is the diffusion coefficient when the steady state is reached and $D_{(ct)}$ is the diffusion coefficient at any instant of time. If the medium is inhomogeneous it may be that D is distance dependent also. A simple case of this form of inhomogeneity is a surface skin which is especially evident in certain polymers (Petropoulos 1959, Barrer and Petropoulos 1961, Barrie 1963).

5. Adsorption

In a paper in 1953, Champion and Halsey showed on theoretical grounds that the adsorption isotherm of a gas on a smooth homogeneous surface would generally lead to an isotherm, made up of steps at approximately monolayer intervals. In simple terms this is because the site energies are all the same and hence there will be very little multilayer formation until the monolayer is almost completely filled, whereas in a normal heterogeneous surface the steps in the transition from monolayer to multilayer formation are smoothed out.

These theoretical predictions were strikingly fulfilled by the work of Polley et al (1953) who took a normal high area carbon black and heated it under vacuum or with a helium atmosphere at successively higher temperatures. The results of this are illustrated in the figure below.

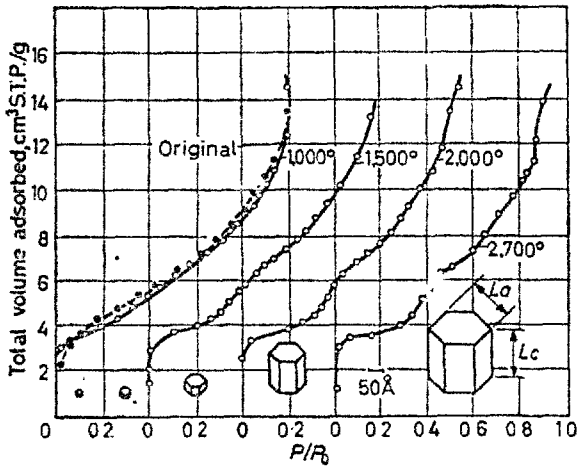

Figure 5.13. Adsorption isotherms of argon on P-33 carbon black at −195°C, showing the effect of temperature of graphitization on the isotherm and on the size of the crystallites. (From Polley *et al.*[158]; by courtesy of the American Chemical Society.)

Further evidence of the homogeneous nature of the surface is shown by the calorimetric heats of adsorption determined by Beebe (1954) and shown in the figure below.

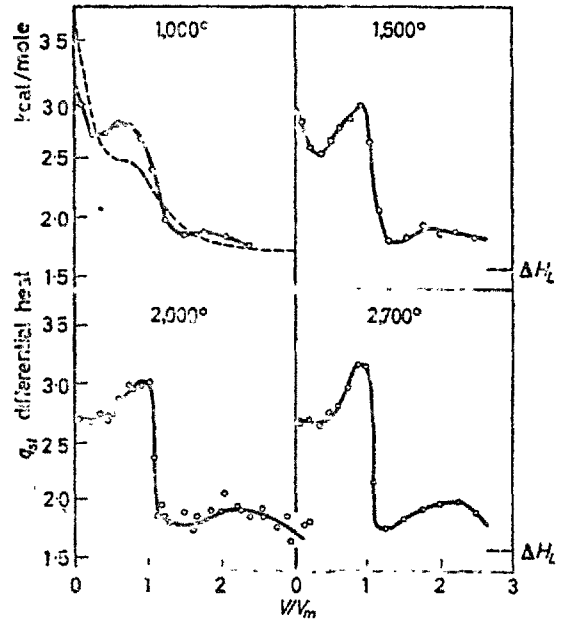

Fig. 5.14. Calorimetrically measured heats of adsorption of argon on Spheron carbon blacks at −195°C, plotted against surface coverage, for blacks graphitized at progressively higher temperatures. The broken line represents untreated black. (From Beebe and Young[159]; by courtesy of the American Chemical Society.)

The very sharp initial decrease in q_{st} is gradually eliminated on going from the untreated sample to the 2700 ^{0} sample. This is due to the initial strongly sorbing sites being gradually removed by progressive sintering. The rise in q_{st} at the monolayer is due to the effect of molecule-molecule interaction. Further discussion of these results can be found in the original papers.

As an example of the extremely homogeneous nature of these graphitised surfaces, it is instructive to quote the work of Adamson and Ling (1961) who derived an expression for the site energy which could be derived from the adsorption isotherm by a

method involving successive approximations. Their result is shown in the figure below.

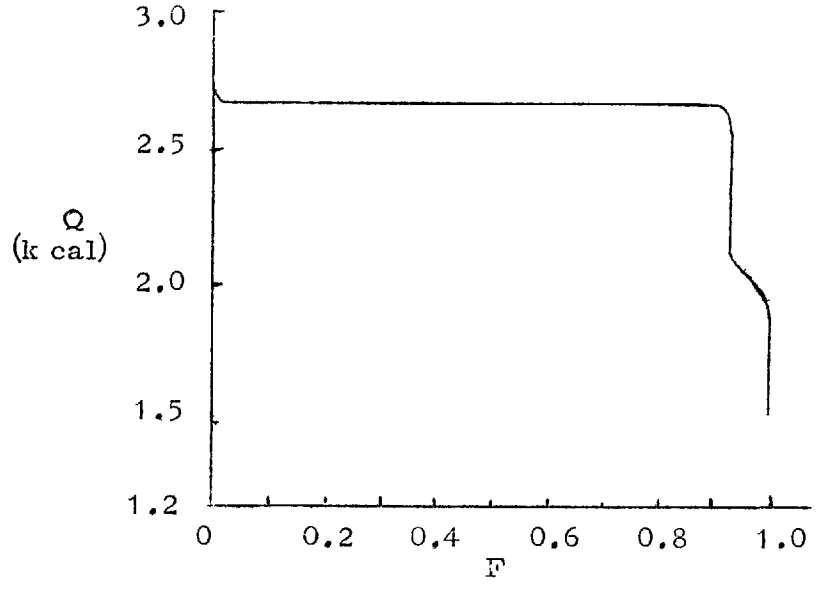

F is fraction of sites with energy $\geq Q$.

6. Thermodynamics of Adsorption

Below is given a very brief outline of the theory used to derive the various thermodynamic quantities of the adsorbed phase. The following notation will be used. $\tilde{A}$ will refer to the molar value of A, and $\bar{A}$ will refer to the differential value of A. The subscript s will refer to the sorbate in the sorbed state, and the subscript g will refer to the sorbate in the gas phase. Other symbols will have their usual meanings, thus S is an entropy and H is an enthalpy, and μ is a chemical potential.

From the Clausius-Clapeyron equation it can easily be shown that

$$\left(\frac{\partial \ell n\, P}{\partial T}\right)_{n_s/n_A} = - \frac{\overline{\Delta H}}{RT^2} \tag{56}$$

where n_s is the number of moles of sorbate in the sorbed state, and n_A is the number of moles of sorbent. Because in general n_A is fixed, the equation is usually written as

$$\left(\frac{\partial \ell nP}{\partial T}\right)_{n_s} = - \frac{\overline{\Delta H}}{RT^2} \tag{57}$$

$-\overline{\Delta H}$ is sometimes replaced by q_{st} the isosteric heat which is the differential heat needed to desorb the sorbate. Hence q_{st} will have the same value as $\overline{\Delta H}$ but the opposite sign. By using equation (57) it is possible to obtain $\overline{\Delta H}$ or q_{st} directly from the adsorption results.

Since the isotherms are measured at equilibrium, then

$$\overline{\Delta G} = \Delta\mu_s = \mu_s - \mu_g = 0$$

where μ_s and μ_g are the chemical potentials of the sorbed phase and the gas phase respectively. We may therefore write

$$(\overline{H}_s - \widetilde{H}_g) - T(\overline{S}_s - \widetilde{S}_g) = 0$$

where H_s, H_g, S_s and S_g are the enthalpies and entropies which correspond respectively with μ_s and μ_g. This last expression then gives us

$$\frac{\overline{\Delta H}}{T} = \frac{\overline{H}_s - \widetilde{H}_g}{T} = \overline{S}_s - \widetilde{S}_g = \overline{\Delta S}$$

rearranging the above expression thus gives us

$$\overline{S}_s = \widetilde{S}_g + \frac{\overline{\Delta H}}{T}$$

$$= S^0_g(P, T) + R\ell n\, P^0/_P + \frac{\overline{\Delta H}}{T} + \alpha P \tag{58}$$

where αP is the correction term for gas imperfections, and $S^0_{g(P,t)} + R\ell n^{P^0}/p$ is the expression for $\tilde{S}_g$ in terms of the standard entropy S^0_g at the standard pressure P. The integral entropy $\tilde{S}_s$ follows easily from this by the definition

$$\tilde{S}_s = \frac{1}{n_s} \int_0^{n_s} \tilde{S} dn_s \qquad (59)$$

II. EXPERIMENTAL

1. Apparatus

The apparatus was similar to that of Ash, Barrer and Pope (1963) and of Barrer and Gabor (1959). The pumping system is shown in fig. 1 and consists of a single stage mercury diffusion pump,made by the glassworkshop, and a good rotary oil pump to provide the backing pressure. A 5-litre buffer was included on the low pressure side of the diffusion pump so that it could be left switched on and working for several hours if need be without the rotary pump. An old rotary pump was used for the low vacuum, and a by-pass was included so that large quantities of gas in the high vacuum apparatus could be removed with this pump.

The rest of the apparatus was split into two main parts:

1. the diffusion system;
2. the adsorption system.

The flow system is shown in fig. 2 and consists of an ingoing side whose pressure could be kept constant by a Toepler pump, and an outgoing side whose pressure was always kept a small fraction (less than 1%) of the ingoing pressure by means of buffer volumes which could be varied between 500 cc (no buffers) and 5o litres (all buffers). The pressure of the outgoing side was measured by means of a McLeod gauge. The pressure at the ingoing side was measured by means of a manometer for pressure greater than 2 cm of mercury and with a small McLeod gauge for pressures between 2 cm and .05 cm o f mercury. When the flow rate was very large it was necessary to buffer the ingoing as well as the outgoing side, and the ingoing side was provided with a one-litre and a five-litre buffer volume for this purpose.

(a) Adsorption system.

A conventional volumetric adsorption system was used (fig. 3). The gas burette was surrounded by a water jacket which reduced the effect of room temperature fluctuations.

(b) Thermostat baths.

The following types of thermostat bath were used depending on the temperature range:

250-30 °C. A silicone oil bath was used for this range. The actual container was made of copper which was wound round with asbestos heating wire. Most of the heat necessary to maintain the temperature of the bath was supplied by this heater. A small 15-watt light bulb controlled by a Sunvic bimetallic senser and relay was used for the fine adjustment of the temperature. By this means it was possible to maintain the temperature constant to within ±0.1 °C even at the very high temperatures.

0 °C. A Dewar flask of melting ice was used for this temperature, and since it was the most convenient temperature to obtain, this was the temperature used for most of the check runs on the plug.

0 - -80 °C. A double Dewar flask system as shown in fig. 4 was used for this range. The gap between the inner and the outer Dewar was filled with solid Cardice or with liquid nitrogen. The rate of removal of heat from the inner Dewar was regulated by adjusting the pressure of the gas in the leaky Dewar. Methanol was found to be the best thermostatting liquid to use in this range.

-90 - -120 °C. The system was the same as for the range 0 °C - -80 °C except that 40/60 petroleum ether was used as the thermostatting liquid since below -80 °C methanol became very viscous. It was found that water vapour in the atmosphere formed crystals on the sides of the inner Dewar flask and that this allowed the petroleum ether to syphon out of the Dewar by means of capillary attraction.

It was found, however, that by the addition of even as little as 2 or 3 cc of methanol to the petroleum ether the ice crystals were immediately dissolved.

Below -120 °C. A normal liquid nitrogen bath was used for the temperature 77.6 °K and a liquid oxygen bath was used for 90 °K. The temperatures of the thermostat baths were measured by various methods: mercury thermometers, SO_2, CO_2, and O_2 vapour pressure thermometers, and also copper/constantan thermocouples which were calibrated against the vapour pressure thermometers and also the mercury thermometers.

(c) Gases used.

The gases H_2, He, Ne, Kr, Xe, ~~CO_2~~, etc., were all supplied spectrally pure, by British Oxygen Company, except for Xe which contained a maximum of 1% Kr, and the Kr which contained a maximum of 1% Xe. The SF_6 was supplied by the Matheson Company in a small steel cylinder which was connected to the system by rubber pressure tubing. The system was then pumped out and the pumps cut off. The SF_6 was admitted into the system and frozen out with liquid nitrogen. It was then pump ed out by the low vacuum pump to approximately 0.5 mm of mercury, after which the pumps were cut off and the SF_6 was allowed to expand into the storage vessel. This alternate freezing, pumping and expansion was repeated several times.

(d) Porous media.

Plugs were constructed of two materials supplied by the Cabot Company:

i) Graphon. This is a highly graphitised carbon black with a surface area of approximately 80 m^2/g, and a density of 1.97 g/cm^3. It is prepared by heating a Carbolac powder (Spheron 6)

of much higher surface area to about 2700 ^{0}C in vacuo or in a helium atmosphere. The surface area is much reduced and the crystal size as shown by electron microscope studies increases markedly. The surface becomes energetically homogeneous as shown by stepwise adsorption isotherms, isosteric heats, etc. It is sometimes referred to in the literature as Spheron 6 (2700 ^{0}).

ii) Black pearls 2. This is a similar material to the Graphon but it is not so homogeneous. The surface area is about 200 m^2/g and it has a density of 1.71 g/cm^3.

2. Experimental procedure

(a) Preparation of the plug sample

The diameter of the plug holders was first measured by means of a cathetometer, but this did not give very reproducible results. The diameter was then re-checked using the apparatus shown in fig. 5. A known weight of mercury was placed inside the plug and the difference in height of the mercury column measured before and after the addition by lowering the cathetometer telescope until the needle was just making contact with the mercury and thus closing the circuit. By this means it was possible to measure the diameter of the plug holder at several points along its length. This was found to give a high degree of reproducibility (r, .306, .304, .303, .303, .308, .304). The plug was prepared by weighing out the powder in a series of increments of approximately 0.2 g each, and then compressing them one after another to a length such as to give the required porosity. A Dennison press was used for this with a specially made set of steel plungers. The length between the ends of the plungers was measured after each compression by means of a pair of Vernier callipers. The length of the increment was then calculated from the known original length of the plungers.

The force exerted by the press was increased in stages till the increment had reached a length equivalent to the same porosity for each increment in turn. By making the plug in these small increments it was hoped to reduce the variation in the porosity along the plug to a minimum. A total force of about 1700 lb was needed to compress each increment. A diagram of the plug holder is shown in fig. 5.

(b) Outgassing

The plug was outgassed slowly by raising its temperature, in stages of 50 °C, from room temperature to 350 °C over a period of two days. The adsorption sample of powder was outgassed in a similar manner and, as might be expected from the method of manufacture, there was no appreciable loss in weight on degassing for either the Graphon or the Black Pearls.

(c) Diffusion experiments

In the method used in this laboratory, gas at a known pressure was suddenly let into one end of the plug which was thermostatted. The pressure at the outgoing side was measured at regular intervals. A typical graph is shown in fig. 6. The time lag and the rate of rise of pressure were measured when the system had reached the steady state of flow. Using the previously evaluated volume of the outgoing side, it was thus possible to determine the total flux per unit cross-section using equation (60)

$$J_T = V \frac{dP}{dt} \cdot \frac{1}{R.T_R} \cdot \frac{1}{A_C} \qquad (60)$$

where V is the volume of the outgoing side in cc, dP/dt is the rate of rise of pressure in dynes per cm^2 per sec, T_R is the room temperature, and A_C is the cross-sectional area of the plug. The permeability is given by equation (47):

$$K = \frac{J_T \cdot \ell}{C_g'^0 - C_g'^{\ell}} \tag{47}$$

which rearranges to

$$K = V \cdot \frac{dP}{dt} \cdot \frac{\ell}{A_C} \cdot \frac{T_P}{T_R} \cdot \frac{1}{P^0} \tag{61}$$

where P^0 is the pressure at the ingoing face in dynes per cm^2 and T_P is the temperature of the plug.

The experiments were taken to at least five times and usually to more than eight times the time lag. This was in order to obtain an accurate extrapolation back to the time axis for the time-lag determination. The flux or the time lag was sometimes so great that even with the maximum buffer volume on the outgoing side it was not possible to keep the pressure less than 1% of that at the ingoing side. The time lag could not then be determined, but the outgoing side was opened to the pumping system until it was certain that the experiment was in the steady state. The pumps were then cut off and the rate of rise of pressure measured.

(d) Calibration of the outgoing side volumes

The outgoing side buffer volumes were calibrated by expansion of helium from the known volume of the McLeod gauge bulb and at a known pressure into the buffer volume. After ten minutes to allow the temperature of the gas to come to room temperature the pressure was again measured. By simple application of the gas laws, the volume of the outgoing side was then obtained. For the larger volumes expansion from an already known buffer volume was used, since the greater the difference between the first and final volume the smaller the accuracy of the determination.

(c) Adsorption experiments

A conventional volumetric technique was used for the powder samples. Since marked differences between adsorption isotherms measured on plugs of different porosities and on the powder have been observed (Barrer and Strachan) it was desirable to compare the adsorption results for the powder and the plug. An adsorption system was included in the diffusion part of the apparatus and by this means it was hoped to measure the adsorption isotherm of the plug in situ. This was of limited use, however, since in the regions of adsorption large enough to be accurately measured the time lag was very large. It was necessary therefore to wait a very long time for equilibration between readings and because of this the surface area was only measured at liquid oxygen temperatures using argon. Five to six hours were allowed for equilibration between each reading.

3. Experimental errors

(a) Adsorption measurements

The errors in the adsorption results appeared to be fairly small depending on the size of the adsorption, generally about ±1% and never more than ±4% at the highest temperatures.

(b) Isothermal flow measurements

TABLE 1

Measurement	Error	Error in reproducibility	Absolute error
1. Ingoing pressure	±1%	1%	1%
2. Plug (i) length	±.01 cm	0	1%
(ii) diameter	±.003 cm	0	4%
(iii) wt. of C	±.01 g	0	1%
(iv) dens. of C	±1.5%	0	1.5%
3. Temperature of plug	±4 °C	.5% max	.5%
4. Outgoing pressure	±1% max	1%	1%
5. Time	±1 sec	0	0
6. Vol. of outgoing side	±1%	1%	1%
7. Room temperature	±2 °C	0	0

The total absolute error therefore has a maximum value of ±11% whilst the error in reproducibility has a maximum value of ±3.5%. In general the actual errors would be less than these. The error in the pressures on the outgoing side was due to sticking of the mercury in the McLeod gauges. This could be partly eliminated by using carefully purified mercury prepared by Mr A. Fox of this department. Heating of the capillaries of the McLeod gauge with a gentle gas flame whilst at the same time pumping with the mercury pump also reduced sticking. Temperature variations in the thermostatic baths were difficult to avoid between the temperatures 0 °C to -120 °C but could be kept to less than ±0.4 °C which did not generally comprise a large source of error in the calculated permeabilities.

FIG. 1

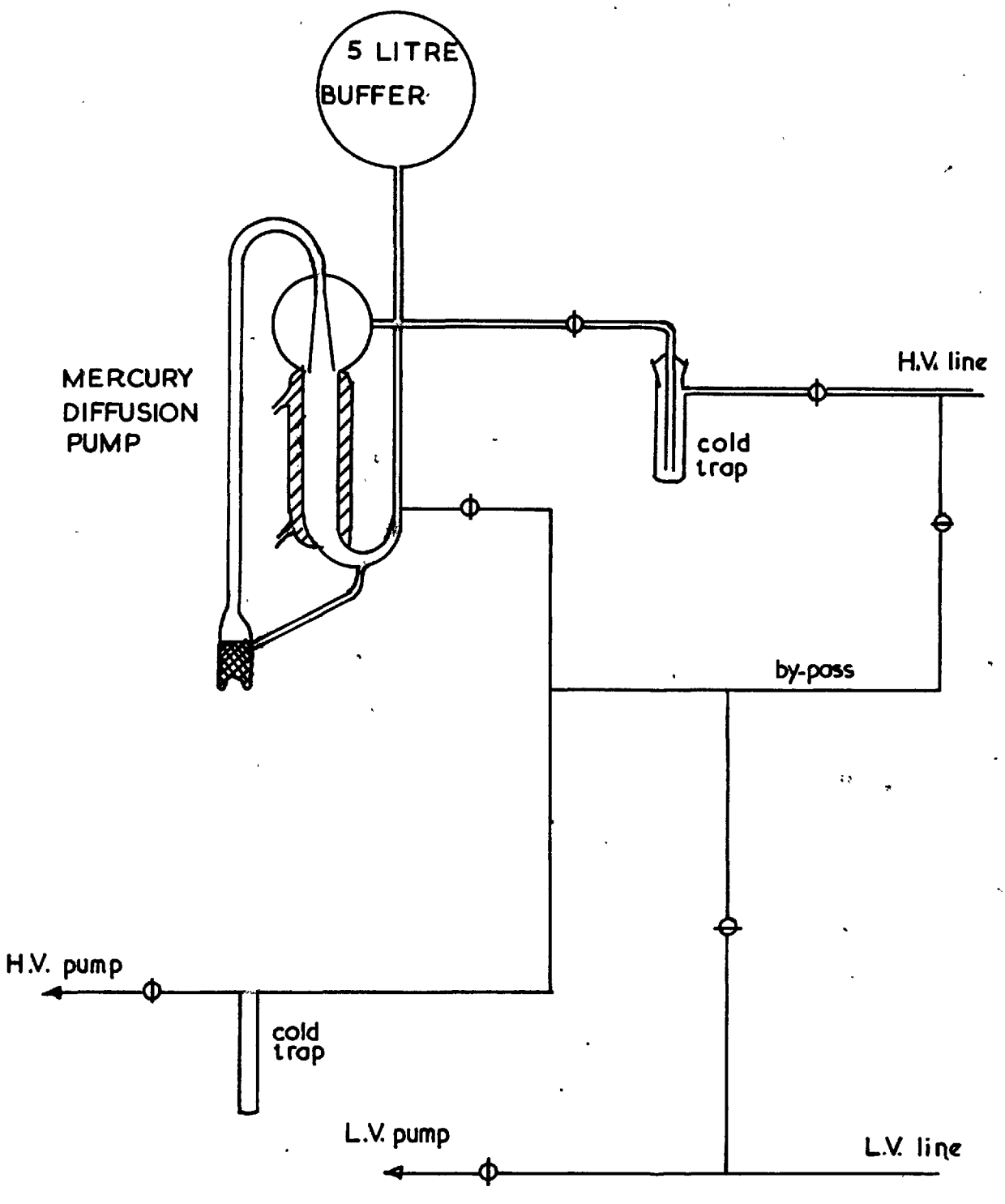
5 LITRE
BUFFER
MERCURY
DIFFUSION
PUMP
H.V. line
cold
trap
by-poss
H.V. pump
cold
trap
L.V. pump
L.V. line

40

DIFFUSION APPARATUS

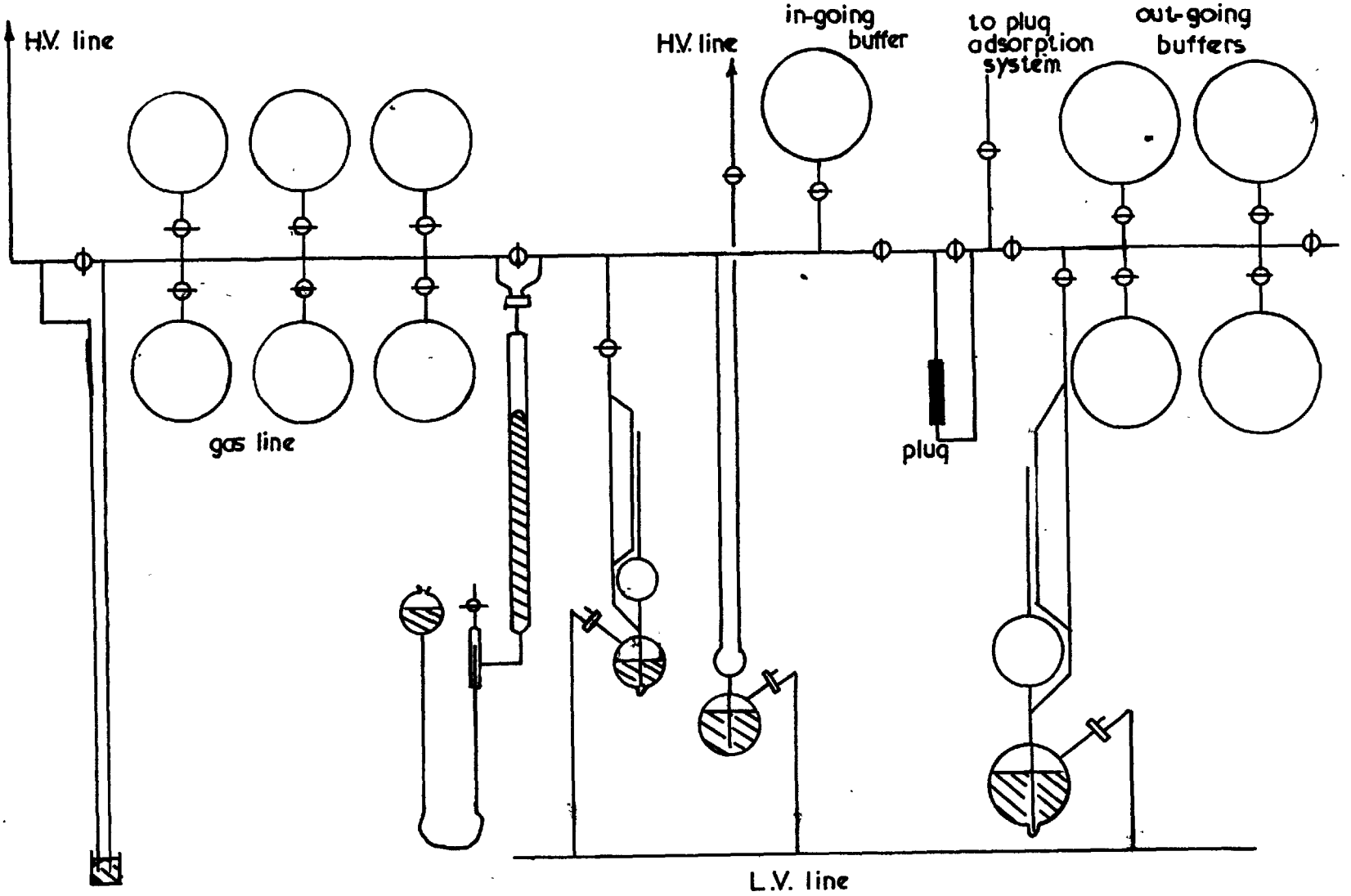

FIG. 2

FIG.3

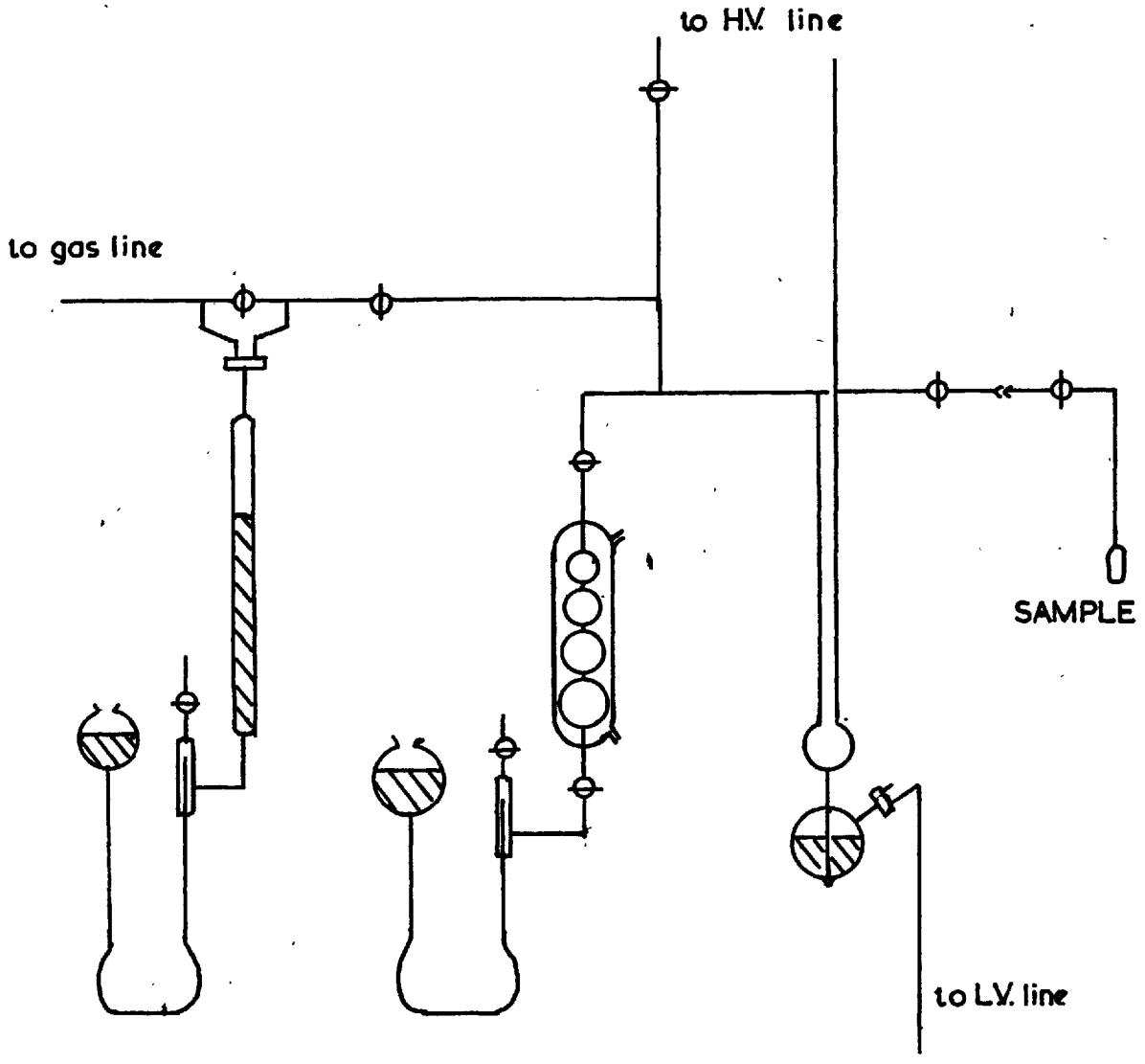

FIG. 4

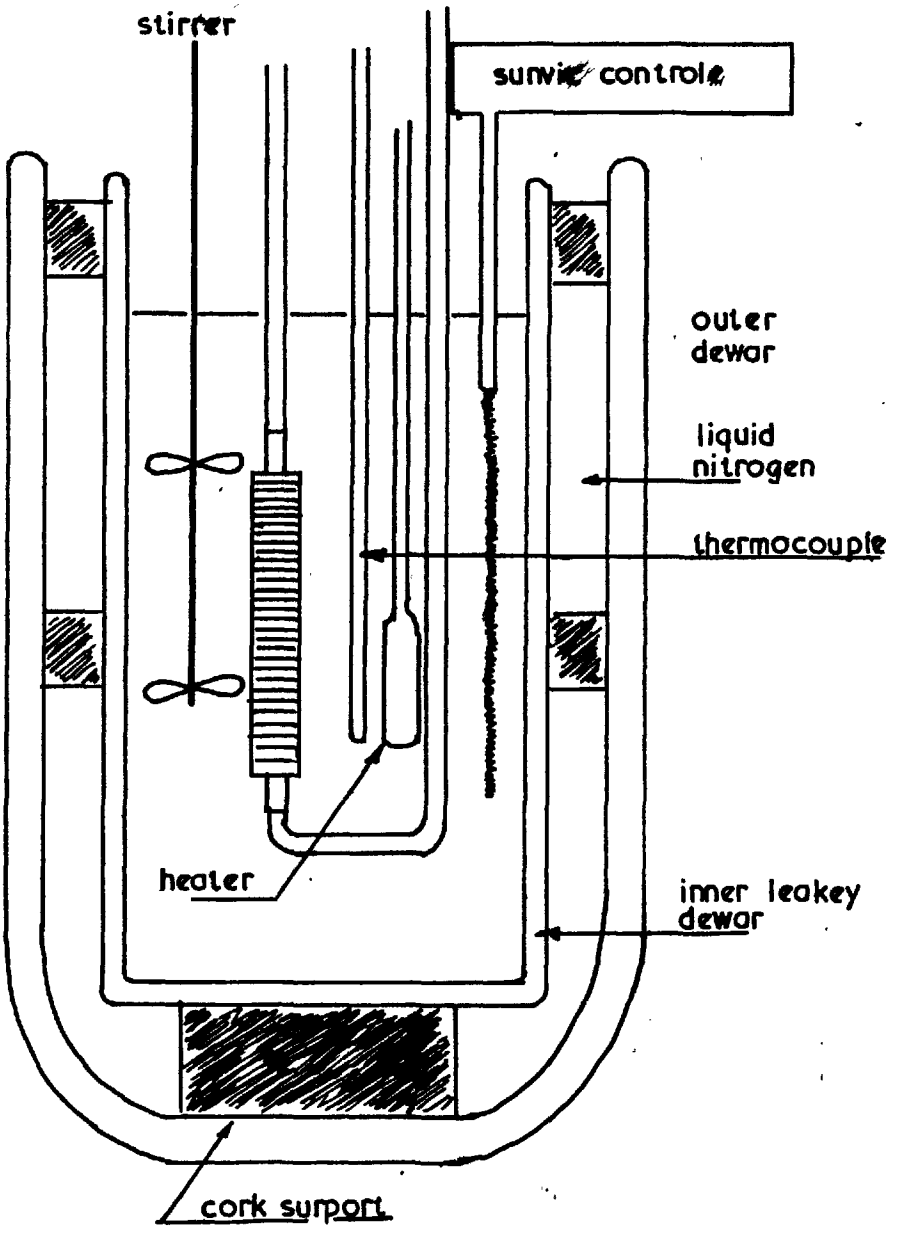
stirrer
sunvic controle
outer dewar
liquid nitrogen
thermocouple
heater
inner leakey dewar
cork surport

FIG. 5

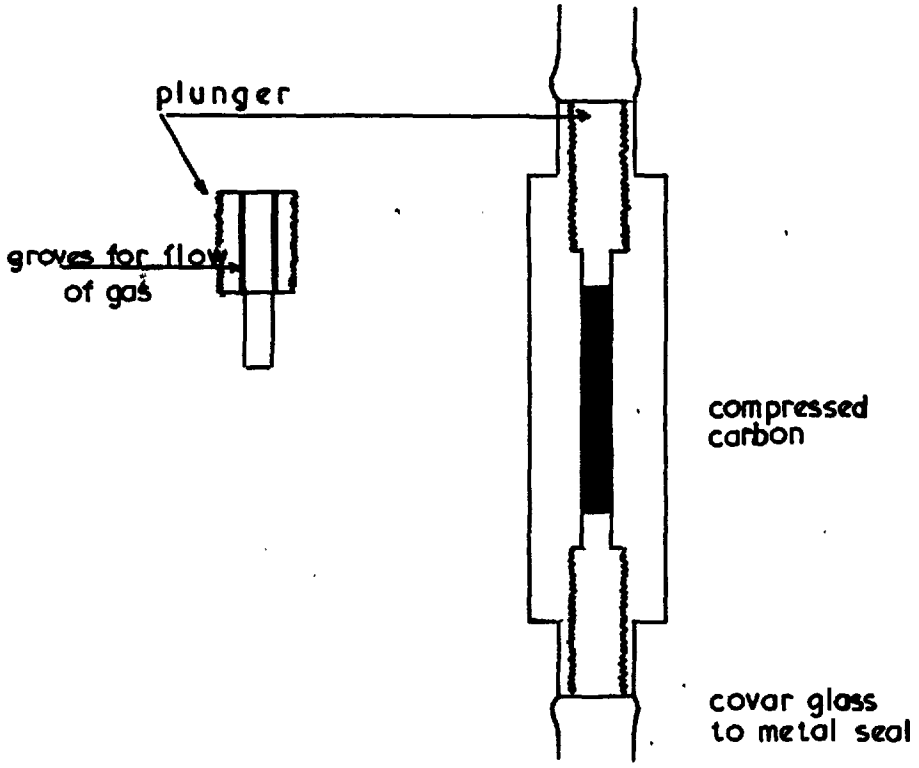

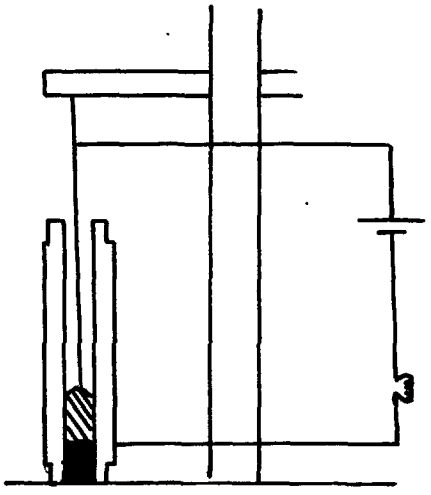

apparatus for determining plug dia.

FIG. 6

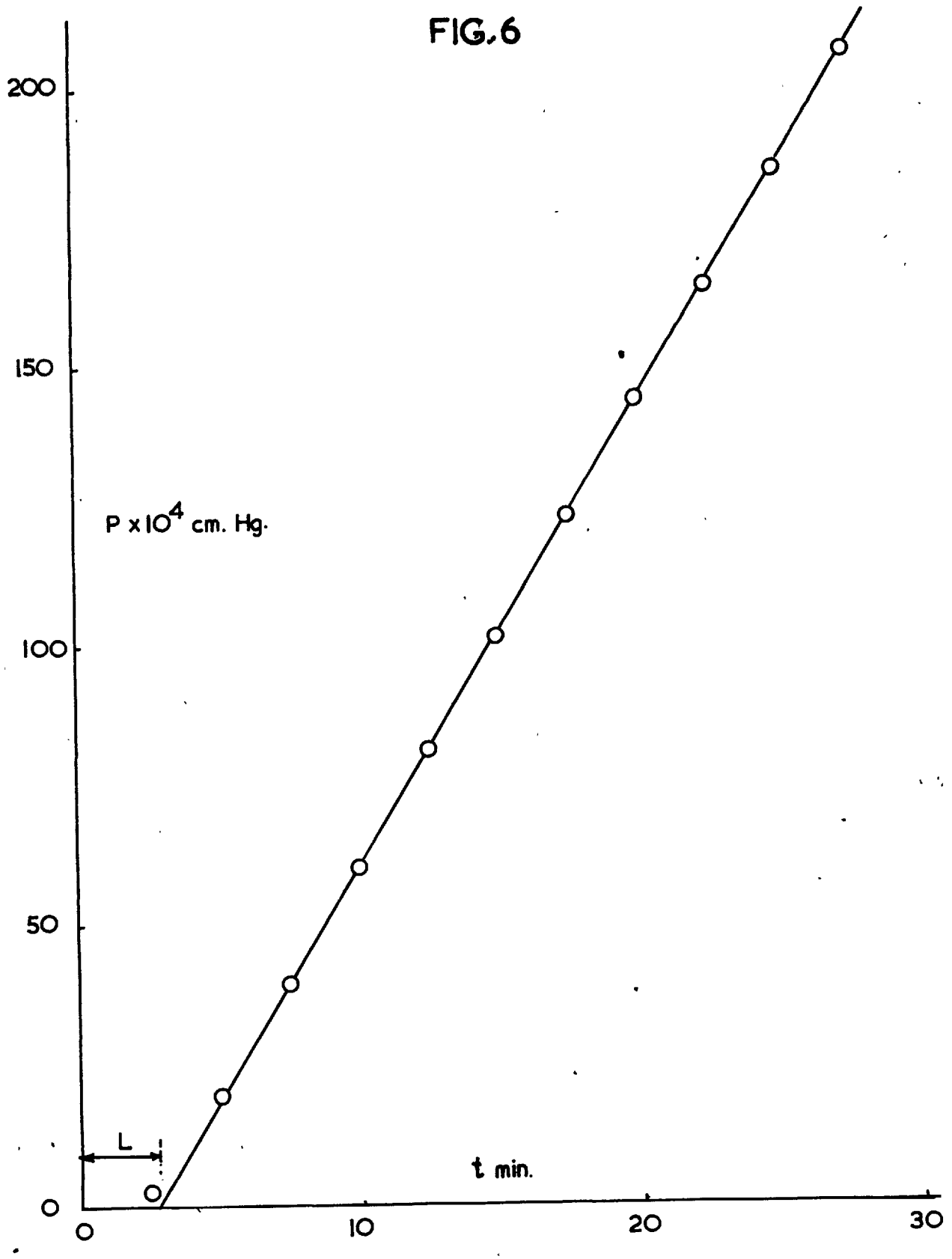

III. RESULTS

A series of preliminary results was obtained on a Black Pearl and a Graphon plug. The numerical results are listed in the Appendix : and are shown in a graphical form in fig. 7. At the temperature used in obtaining these results (31 ^{0}C) all the gases employed (He, Ne, Ar, Kr and Xe) gave straight line plots for K and L against pressure.

As an example of the relative quantities of surface flow for the different gases the values of $K\sqrt{M}$ are shown plotted against the polarisability (α) in fig. 8. For pure gas-phase flow $K\sqrt{M}$ should be a constant, as can be seen the experimental values fall on a smooth curve and it has been suggested that this may find some use as an empirical correlation (Aylmore and Barrer 1966).

When these preliminary experiments were completed, two new plugs of Graphon and Black Pearls were constructed and a second series of results obtained. It was decided to study the surface flow over as wide a region as possible, so as to obtain information from the multilayer region right down to the Henry's Law region. Adsorption isotherms were determined at every temperature at which diffusion results were obtained. The gases used for these experiments were helium from 333 ^{0}K to 77.6 ^{0}K argon from 333 ^{0}K to 77.6 ^{0}K and SF_6 from 473 ^{0}K to 183 ^{0}K. The numerical values of the diffusion results are given in the Appendix 2 and 3, and the numerical values of the adsorption results in Appendix 4 and 5.

1. Diffusion Results

(a) Helium diffusion

The time lag and the permeability plots for helium behaved as would be expected for pure gas-phase flow. $K\sqrt{T}$ and $L\sqrt{T}$ were

FIG. 7

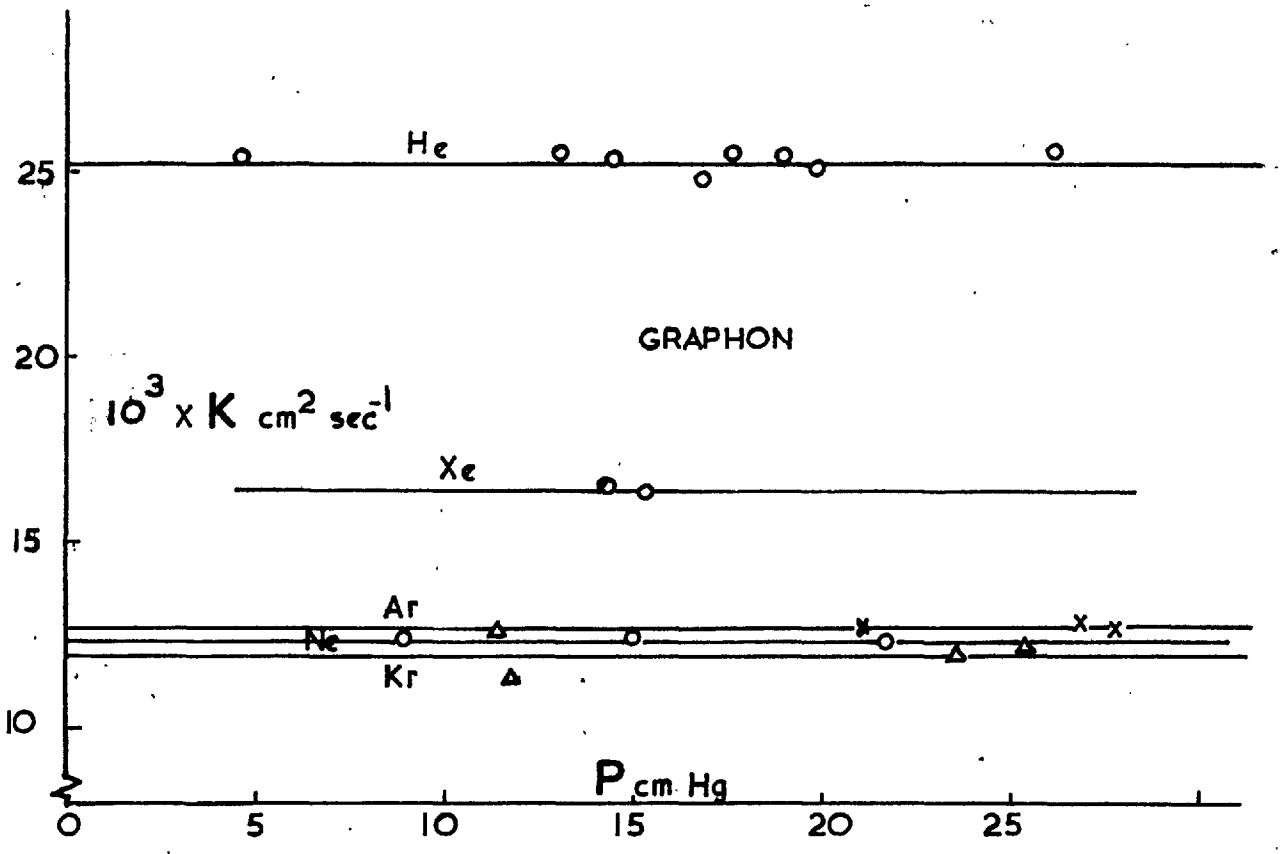
He
GRAPHON
$10^3 \times K\ cm^2\ sec^{-1}$
Xe
Ar
Ne
Kr
25
20
15
10
0
5
10
15
20
25
P cm Hg

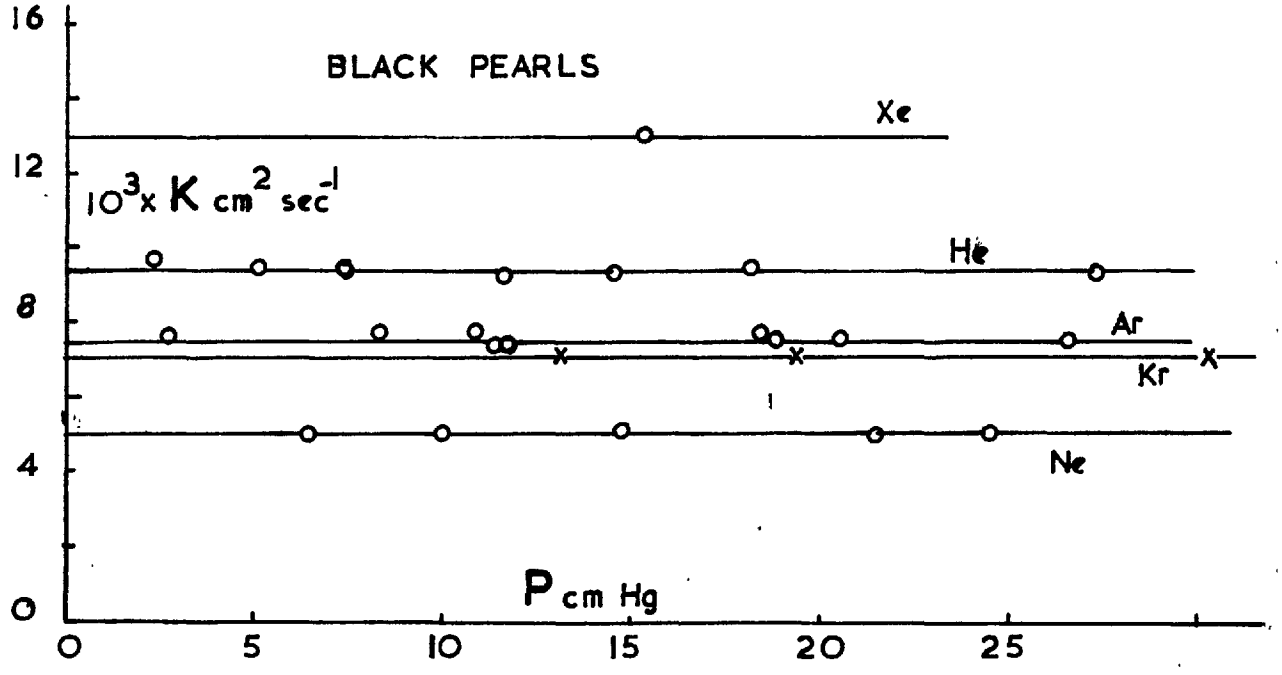
BLACK PEARLS
Xe
$10^3 \times K\ cm^2\ sec^{-1}$
He
Ar
Kr
Ne
16
12
8
4
0
5
10
15
20
25
P cm Hg

FIG. 8

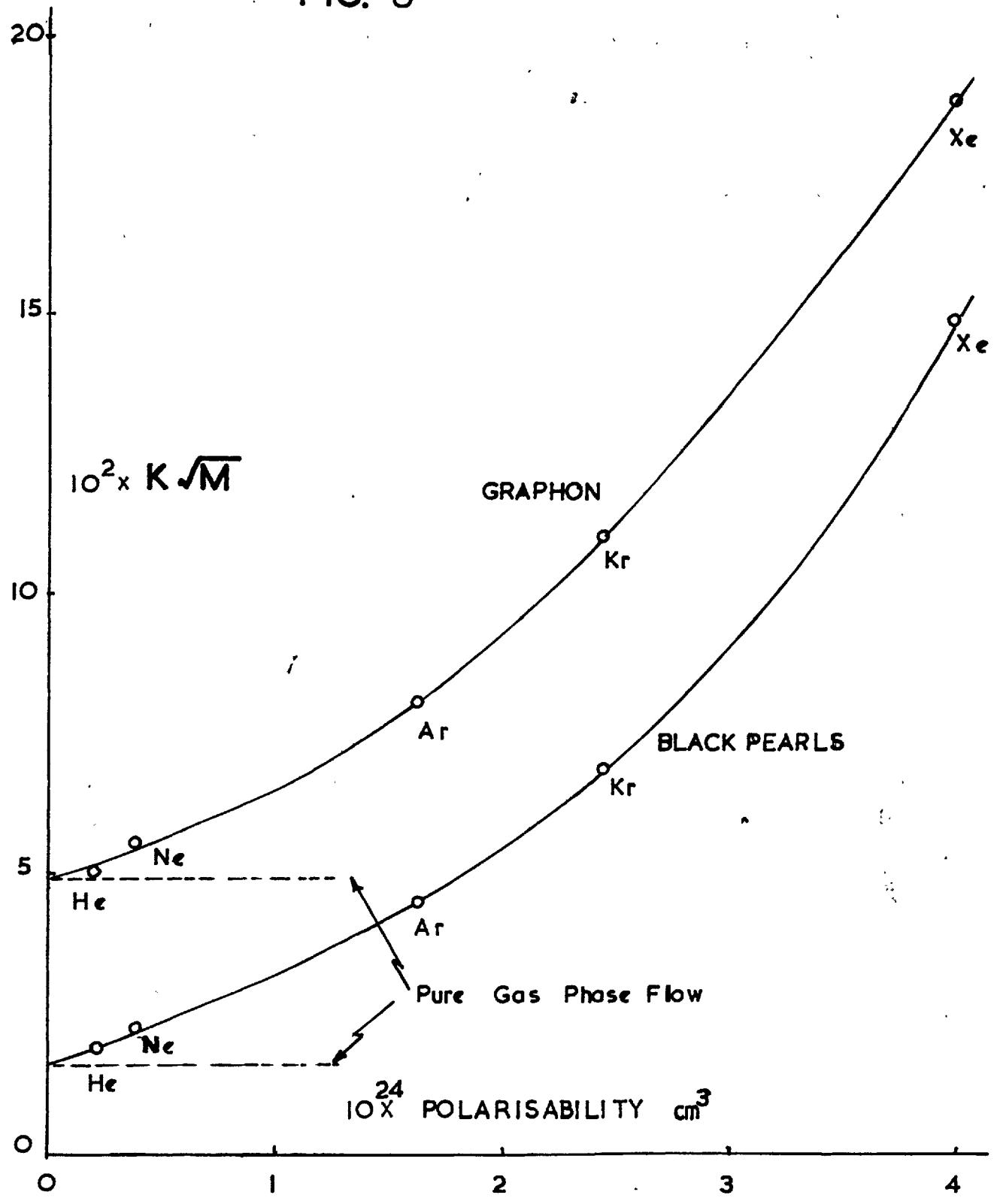
20
15
10
5
0
0
1
2
3
4
$10^2 \times K\sqrt{M}$
$10^{24} \times$ POLARISABILITY cm^3
GRAPHON
BLACK PEARLS
Xe
Xe
Kr
Kr
Ar
Ar
Ne
Ne
He
He
Pure Gas Phase Flow

almost constant in the range 323 °K to 153 °K. There was, however, some indication of surface flow taking place at the two lowest temperatures 90 °K and 77.6 °K. This was shown by a slight increase in the quantities $K/\sqrt{T}$ and $L\sqrt{T}$ with decreasing temperature.

TABLE 2

	Black Pearls		Graphon	
Temp. °K	$10^4 K/\sqrt{T}$ $cm^2 sec^{-1} deg^{-\frac{1}{2}}$	$L\sqrt{T}$ $sec\ deg^{\frac{1}{2}}$	$10^4 K/\sqrt{T}$ $cm^2 sec^{-1} deg^{-\frac{1}{2}}$	$L\sqrt{T}$ $sec\ deg^{-\frac{1}{2}}$
323	3.15	2013	8.68	665
303	3.17	2134	8.68	665
273	3.17	2032	8.74	644
231	3.20	2067	8.74	699
195	3.24	2025	8.68	656
153	3.22	2016	8.77	631
90	3.74	2305	9.62	636
77.6	4.06	2546	9.82	710

The discrepancies at 90 °K and at 77.6 °K are too large to be explained as an experimental uncertainty due to the very low temperatures, and are almost certainly due to surface flow.

(b) Argon diffusion

With argon the permeability and the time lag indicated large surface flows in the Henry's Law region and these effects increased markedly with decreasing temperature (see fig. 9-12 and tables 3 and 4 below).

TABLE 3

Graphon

Temp. ^0K	$Kx10^3$ cm^2sec^{-1}	$Kx10^3$(calc) cm^2sec^{-1}	L sec	L(calc) sec
323	7.71	4.94	128	115
303	7.90	4.78	138	118
273	8.09	4.54	167	124
231	8.92	4.17	215*	137
195	10.38	3.83	305*	149
153	16.0*	3.40	540*	168

TABLE 4

Black Pearls

Temp. ^0K	$Kx10^3$ cm^2sec^{-1}	$Kx10^3$(calc) cm^2sec^{-1}	L sec	L(calc) sec
323	4.45	1.79	432	348
303	4.69	1.76	453	361
273	5.11	1.67	572	380
231	6.20	1.54	893*	411
195	8.20	1.39	1336*	447
153	16.1*	1.23	5600*	507

All calculated values are derived from the helium results at 323 ^0K ($K^{He}\sqrt{\frac{M^{He}}{T}} = K\sqrt{\frac{M}{T}}$ and $L^{He}\sqrt{\frac{T}{M_{He}}} = L\sqrt{\frac{T}{M}}$).

* Extrapolated values to $C_G'^0 = 0$.

As the temperature was lowered and the gas moved out of the Henry's Law range, the time lag for both graphon and black pearls became pressure dependent at 231 ^{0}K. As the temperature was lowered further still the permeability became pressure dependent also at 153 ^{0}K. At liquid nitrogen temperatures it was very pressure dependent indeed (figs. 13 - 16). An explanation for this behaviour is given in a later section.

The striking thing about the argon diffusion results is the magnitude of the surface flow. Even with a surface concentration at one atmosphere pressure of 0.2 cc at N.T.P. per g the flow was made up of almost equal parts gas phase and surface transport. At liquid nitrogen temperatures the fraction of surface flow was at the lowest surface concentration more than 500 times the gas-phase flow. The reasons for these very large flows are discussed later.

The overall diffusion coefficient D_t from equation (46) is shown plotted against C_0 at 90 ^{0}K and 77.6 ^{0}K in fig. 20. The results are similar to those reported by Haul and are a confirmation of his results.

The energy of activation for argon was evaluated for the Henry's Law region by using equation (10) and was found to be 1.05 Kcal mole for graphon and 1.19 Kcal for black pearls. Due to experimental inaccuracies it was not possible to evaluate the energy of activation using equation (10) outside the Henry's Law region.

(c) SF_6 diffusion

The time lags were measured only for the Henry's Law range since they became excessively long outside this range. The plots of permeabilities and of J_T against pressure were similar to those for argon. In Table 5 are listed the values of K as experimentally

determined and as calculated from the helium result at 323 ^{0}K. The fraction of surface flow ~~is not so large as for argon but it~~ is still large compared with the results for most other porous materials.

TABLE 5

Temp. ^{0}K	Graphon $Kx10^3$ cm^2sec^{-1}	$Kx10^3$(calc) cm^2sec^{-1}	Black Pearls $Kx10^3$ cm^2sec^{-1}	$Kx10^3$(calc) cm^2sec^{-1}
473	6.0	3.1	3.8	1.13
423	6.3	3.0	4.5	1.07
373	6.9	2.8	5.5	1.01
333	7.9	2.6	7.4*	0.95
304	9.3	2.5	9.8*	0.91
273	11.9	2.4	14.4*	0.86
253	15.5	2.3		

* Extrapolated values to $C'^0_g = 0$.

The results are also shown graphically in figs. 21-27. The overall diffusion coefficient calculated from equation (46) is also shown plotted against surface coverages in fig. 28. These results will be discussed later where the very unusual form of this curve is explained. It should again be emphasised that not too much reliance should be placed on the actual numerical values of the diffusion coefficient outside the Henry's Law region since they are derived from the slopes of experimental graphs and as such are liable to large errors. The energy of activation (ΔE^*) for surface diffusion in the Henry's Law region was found to be 2.2. Kcal for graphon and 1.8 Kcal for black pearls. The ratio $\Delta E^*/\Delta\bar{H}$ was 0.48 for graphon and 0.34 for the black pearls.

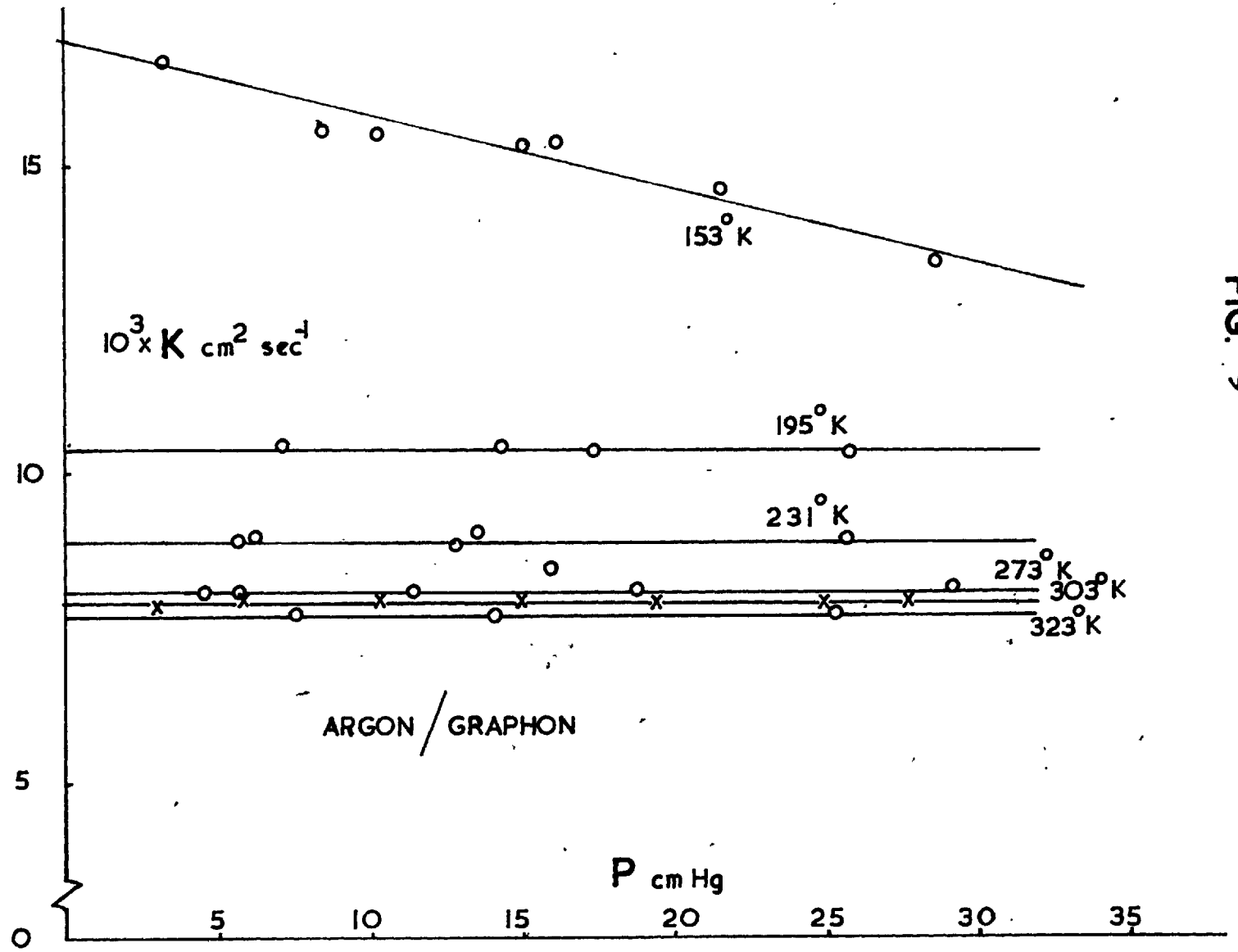
15
10
5
0
153° K
195° K
231° K
273° K
303° K
323° K
$10^3 \times K$ cm^2 sec^{-1}
ARGON / GRAPHON
P cm Hg
5
10
15
20
25
30
35

FIG. 6

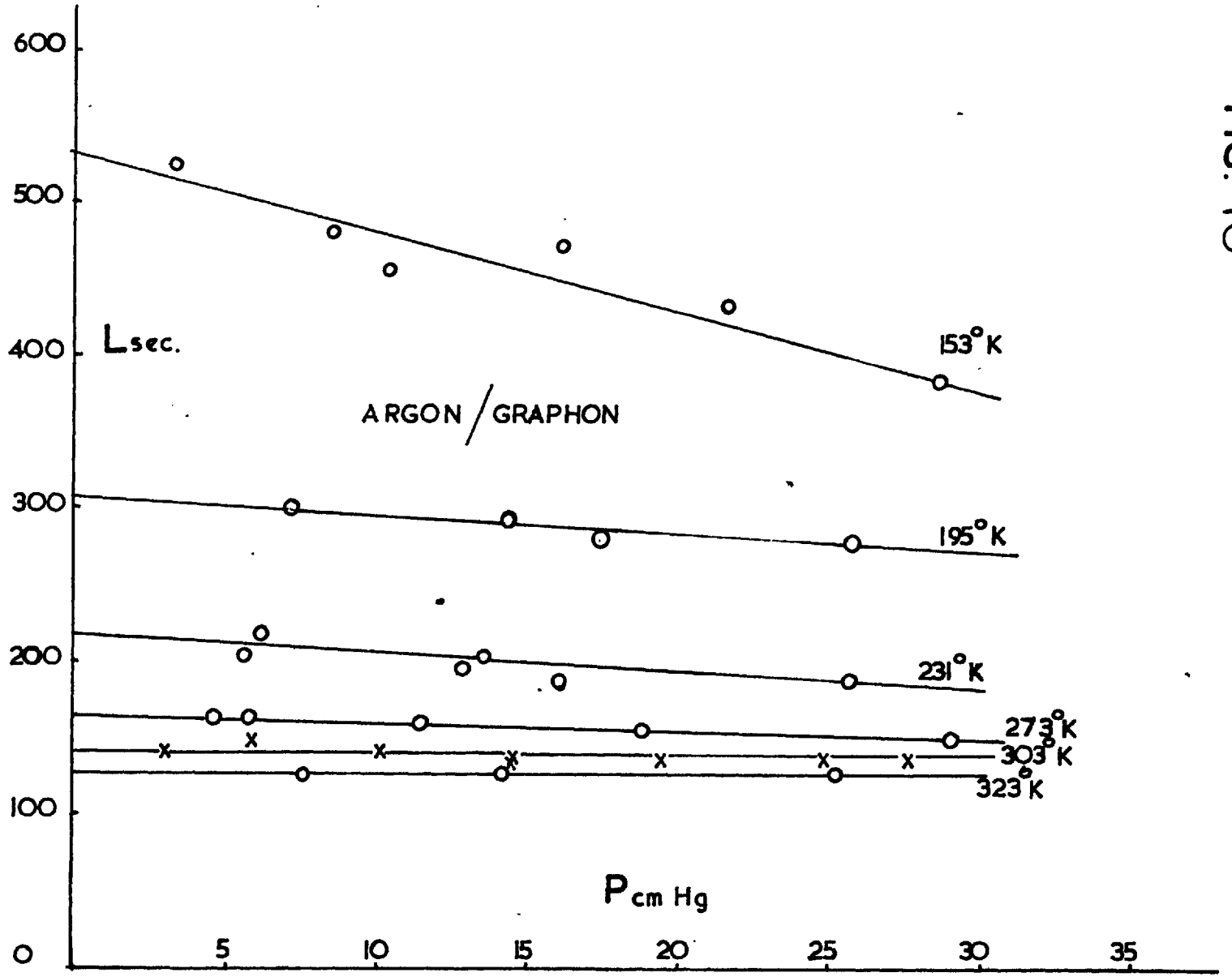
600
500
400
300
200
100
0
Lsec.
ARGON / GRAPHON
153°K
195°K
231°K
273°K
303°K
323°K
5
10
15
20
25
30
35
P cm Hg

FIG. 10

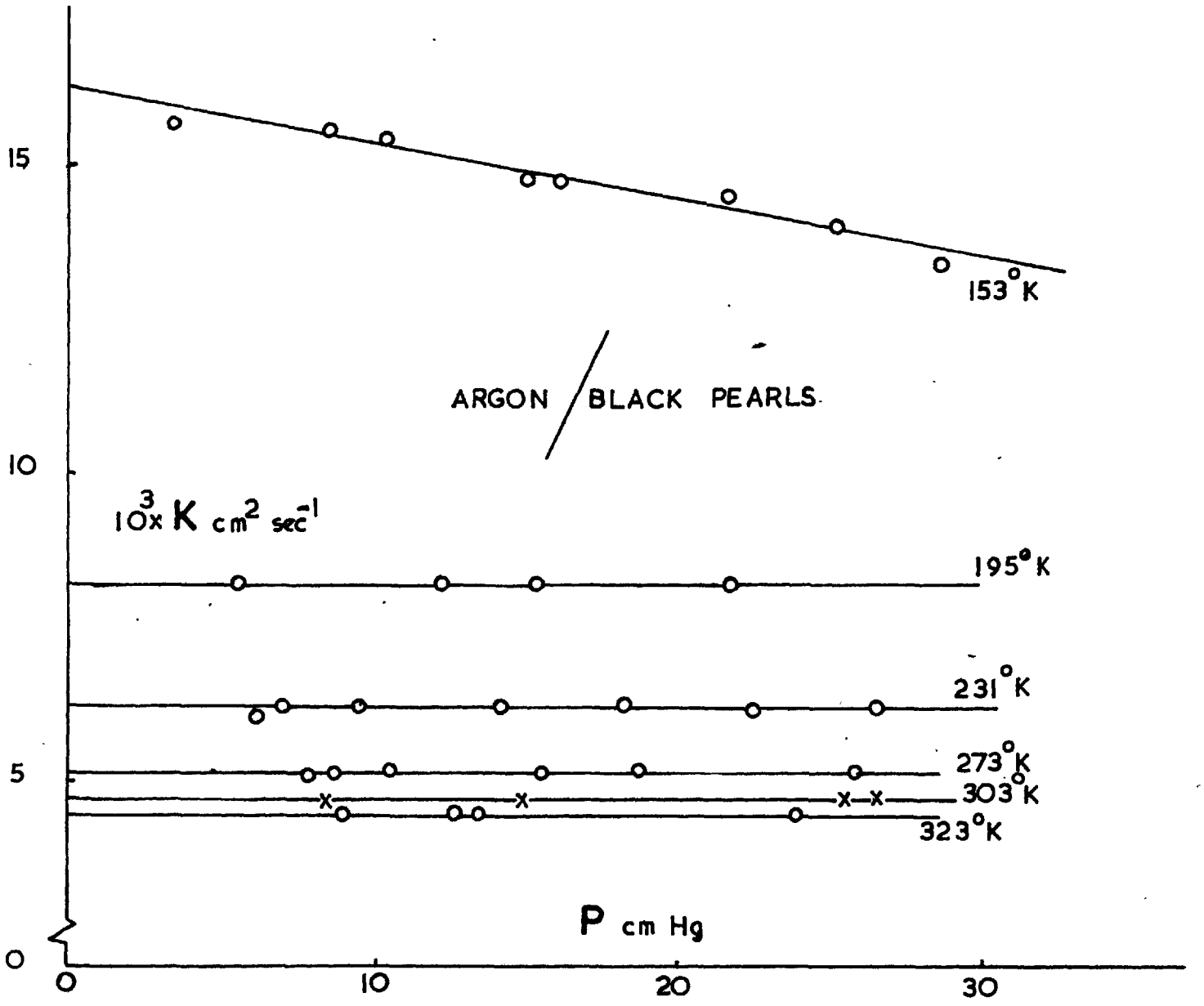
15
10
5
0
$10^3 \times K\ cm^2\ sec^{-1}$
ARGON / BLACK PEARLS
153°K
195°K
231°K
273°K
303°K
323°K
P cm Hg
0
10
20
30

FIG. 11

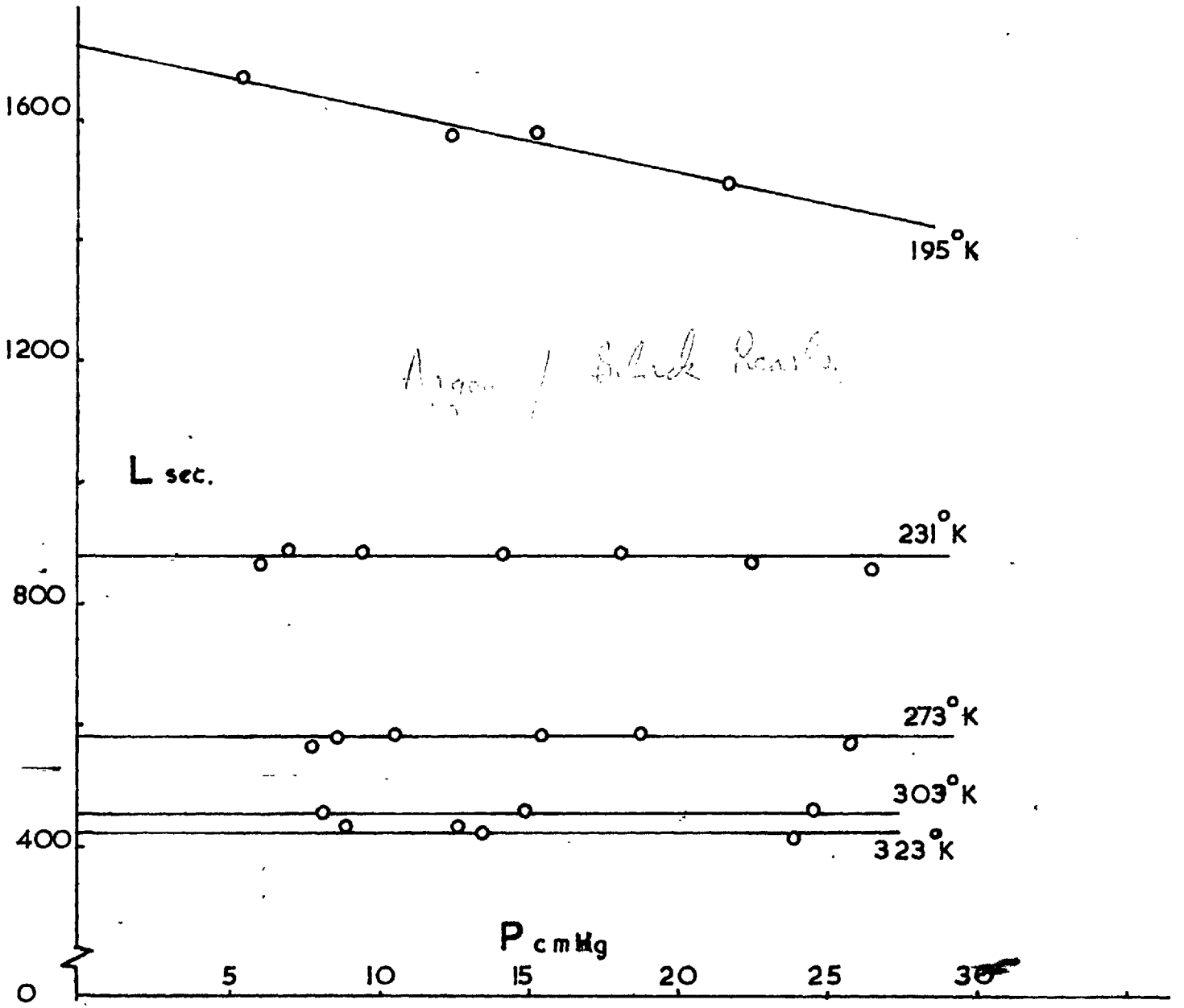
1600
1200
800
400
0
L sec.
195°K
231°K
273°K
303°K
323°K
P cm Hg
5
10
15
20
25
30

FIG. 12

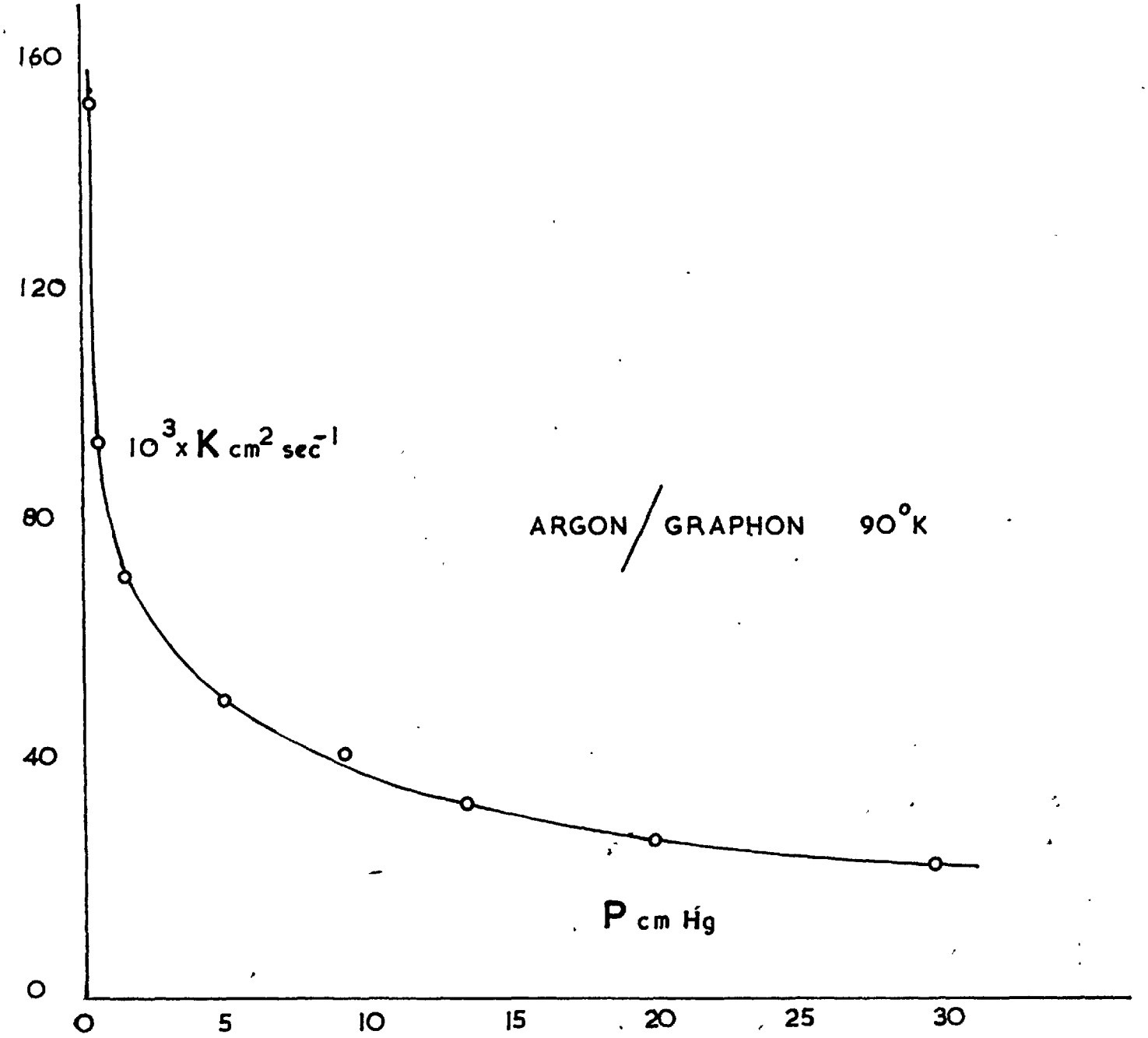
160
120
80
40
0
$10^3 \times K\ cm^2\ sec^{-1}$
ARGON / GRAPHON 90°K
P cm Hg
0
5
10
15
20
25
30

FIG. 13

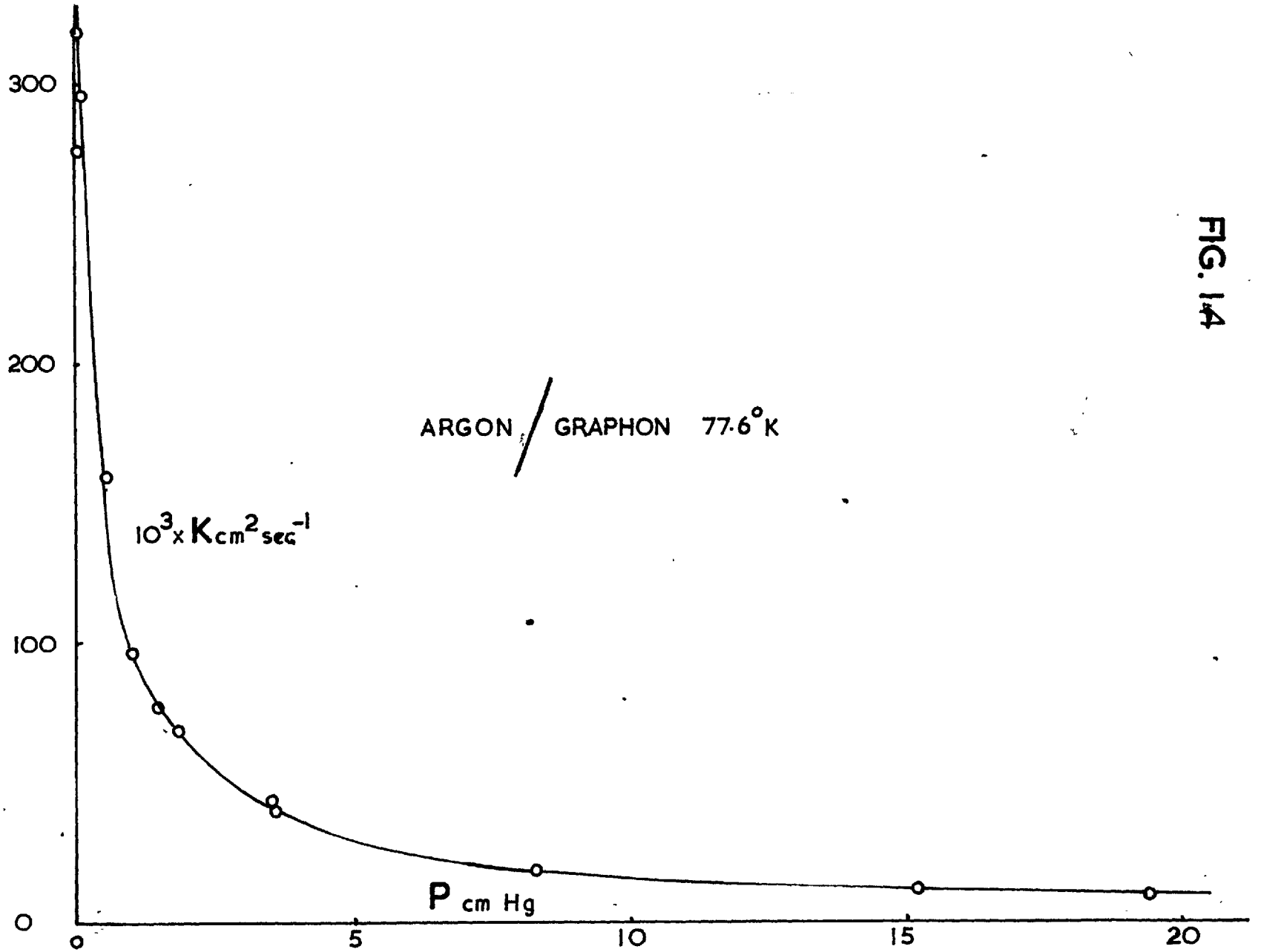
300
200
100
0
ARGON / GRAPHON 77·6°K
$10^3 \times K_{cm^2 sec^{-1}}$
P cm Hg
0
5
10
15
20

FIG. 14

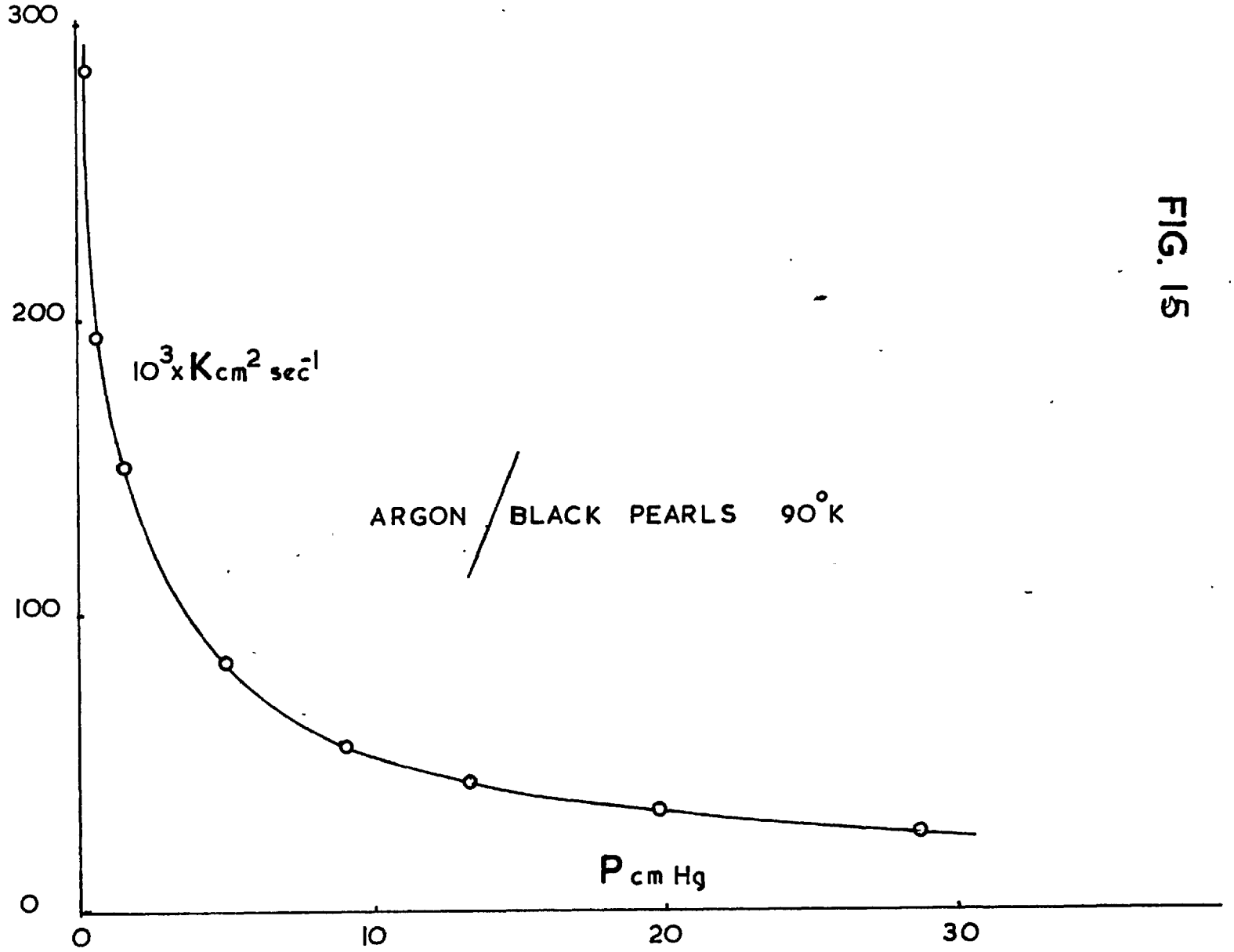
300
200
100
0
$10^3 \times K cm^2 sec^{-1}$
ARGON / BLACK PEARLS 90°K
P cm Hg
0
10
20
30

FIG. 15

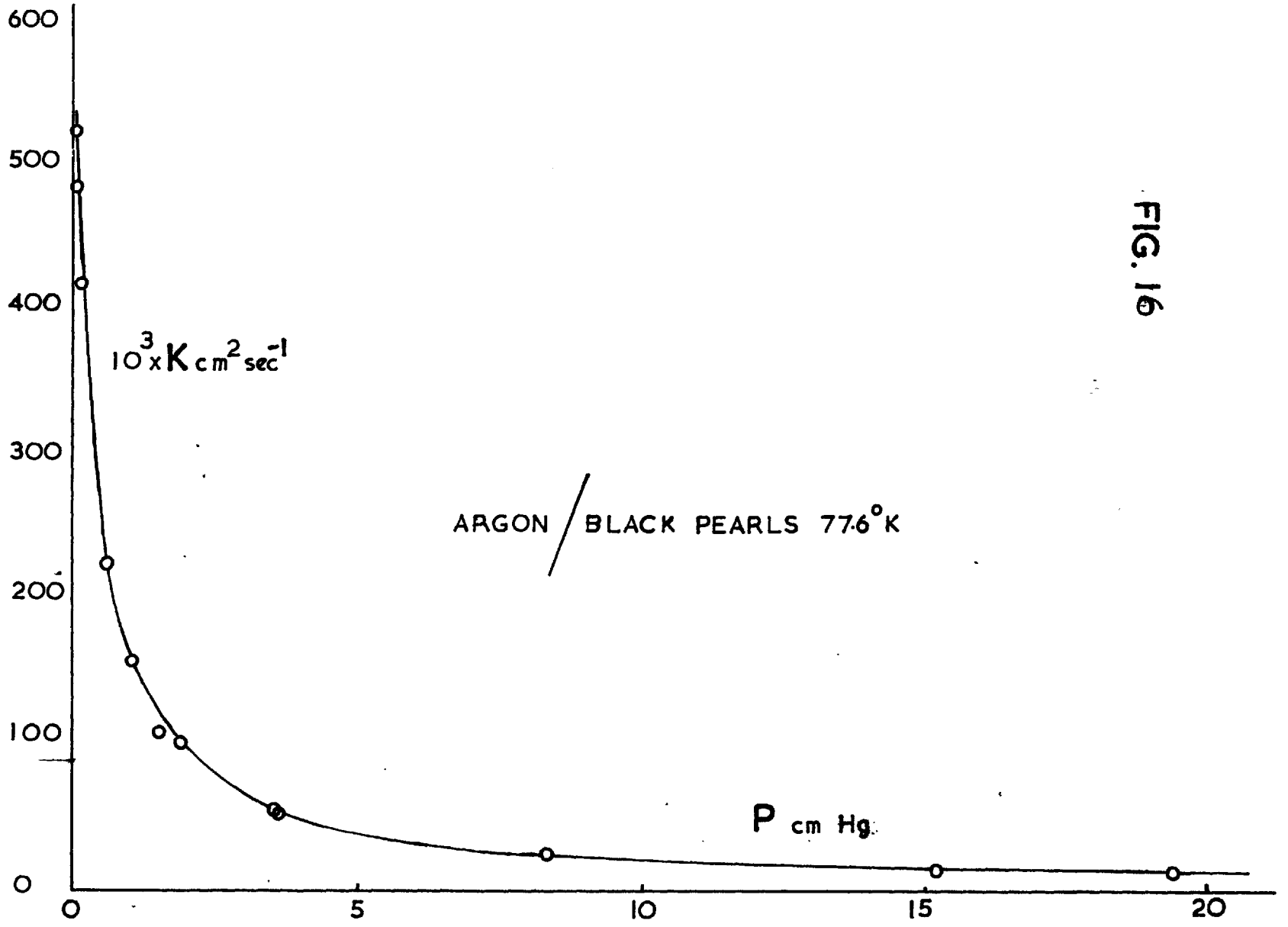
600
500
400
300
200
100
0
$10^3 \times K\ cm^2\ sec^{-1}$
ARGON / BLACK PEARLS 77.6°K
P cm Hg
0
5
10
15
20

FIG. 16

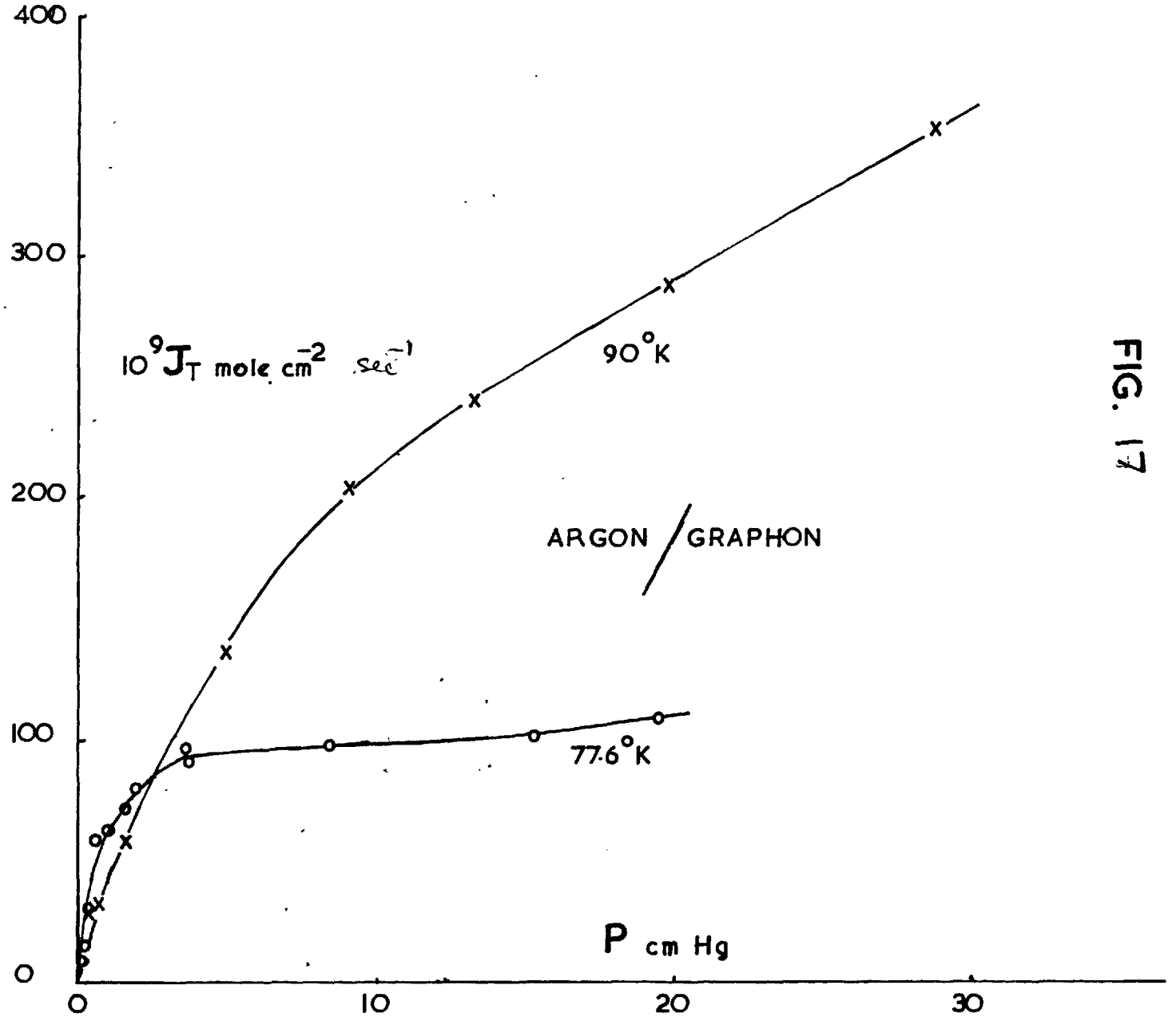
400
300
200
100
0
$10^9 J_T$ mole cm^{-2} sec^{-1}
90°K
ARGON / GRAPHON
77.6°K
P cm Hg
0
10
20
30

FIG. 17

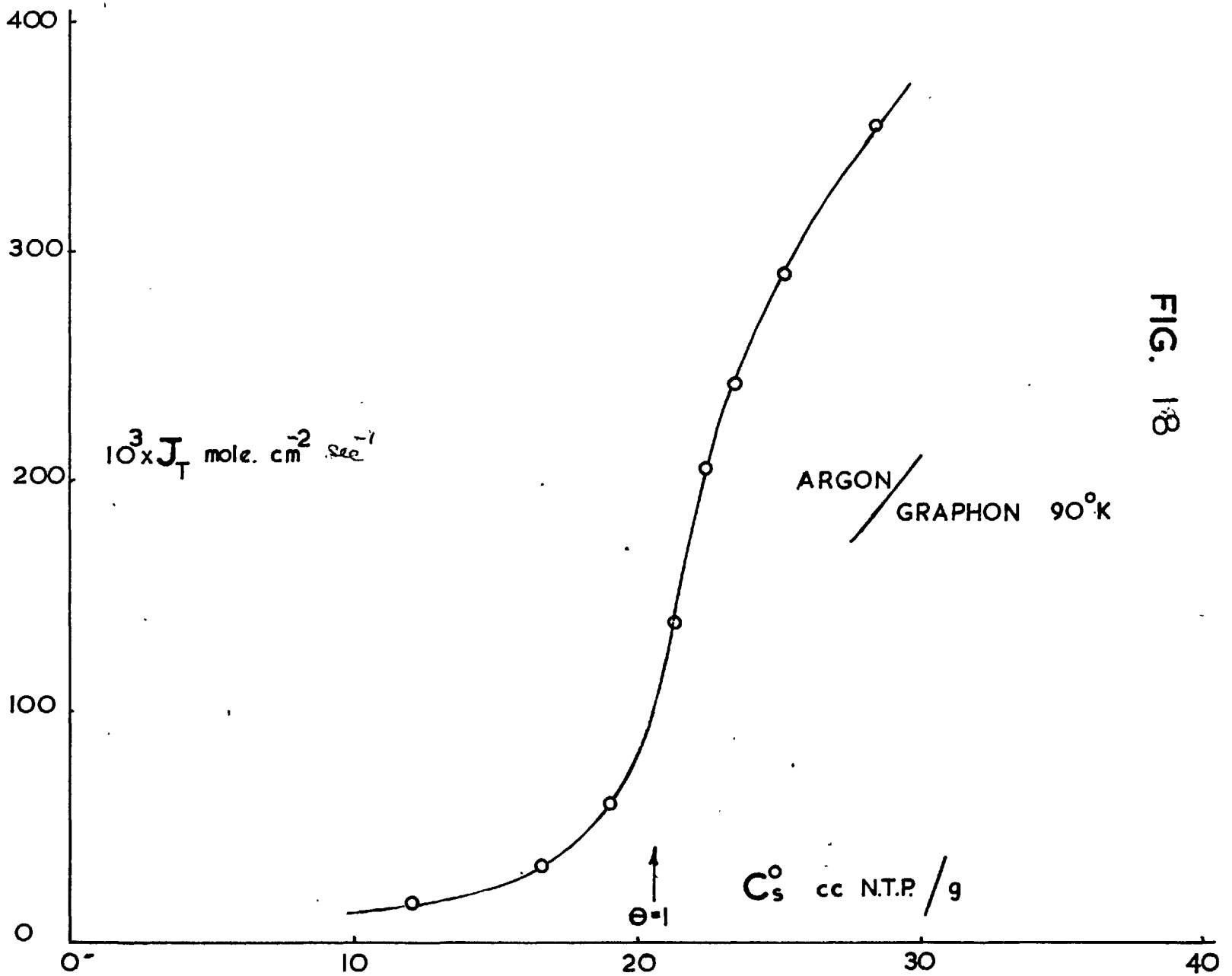
400
300
200
100
0
0
10
20
30
40
$10^3 \times J_T$ mole. cm^{-2} sec^{-1}
ARGON / GRAPHON 90°K
θ=1
C_s^o cc N.T.P. / g

FIG. 18

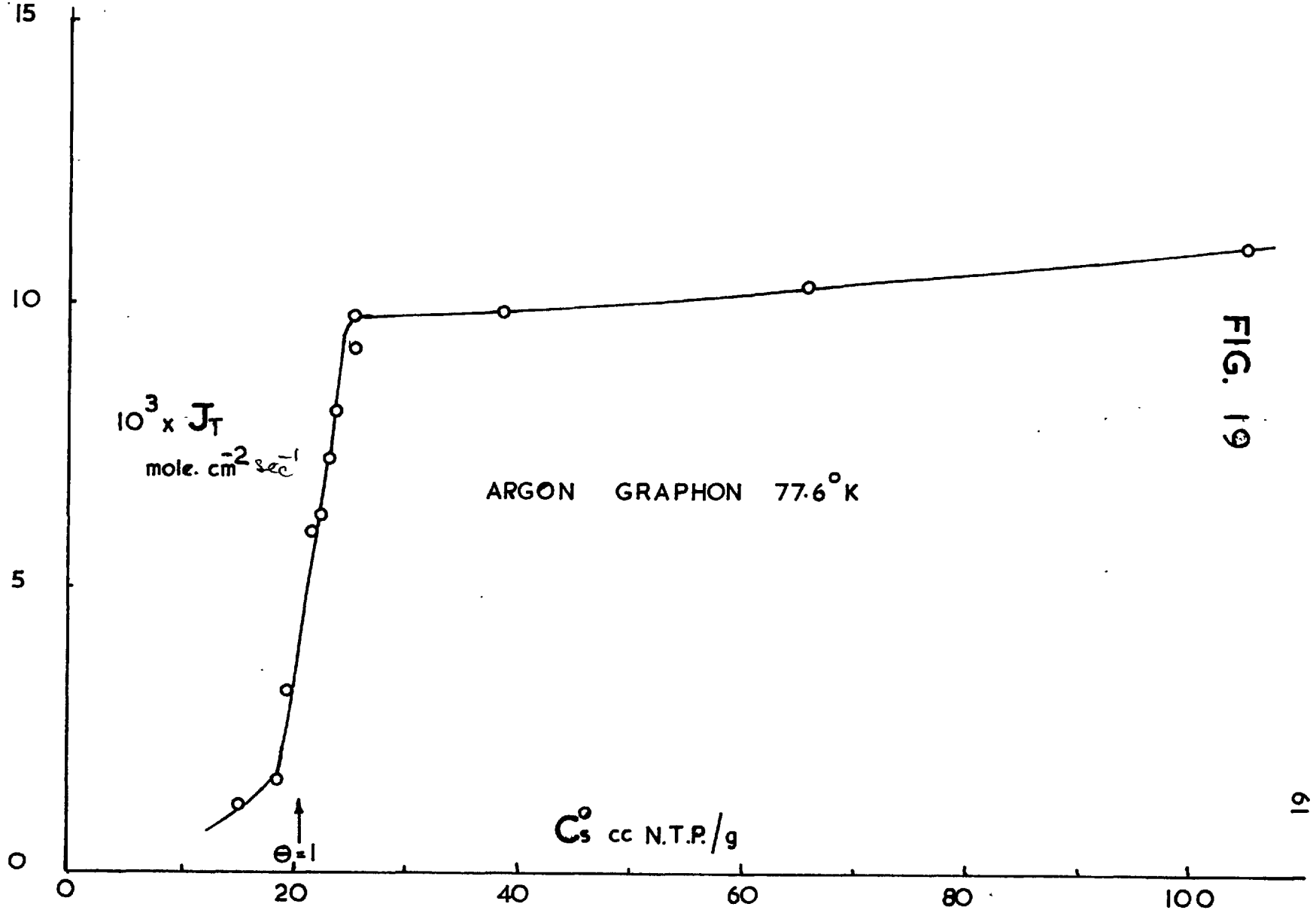
15
10
5
0
$10^3 \times J_T$
mole. cm^{-2} sec^{-1}
ARGON GRAPHON 77.6°K
$\theta = 1$
C_s^o cc N.T.P./g
0
20
40
60
80
100

FIG. 19

FIG. 20

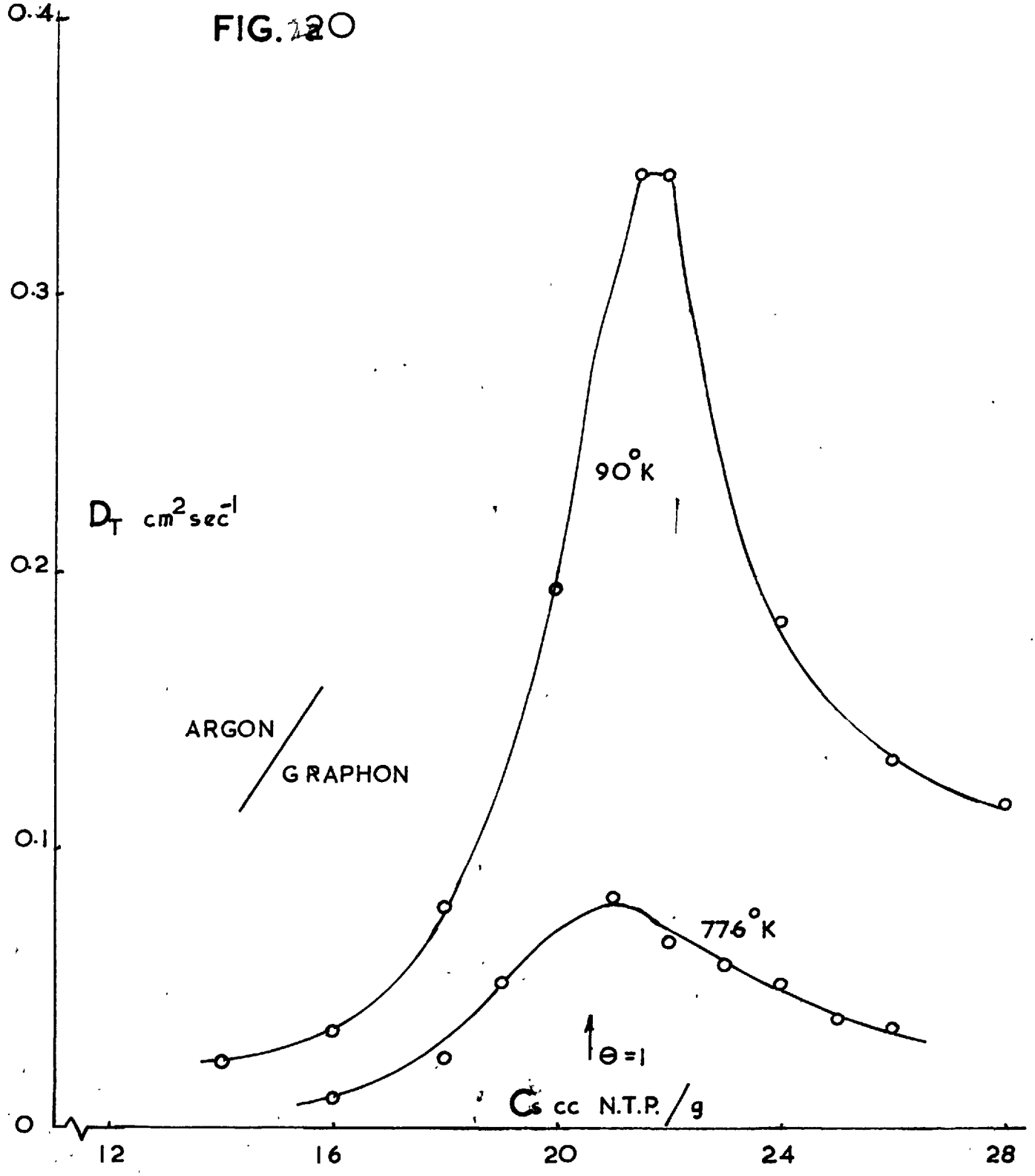
0·4
0·3
0·2
0·1
0
D_T cm^2 sec^{-1}
90°K
776°K
ARGON
GRAPHON
θ=1
C_s cc N.T.P./g
12
16
20
24
28

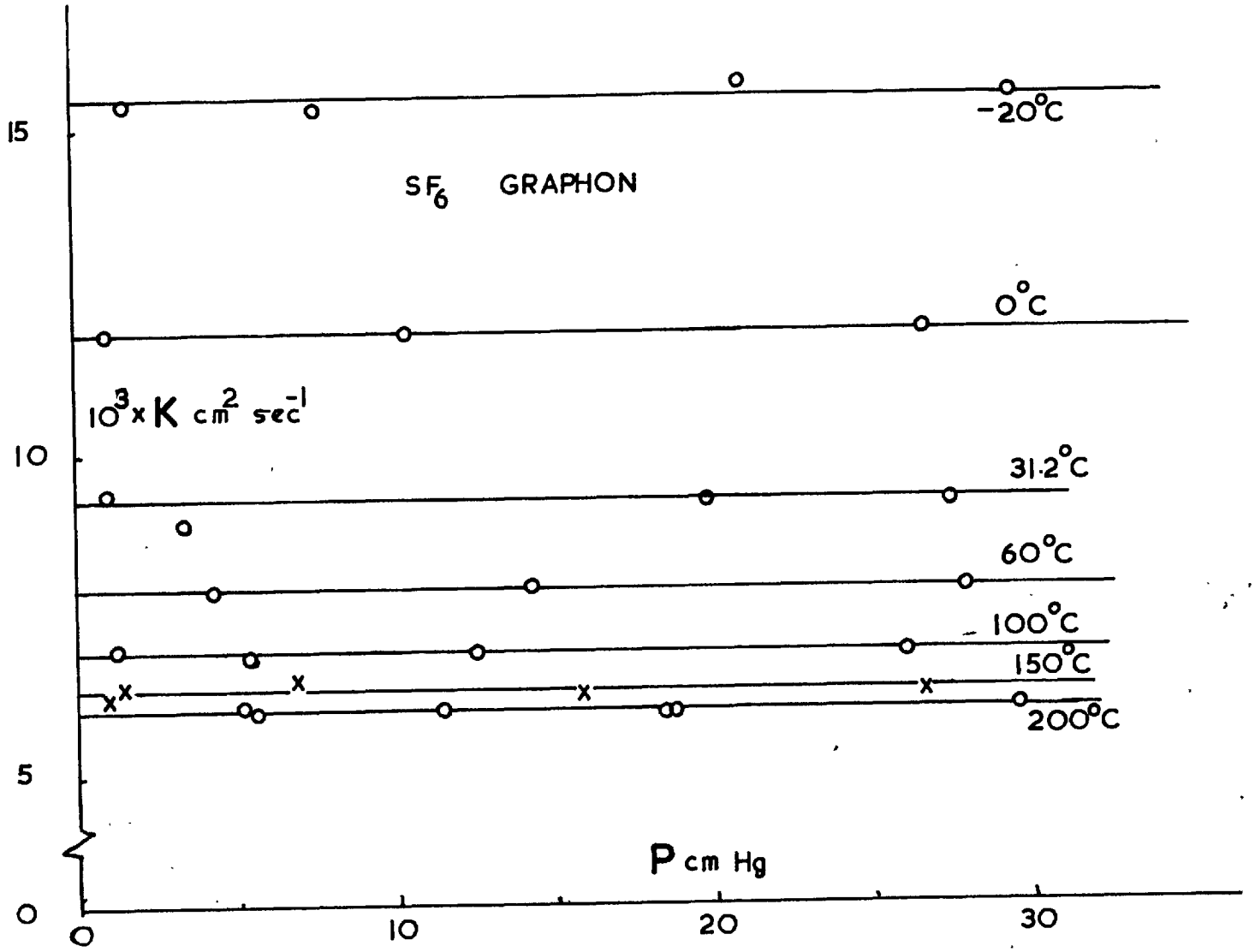
15
10
5
0
SF_6 GRAPHON
$10^3 \times K\ cm^2\ sec^{-1}$
-20°C
0°C
31.2°C
60°C
100°C
150°C
200°C
P cm Hg
0
10
20
30

FIG. 21

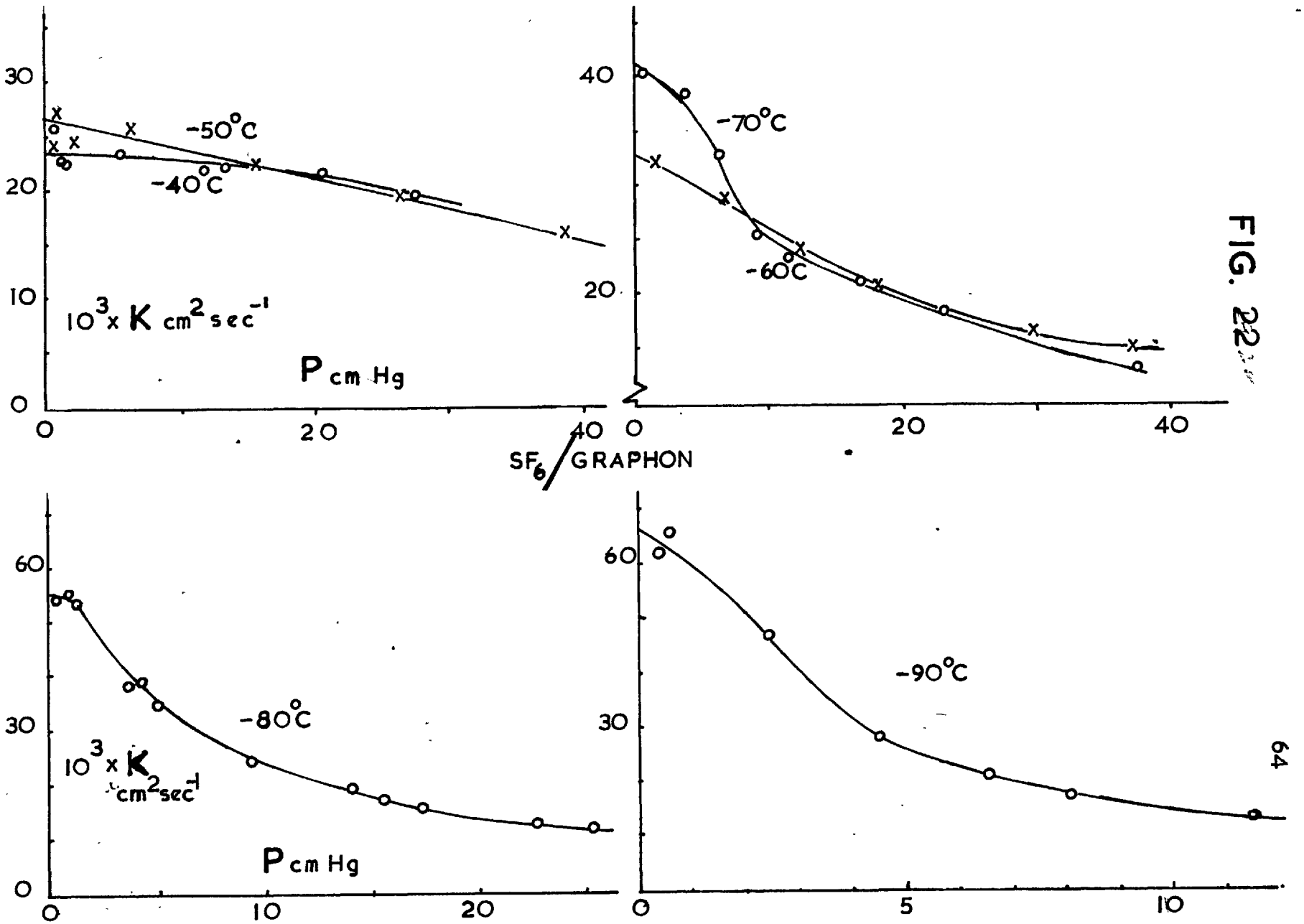
30
20
10
0
-50°C
-40°C
$10^3 \times K\ cm^2\ sec^{-1}$
P cm Hg
0
20
40
40
20
-70°C
-60°C
0
20
40
SF_6 / GRAPHON
60
30
0
-80°C
$10^3 \times K\ cm^2 sec^{-1}$
P cm Hg
0
10
20
60
30
-90°C
0
5
10

FIG. 22

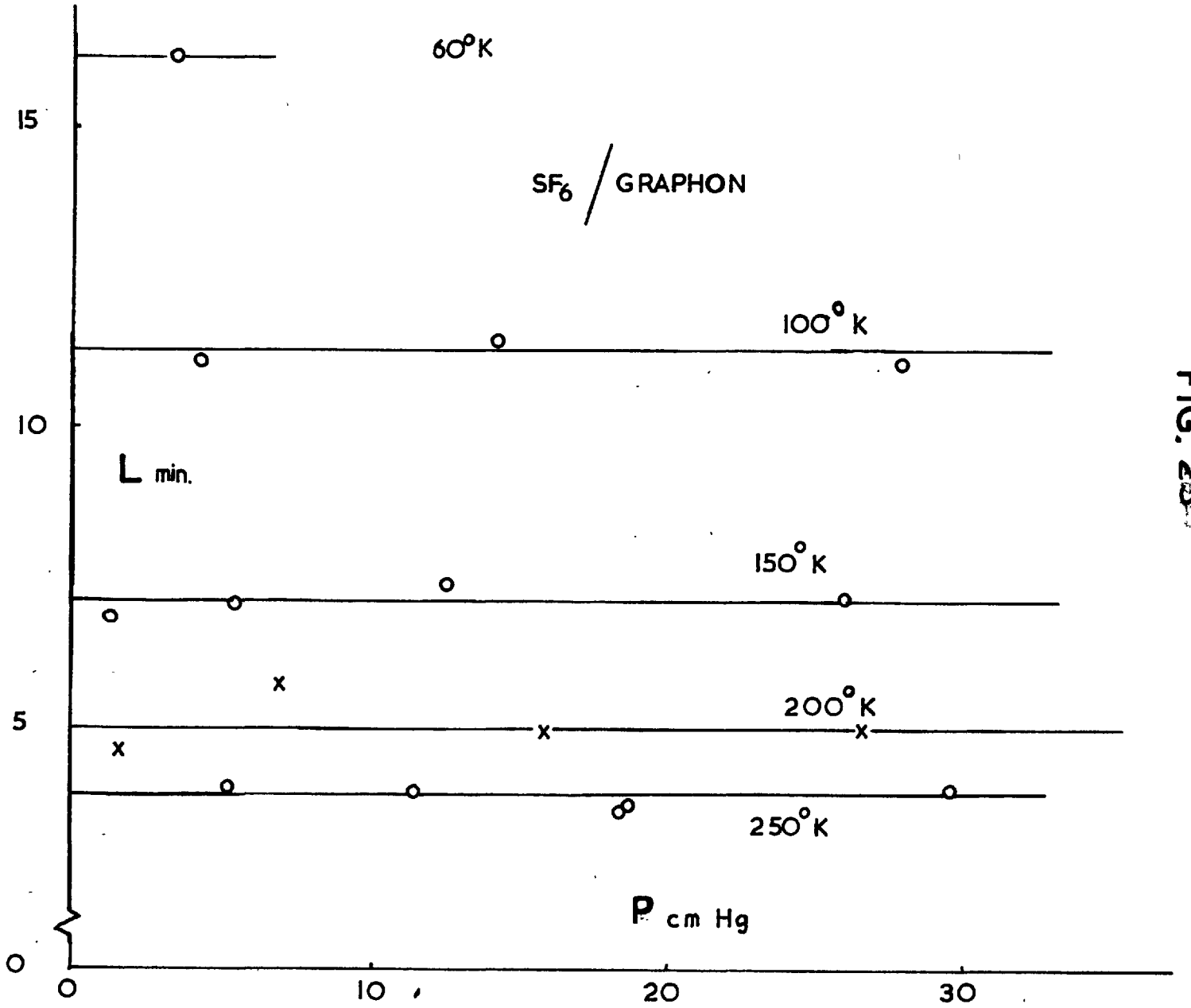
60°K
15
SF6 / GRAPHON
100° k
10
L min.
150° K
5
200°K
250°K
P cm Hg
0
0
10
20
30

FIG. 23

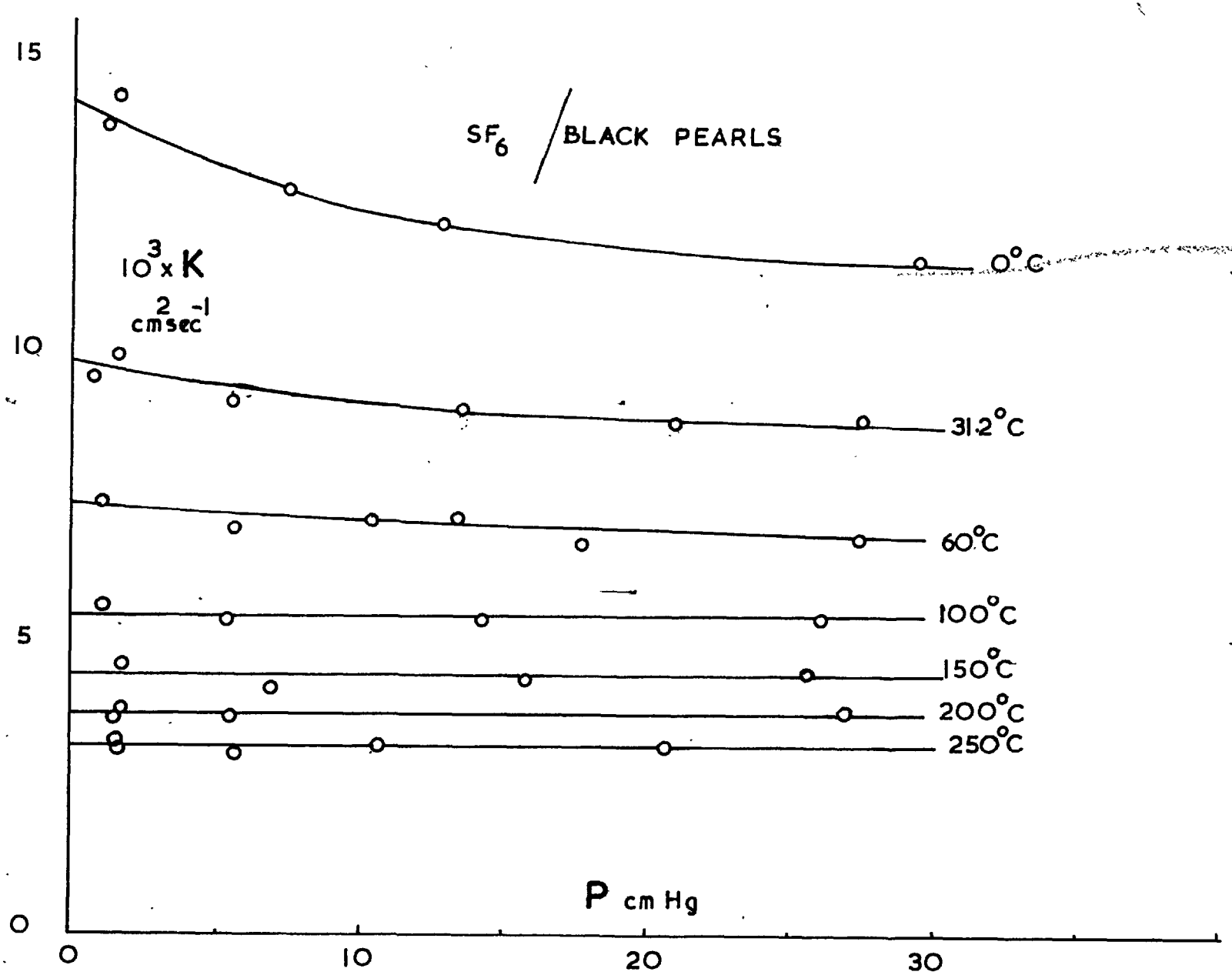
15
10
5
0
SF_6 / BLACK PEARLS
$10^3 \times K$
$cm^2 sec^{-1}$
0°C
31.2°C
60°C
100°C
150°C
200°C
250°C
P cm Hg
0
10
20
30

FIG. 24

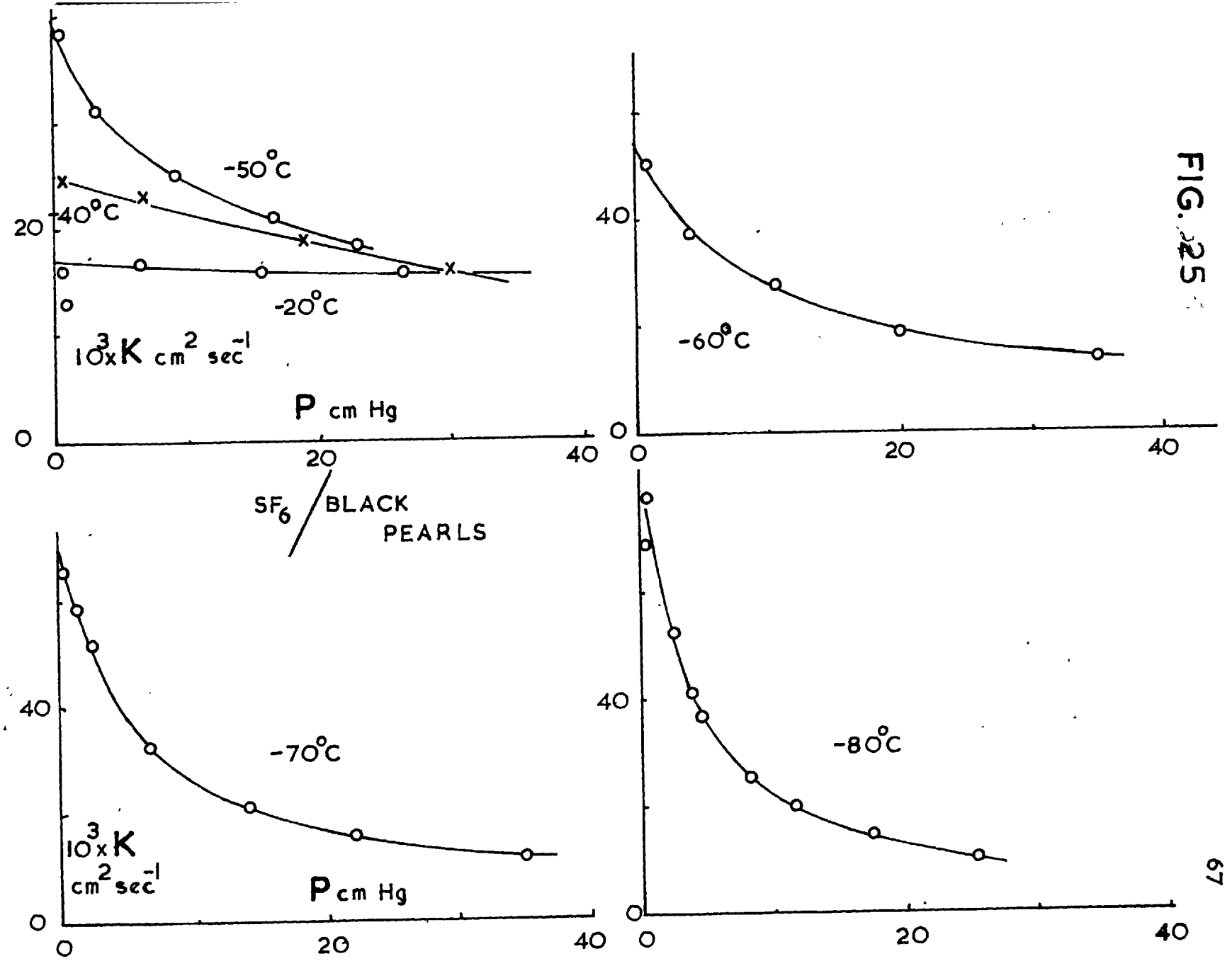
-50°C
40°C
-20°C
$10^3 \times K$ cm^2 sec^{-1}
P cm Hg
0
20
40
-60°C
SF_6 / BLACK PEARLS
-70°C
-80°C

FIG. 25

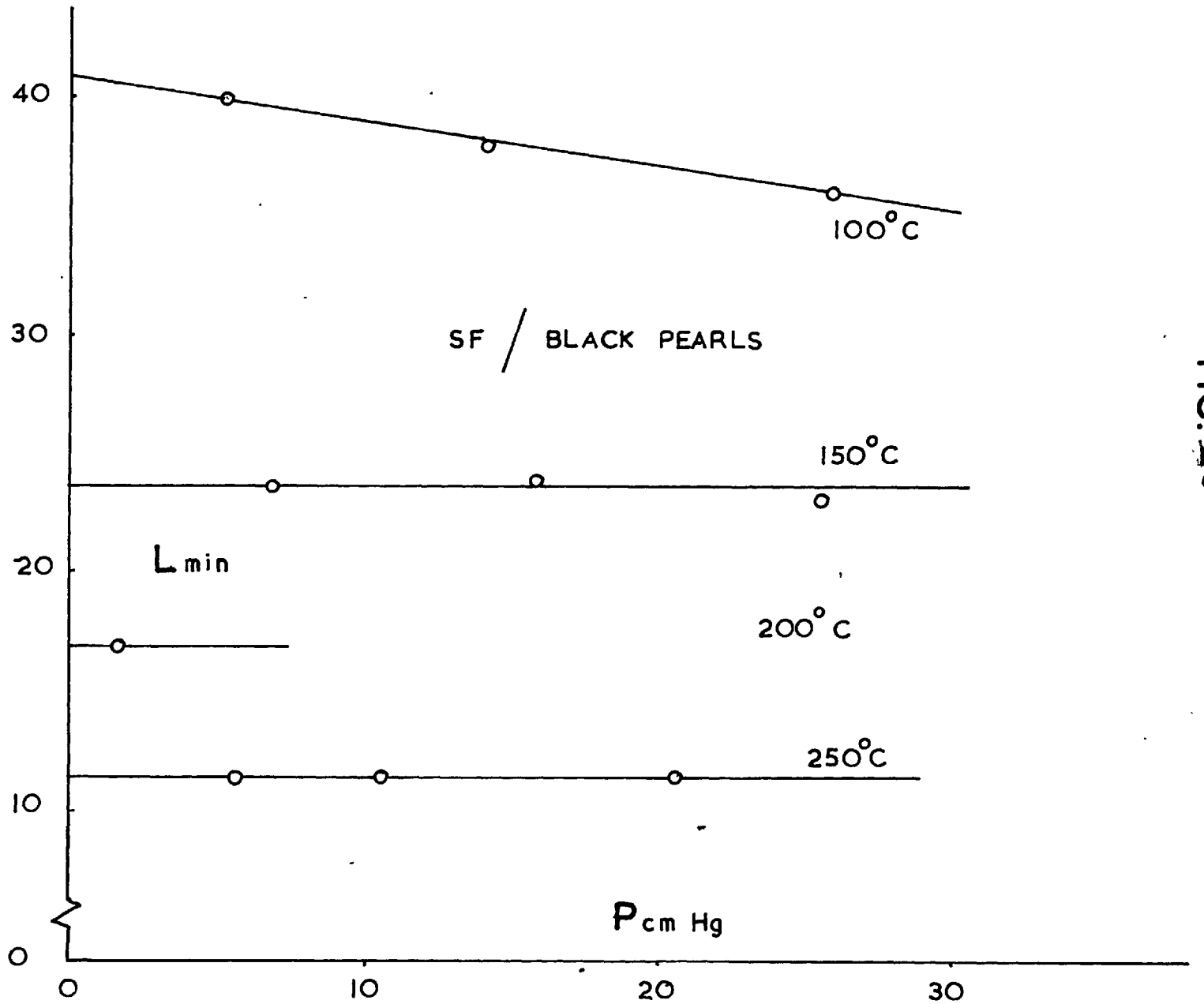
40
30
20
10
0
SF / BLACK PEARLS
100°C
150°C
200°C
250°C
L min
P cm Hg
0
10
20
30

FIG. 26

FIG. 27

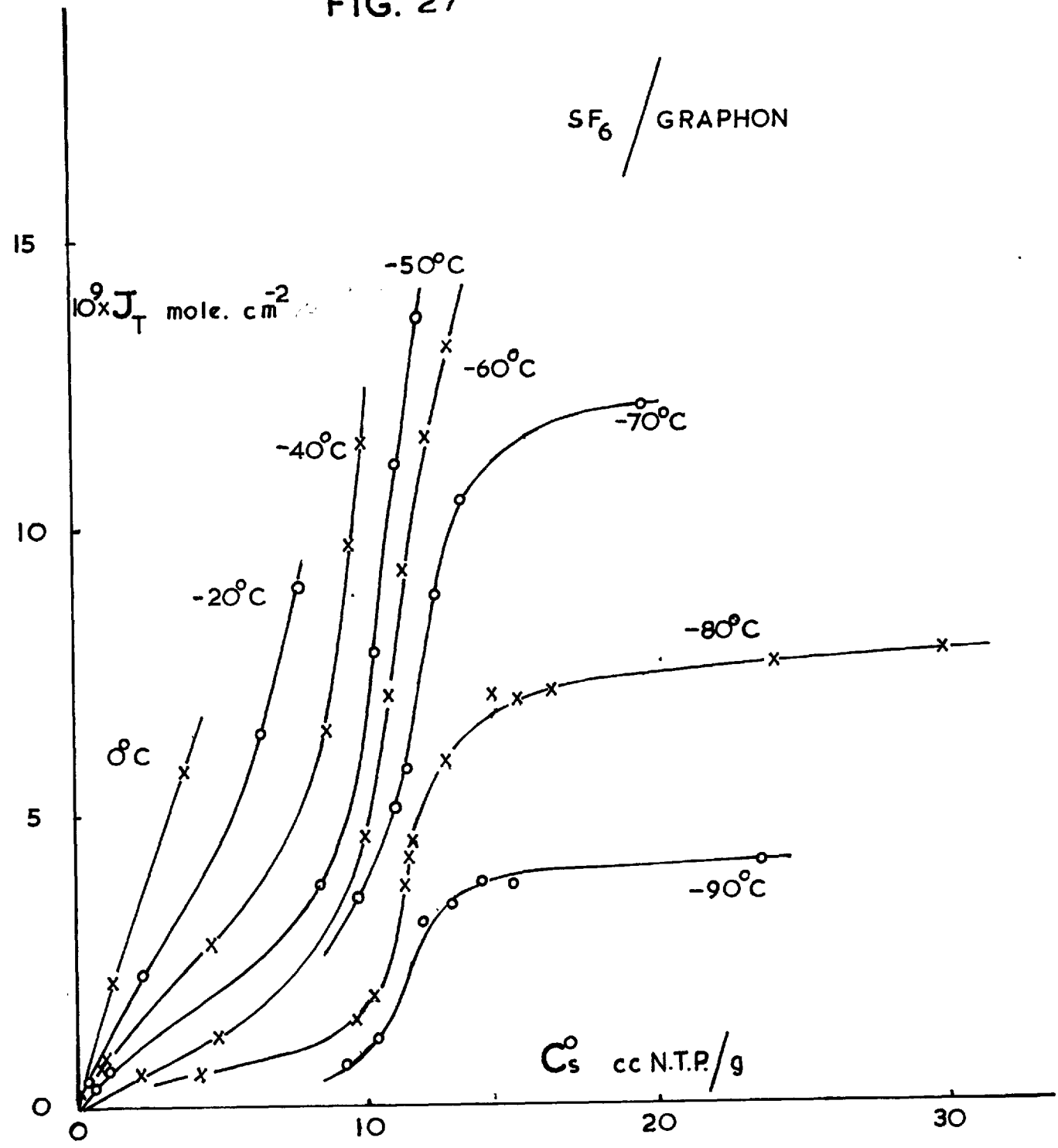
SF6 / GRAPHON
15
10
5
0
$10^9 \times J_T$ mole. cm^{-2}
-50°C
-60°C
-70°C
-40°C
-20°C
-80°C
0°C
-90°C
C_s^o cc N.T.P./g
0
10
20
30

FIG. 28

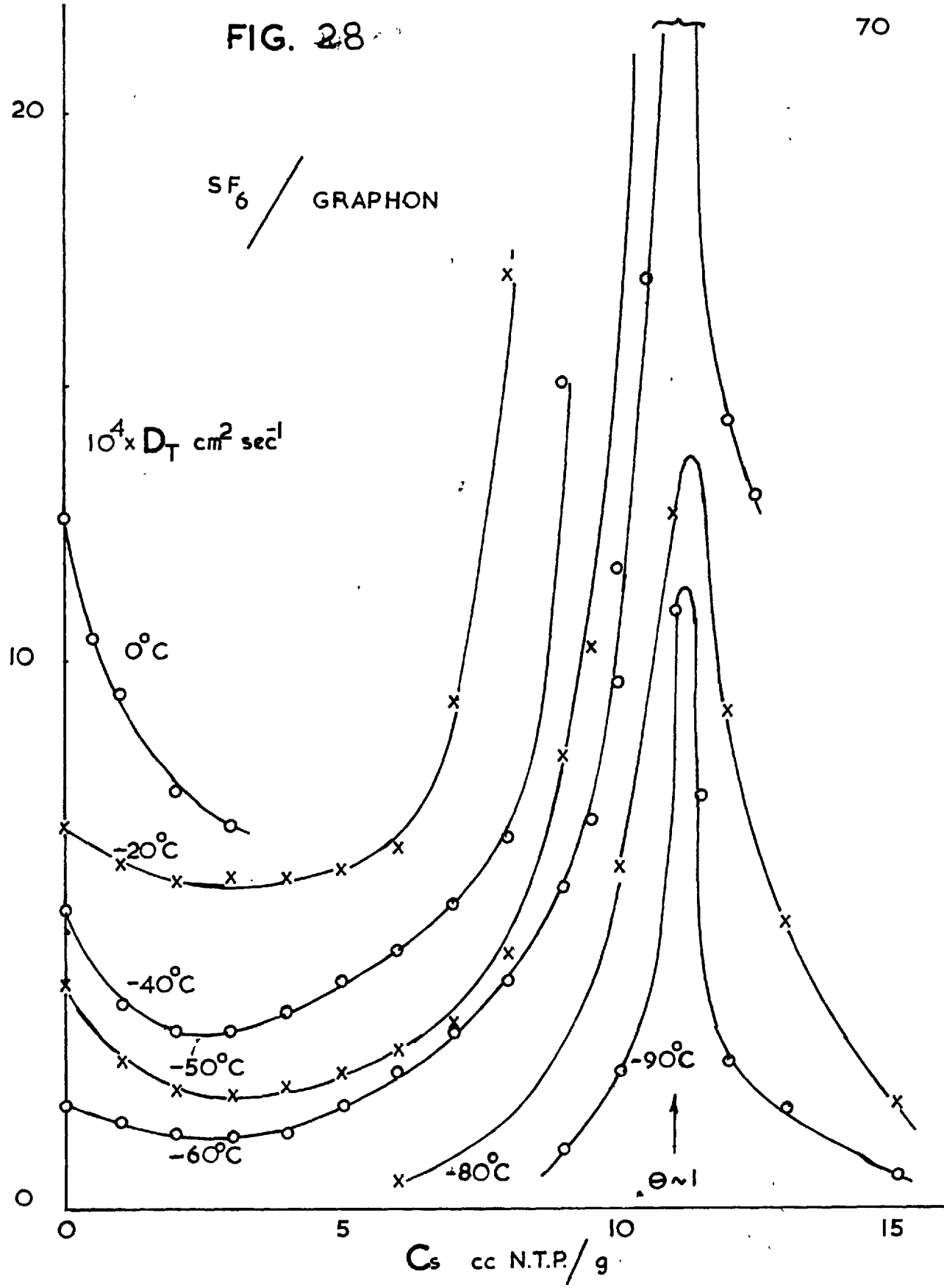
20
10
0
SF_6 / GRAPHON
$10^4 \times D_T$ cm^2 sec^{-1}
0°C
-20°C
-40°C
-50°C
-60°C
-80°C
-90°C
θ~1
0
5
10
15
Cs cc N.T.P./g

2. Adsorption Results

The heat of adsorption was evaluated using equation (57) for both argon and SF_6 on the graphon and the black pearls. The argon results were not very extensive and all that need be said of them is that they are similar to the results already available in the literature (fig. 29). The SF_6 results are far more comprehensive since isotherms were measured over a wide range of temperatures (200 °C to -90 °C) (figs. 31-38). q_{st}, $\overline{S}_s$ and $\tilde{S}_s$ were all evaluated using the methods described in the theoretical section and using the gas state at one atmosphere pressure and -80 °C as the standard state in the calculation of $\overline{S}_s$ and $\tilde{S}_s$.

On examining the heat of adsorption results in fig. 30 it will be seen that for both graphon and the black pearls above a monolayer coverage $q_{st} < Lh(solid)$ when the measurements used to determine q_{st} were the -90 °C and the -80 °C isotherms, which are well below the normal freezing point of SF_6.

Another interesting point coming from the adsorption results is the initial fall in the heat of adsorption on black pearls which is not found in the results for graphon. This fall is due to slight initial energetic heterogeneity found in black pearls but not in graphon. The subsequent rise in q_{st} is due in both cases to increasing molecule-molecule interaction.

It might be thought that the very extensive results for SF_6 would lend themselves to a detailed thermodynamic and statistical analysis. Beebe and Kiselev et al (1964) have attempted this for a large collection of results for various gases including SF_6 with adsorptions up to the monolayer region on homogeneous surfaces similar to graphon. They have then calculated, using the statistical mechanical models of Hill (1946) and Kiselev (1958) for the localized and non-localized adsorption, which of these models best fits the experimental results. For CO_2 they found that a localized model

was in best agreement with the results; with SF_6, NH_3 and CH_4 they found that a non-localized model was in better agreement. However, this sort of treatment is open to question since one of the parameters used (the average area occupied by a single molecule) was determined on a semi-empirical basis and it is a well known result in adsorption work that obtaining fair agreement of the theoretical result with the experimental result is not conclusive evidence as to the reality of the model used, since an entirely different model may also give similar results. The whole problem of differentiating between localized and non-localized adsorption by means of the adsorption isotherm is extremely difficult. The main reasons for these difficulties arise from the relatively simple form of the adsorption isotherm. Unlike, say, emission spectra where the very complexity of the experimental results makes it easy to differentiate between the predictions of various models. There must therefore still be considerable doubt as to the true state of the adsorbed molecules.

Surface area results

The infinity form of the B.E.T. equation can be put

$$V = \frac{V_m a P}{(P^0-P)(1-(a-1)P/P_0)} \tag{62}$$

where V is the volume adsorbed in cc at N.T.P. at the pressure P cm of mercury at a temperature when the saturation vapour pressure is P^0 cm of mercury, and where a is a constant. The above equation is generally rearranged to the form

$$\frac{P}{V(P^0-P)} = \frac{1}{V_m a} + \frac{a-1}{V_m a} P/P^0 \tag{63}$$

Hence a plot of $P/V(P^0-P)$ against P^0/P should give a straight line of slope $a-1/V_m a$ and intercept $1/V_m a$.

Equation (63) should be quite universal and not dependent on the type of adsorption isotherms. Brunauer (1940) has calculated B.E.T. plots for a large variety of isotherms and found quite reasonable agreement, but it is now generally accepted that the B.E.T. equation gives its most reliable results with type II isotherms and large a values.

On application of the equation (63) to the adsorption results obtained in this work we find that whilst for argon at 90 ^{0}K and 77.6 ^{0}K we obtain a line in good agreement with the equation up to relative pressures of 0.20, SF_6 gives poor agreement with the equation over the whole range of relative pressure which indicates that the B.E.T. model is quite inadequate even as an empirical relation in this case. This is almost certainly due to the lateral interaction of the large SF_6 molecules with each other, an interaction which is neglected in the derivation of the B.E.T. equation. Some of the results are shown in fig. 39 and 40 and in the table below.

$\sigma\,(90\,^\circ K) = 13.8\,(\mathring{A})^2$

$\sigma\,(77.6\,^\circ K) = 12.8\,(\mathring{A})^2$

TABLE 6.

Sample	Surface area m^2/g	Gas	Temp. ^{0}K
Graphon powder	76.4	Argon	90
graphon powder	72.7	"	77.6
graphon plug	75.7	"	90
Black Pearls powder	190.5	"	90
Black Pearls powder	195.1	"	77.6
Black Pearls plug	193.6	"	90

There is good agreement between the surface area measurements on the plugs and on the powder samples, and because of this we are able with confidence to use isotherms determined on the powder in the calculations involving the plugs.

FIG. 29

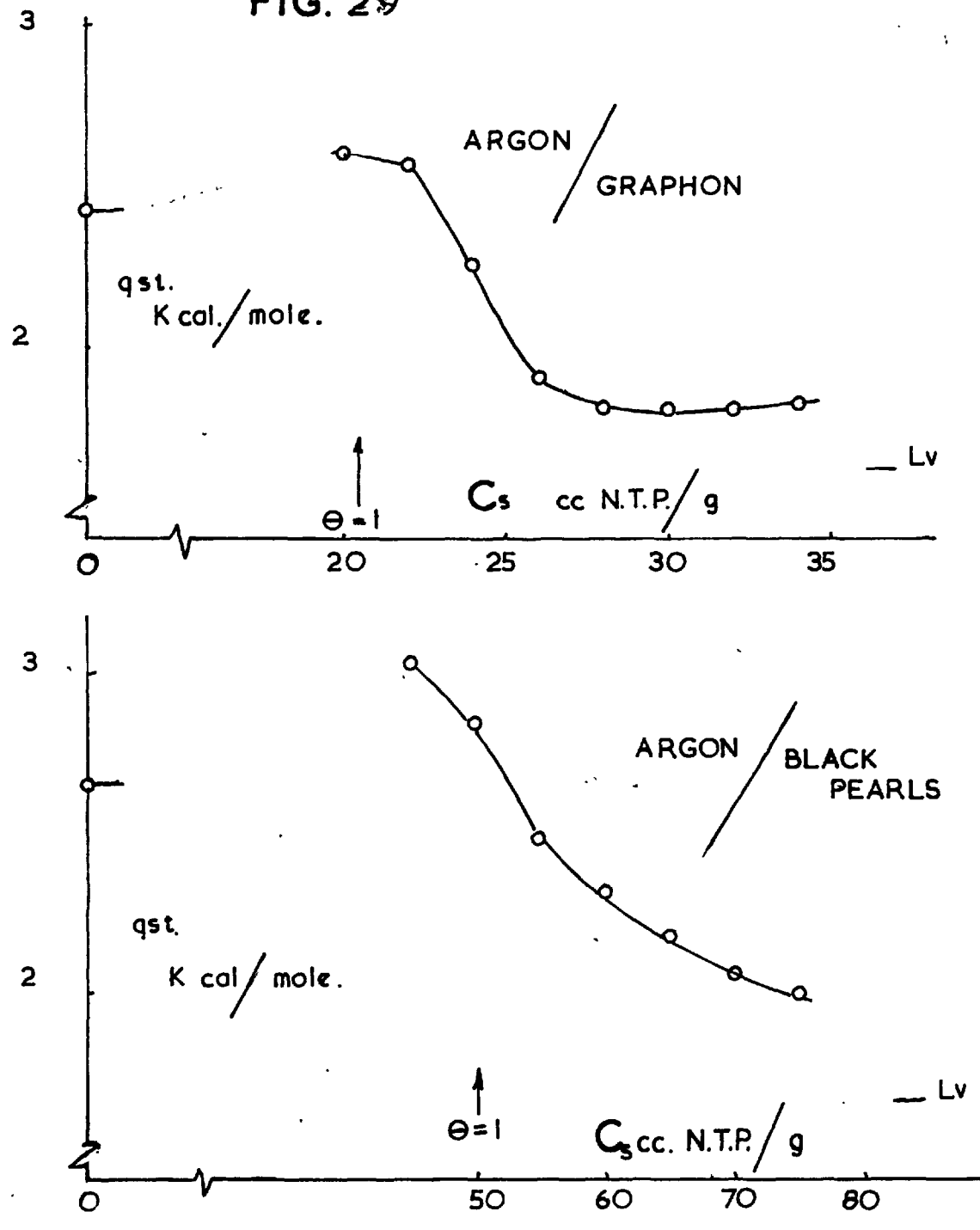
3
2
ARGON
GRAPHON
qst.
K cal./mole.
Lv
θ=1
Cs cc N.T.P./g
0
20
25
30
35
3
2
ARGON
BLACK
PEARLS
qst.
K cal/mole.
Lv
θ=1
Cs cc. N.T.P./g
0
50
60
70
80

FIG. 30

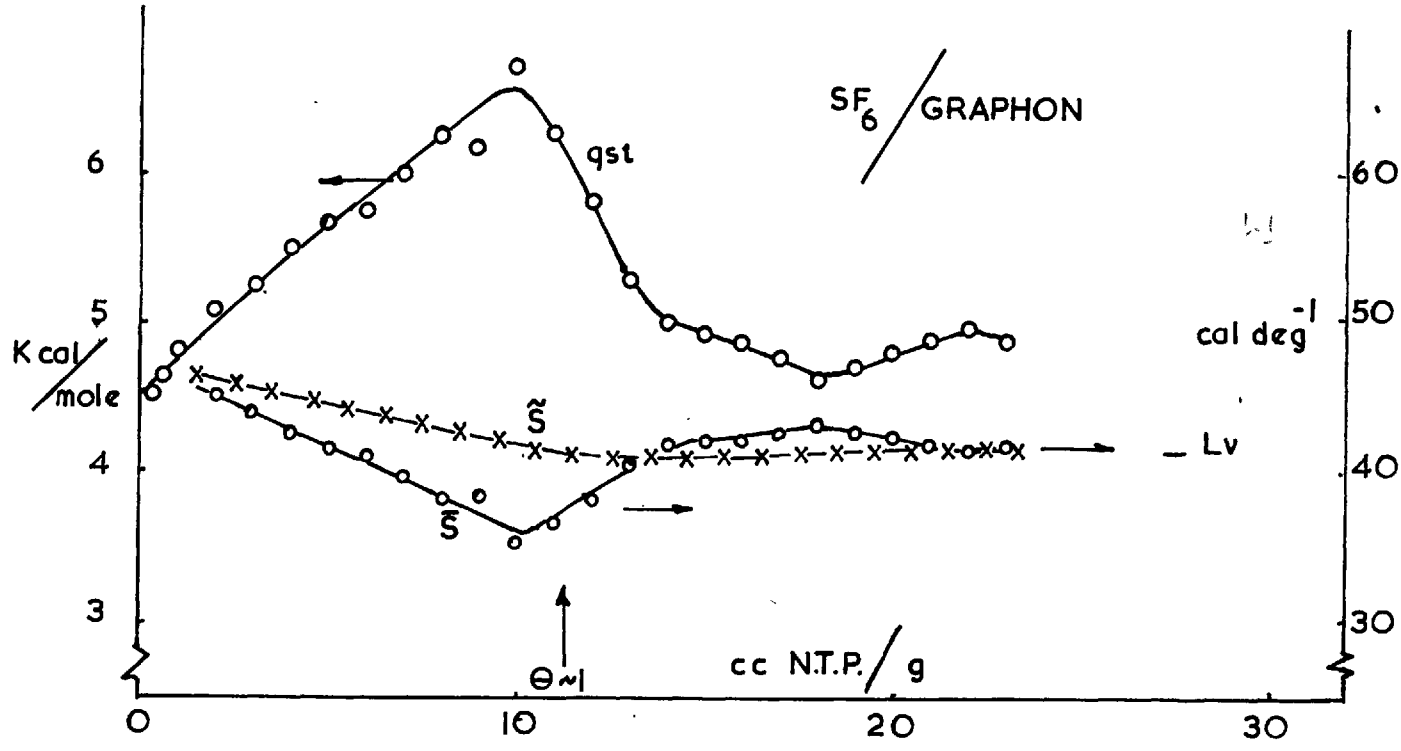
SF6 / GRAPHON
qst
K cal / mole
cal deg-1
Lv
cc N.T.P. / g
θ≈1
0
10
20
30
3
4
5
6
30
40
50
60

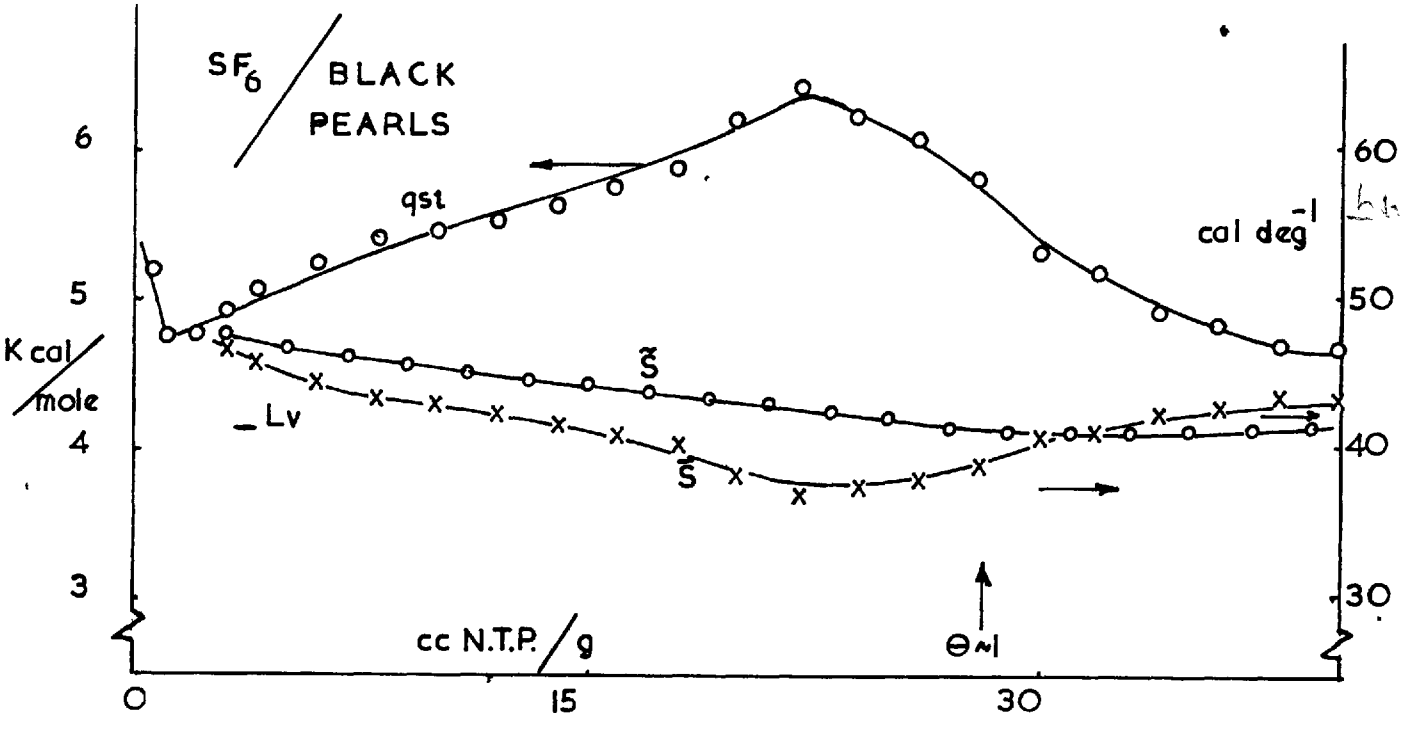
SF6 / BLACK PEARLS
qst
K cal / mole
cal deg-1
Lv
cc N.T.P. / g
θ≈1
0
15
30
3
4
5
6
30
40
50
60

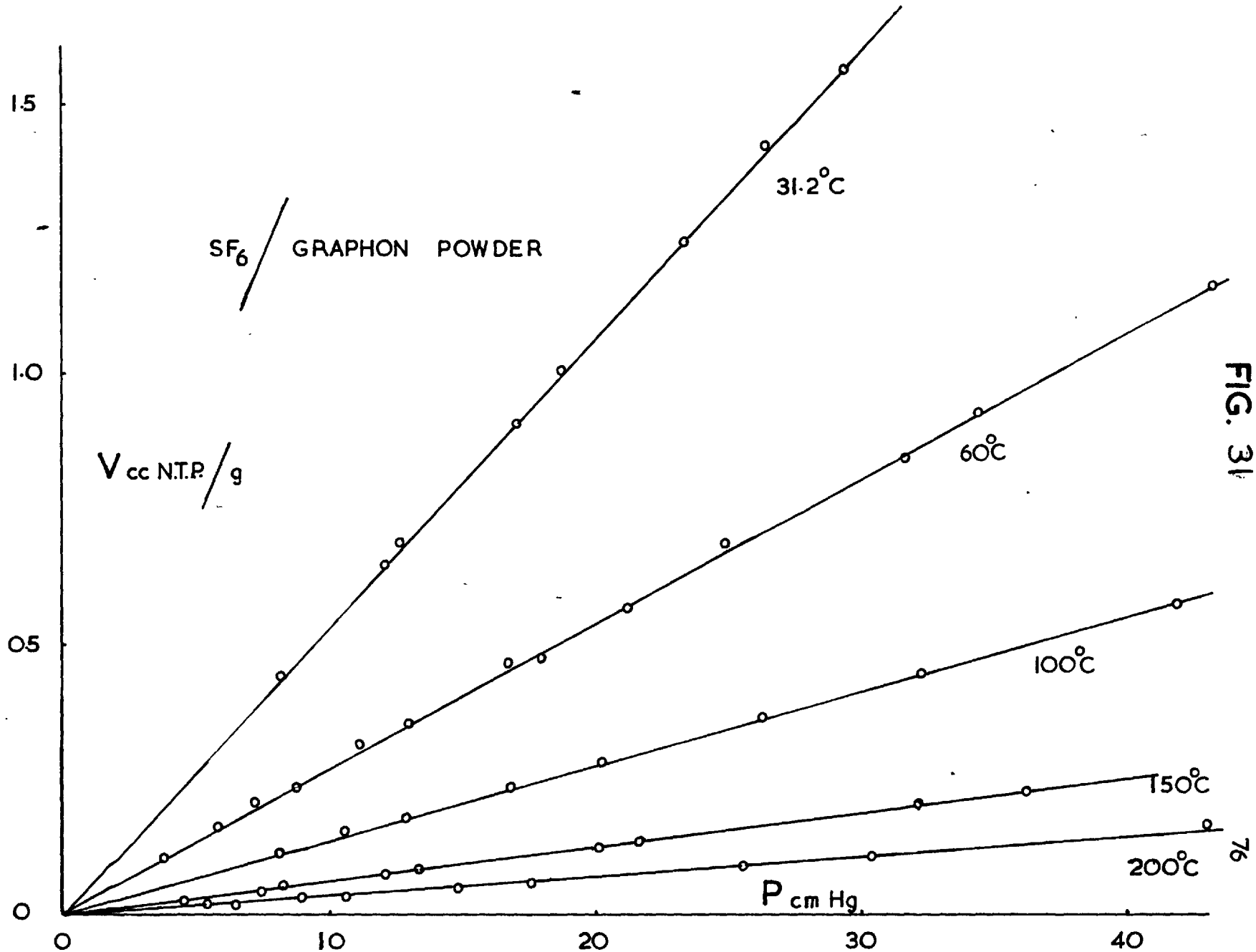
1.5
1.0
0.5
0
0
10
20
30
40
SF6 / GRAPHON POWDER
V cc N.T.P. / g
P cm Hg.
31.2°C
60°C
100°C
150°C
200°C

FIG. 31

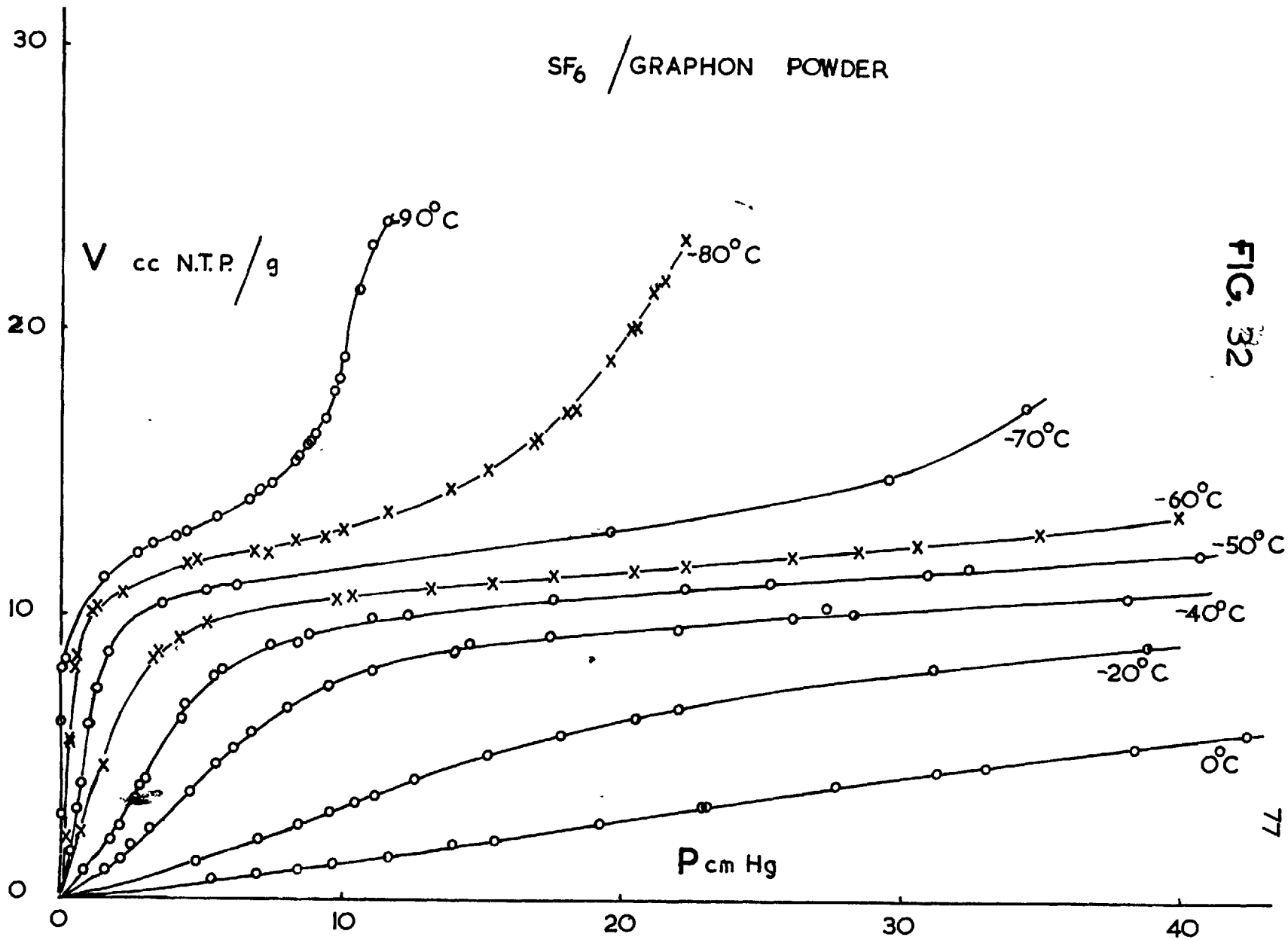
SF6 / GRAPHON POWDER
V cc N.T.P. / g
P cm Hg
-90°C
-80°C
-70°C
-60°C
-50°C
-40°C
-20°C
0°C
0
10
20
30
40

FIG. 32

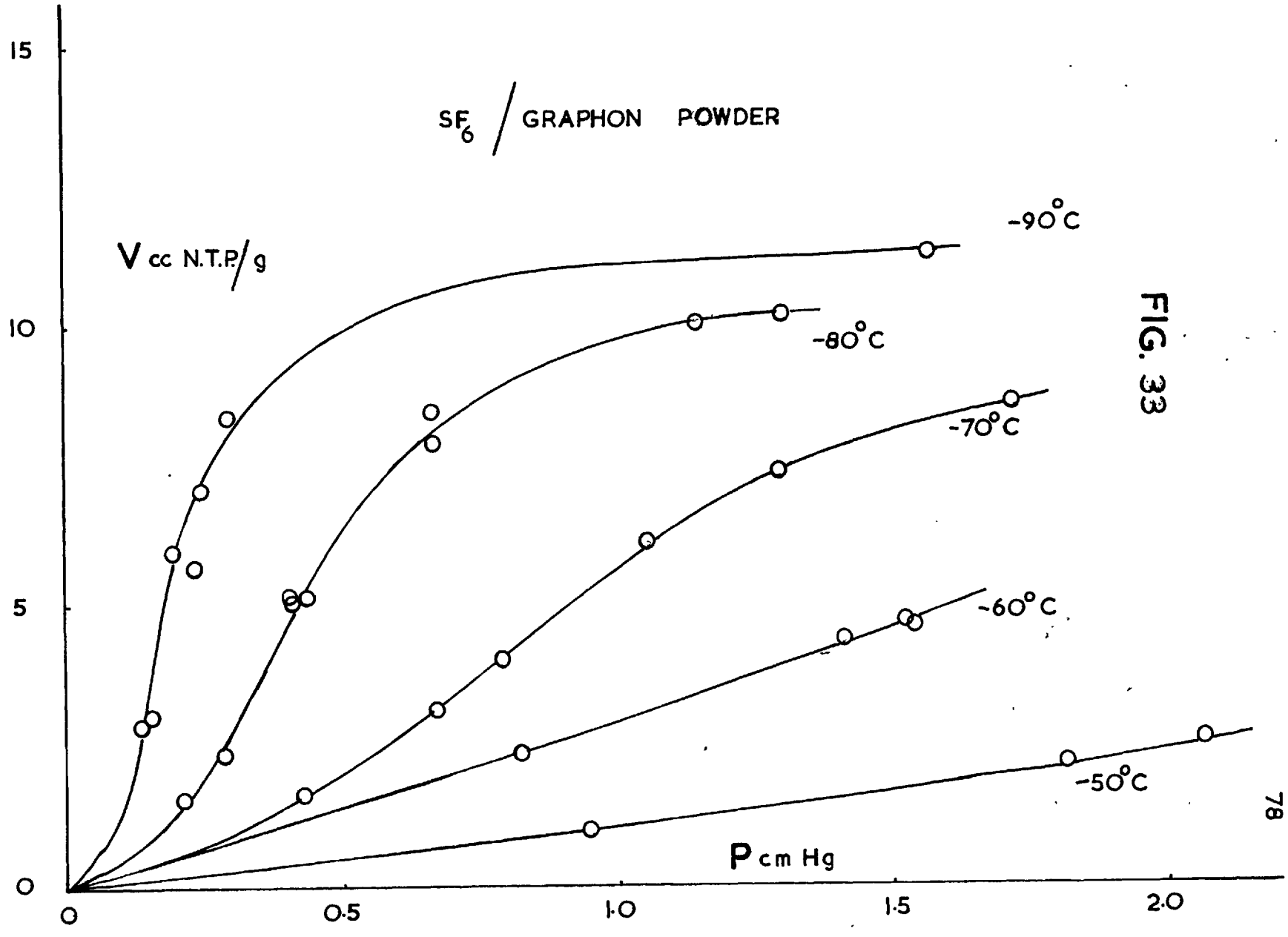
SF6 / GRAPHON POWDER
V cc N.T.P./g
P cm Hg
-90°C
-80°C
-70°C
-60°C
-50°C
15
10
5
0
0
0.5
1.0
1.5
2.0

FIG. 33

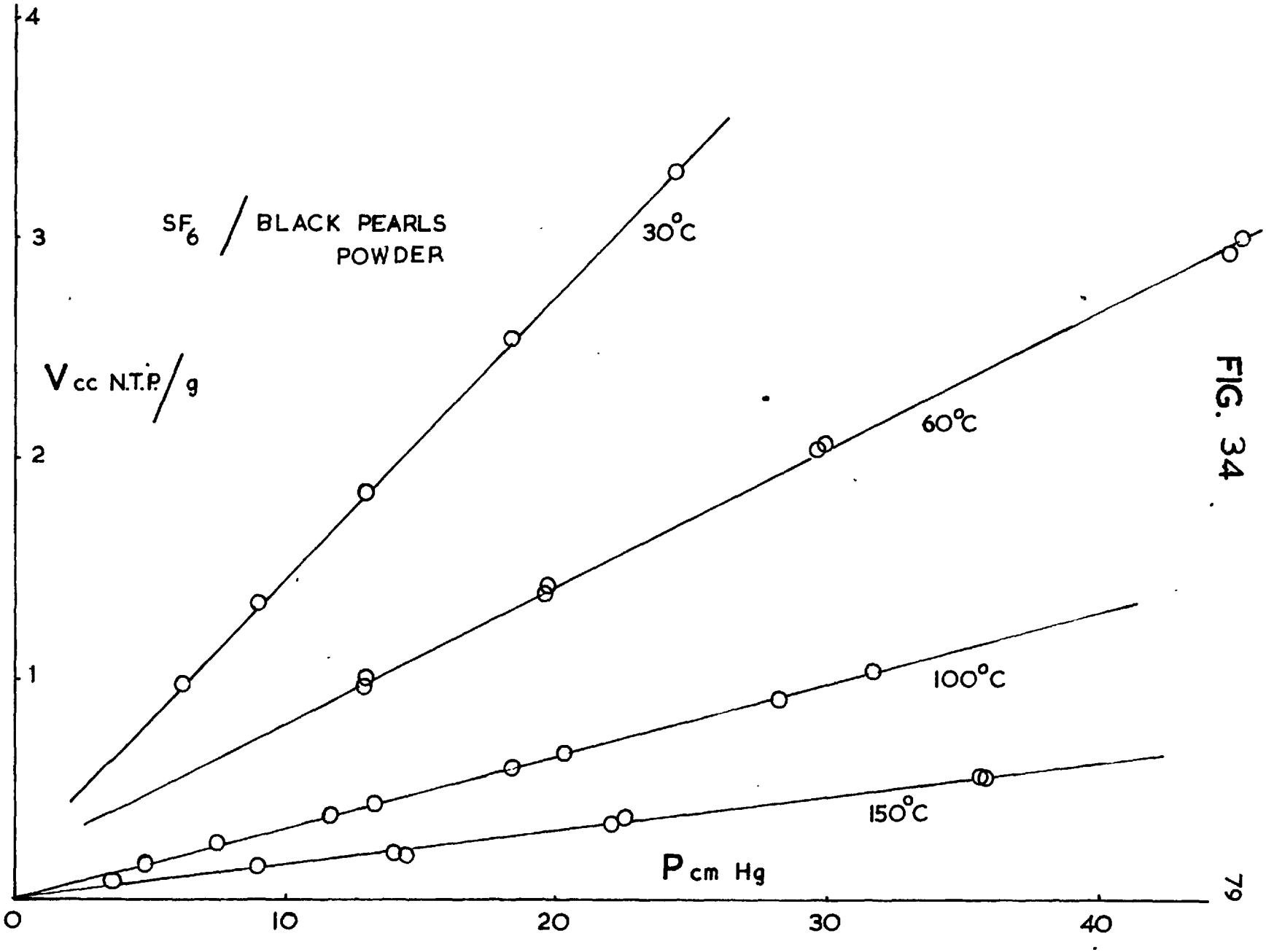
4
3
2
1
0
10
20
30
40
SF6 / BLACK PEARLS POWDER
30°C
60°C
100°C
150°C
V cc N.T.P./g
P cm Hg

FIG. 34

FIG. 35

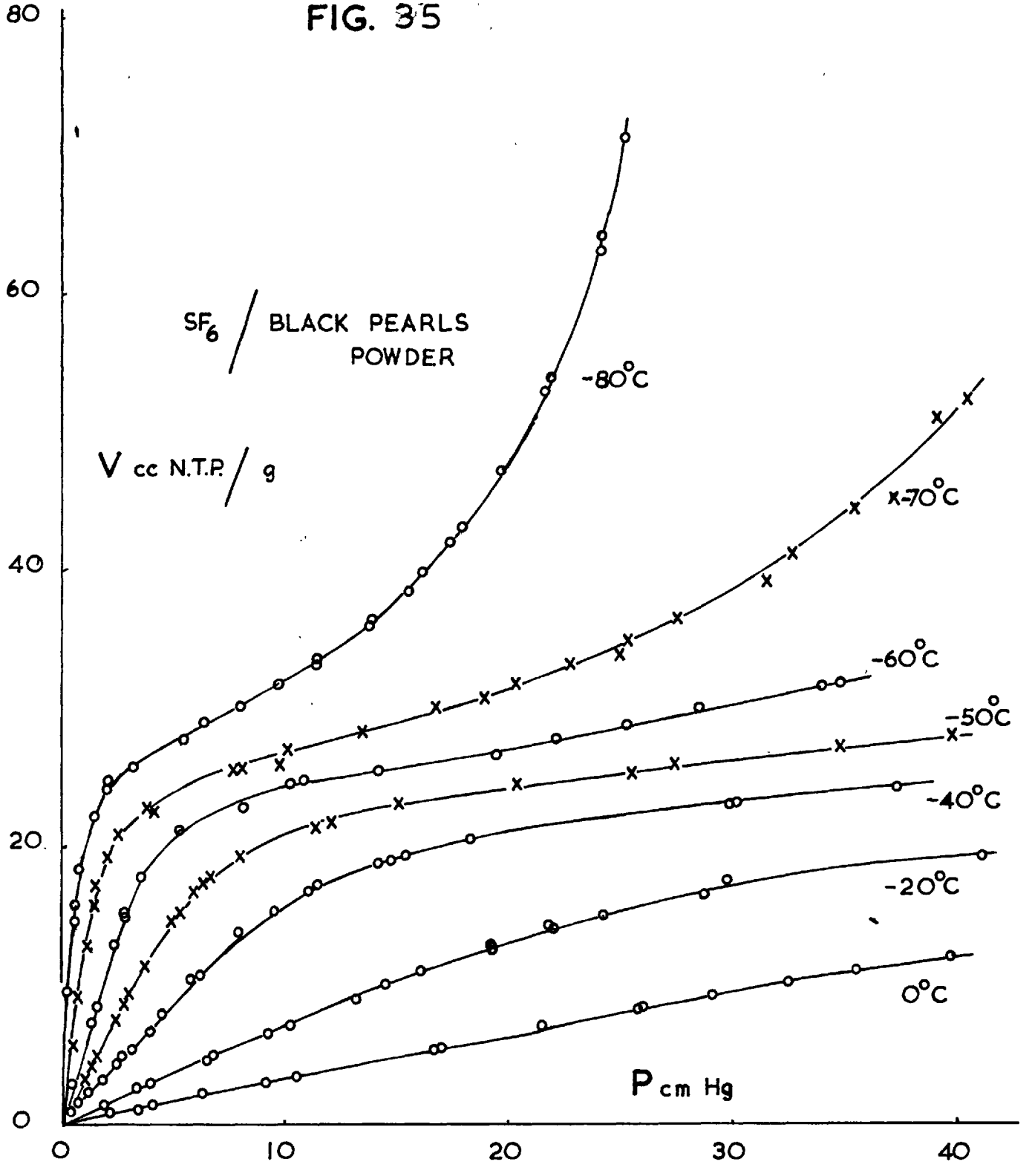
80
60
40
20
0
SF6 / BLACK PEARLS POWDER
V cc N.T.P. / g
-80°C
-70°C
-60°C
-50°C
-40°C
-20°C
0°C
P cm Hg
0
10
20
30
40

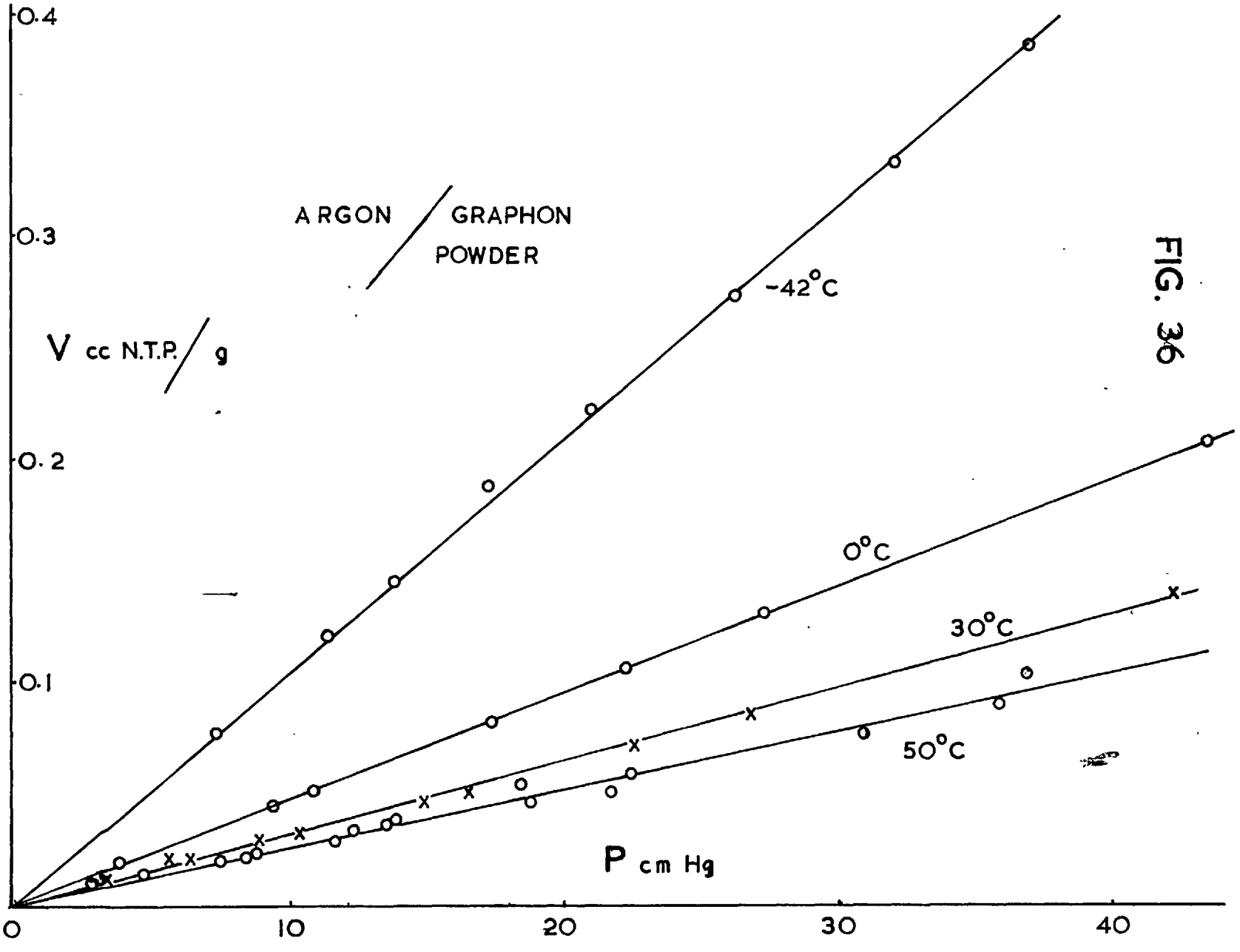
ARGON / GRAPHON POWDER
V cc N.T.P. / g
0·4
0·3
0·2
0·1
-42°C
0°C
30°C
50°C
P cm Hg
0
10
20
30
40

FIG. 36

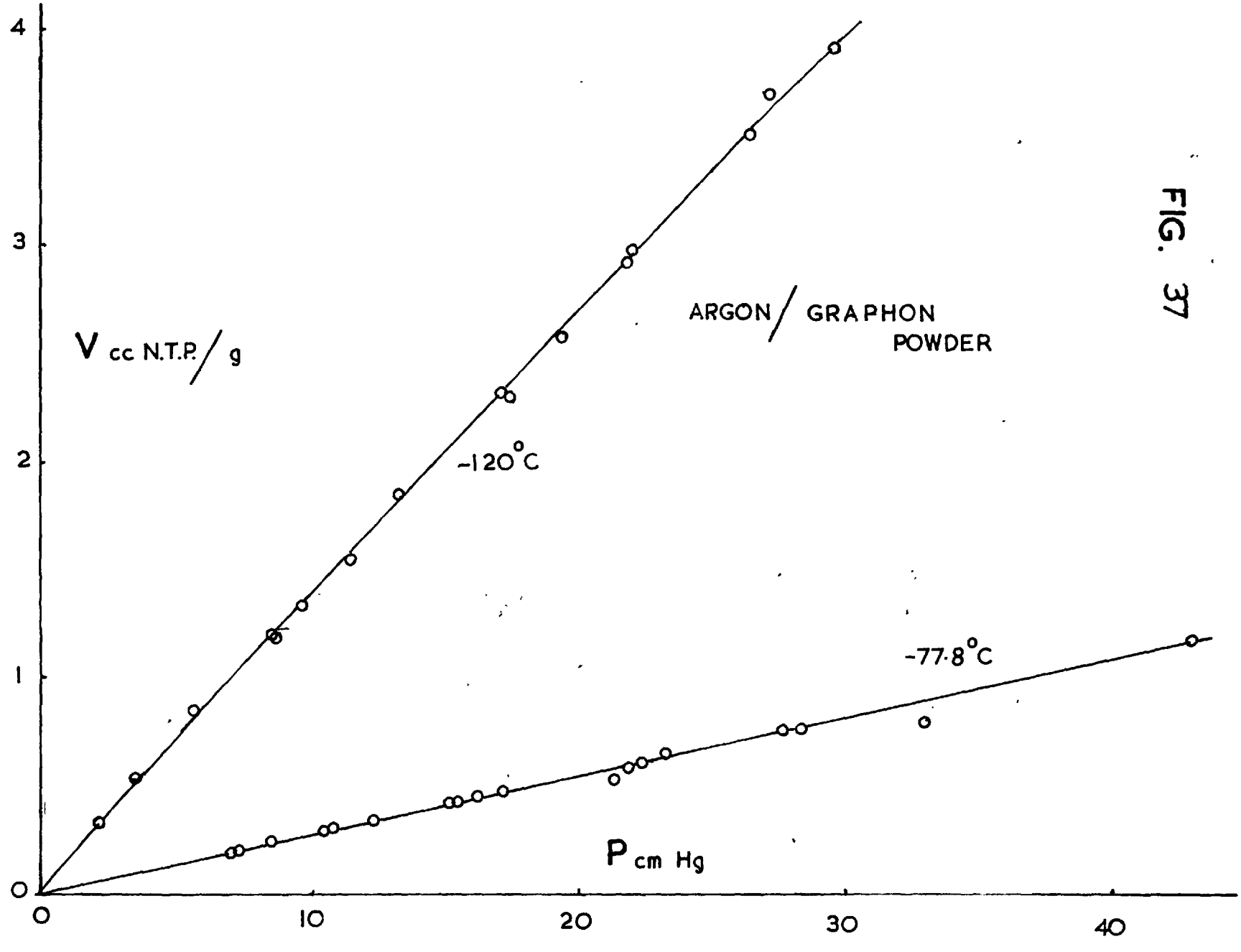
4
3
2
1
0
V cc N.T.P. / g
ARGON / GRAPHON POWDER
-120°C
-77·8°C
P cm Hg
0
10
20
30
40

FIG. 37

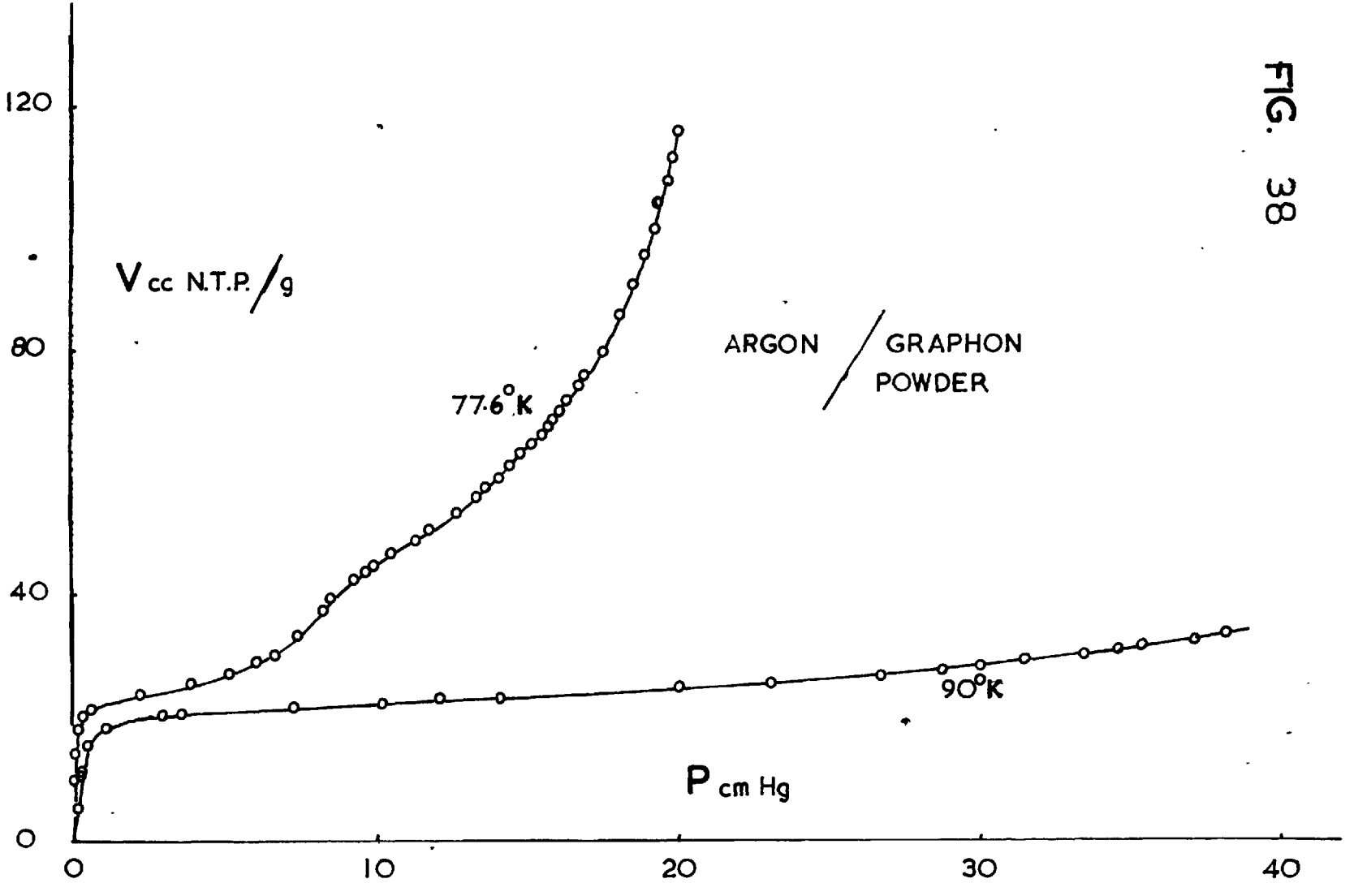
120
80
40
0
V cc N.T.P. / g
77.6°K
ARGON / GRAPHON POWDER
90°K
P cm Hg
0
10
20
30
40

FIG. 38

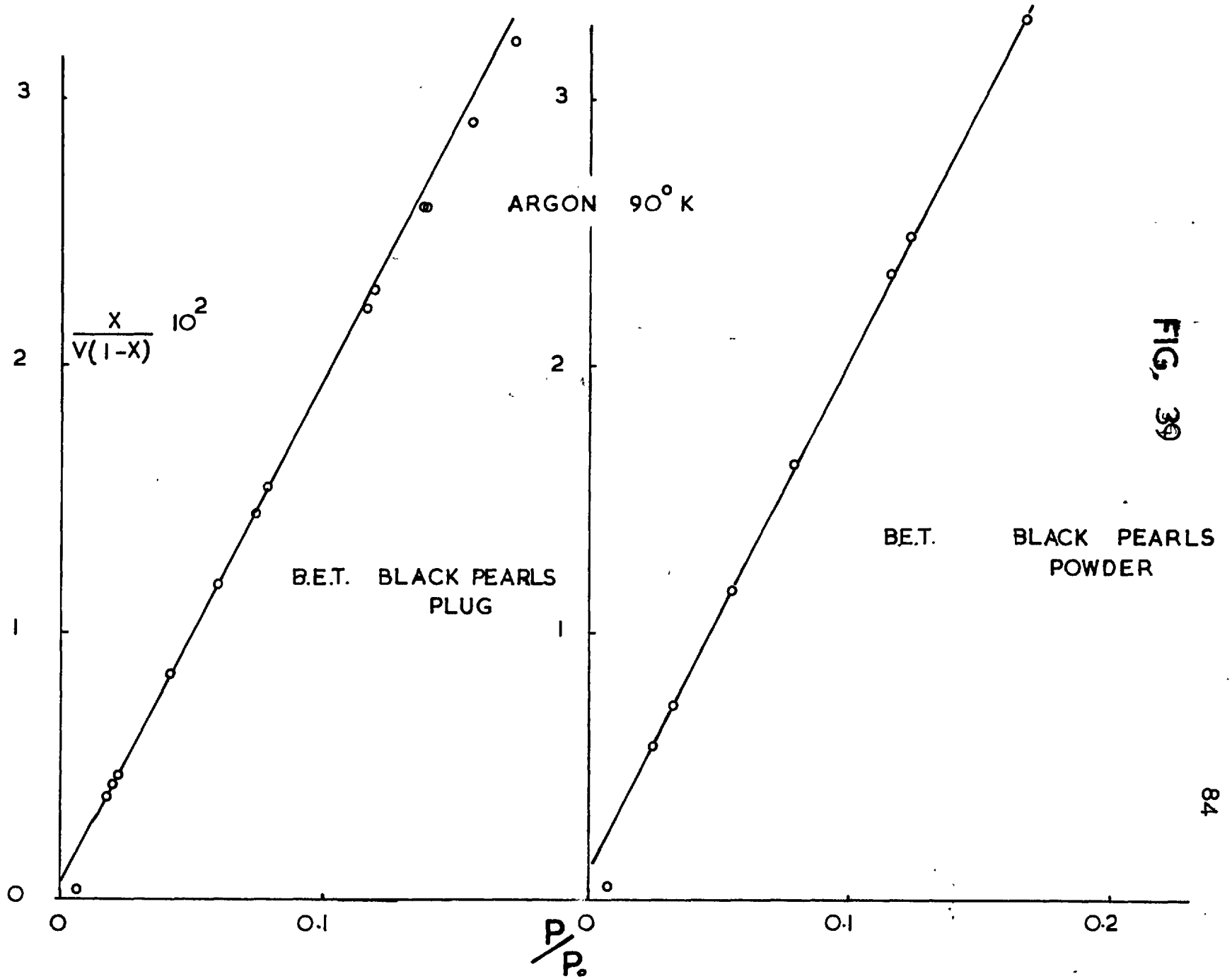
ARGON 90° K
$\frac{X}{V(1-X)}$ 10^2
3
2
1
0
0
0.1
P/P₀
B.E.T. BLACK PEARLS PLUG
B.E.T. BLACK PEARLS POWDER
0.2

FIG. 39

FIG. 40

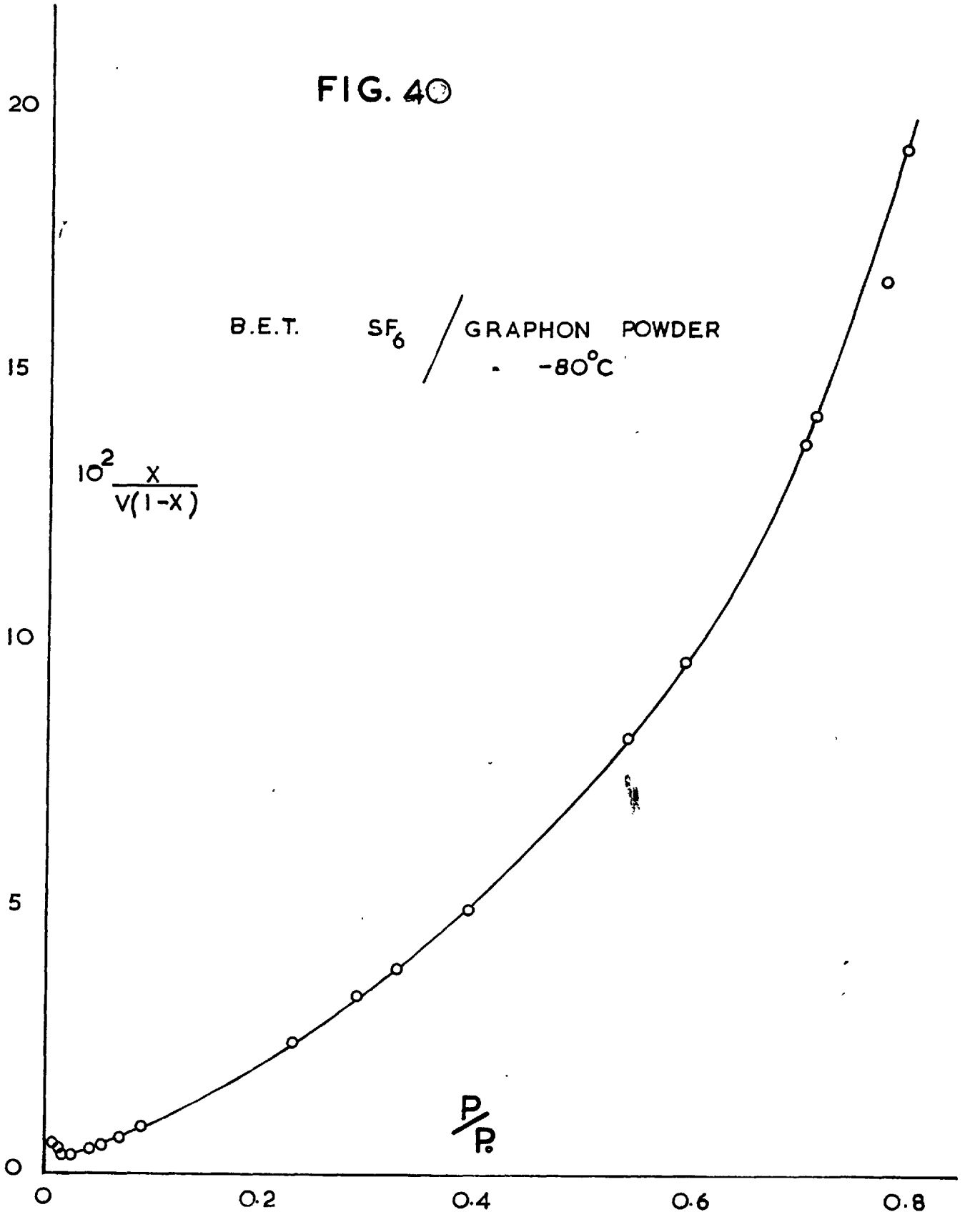
B.E.T. SF_6 / GRAPHON POWDER
- -80°C
$10^2 \frac{X}{V(1-X)}$
20
15
10
5
0
0
0.2
0.4
0.6
0.8
$\frac{P}{P_0}$

IV. DISCUSSION

1. Temperature dependence of J_T

It is instructive to plot J_T against T for constant ingoing pressure. This is done for argon on black pearls and SF_6 on graphon in figs. 41 and 42. The flux rises through a maximum and then falls on progressively decreasing the temperature. This result is a little unexpected at first since the surface concentration at constant pressure is increasing steadily as the temperature falls. The behaviour can be easily explained on looking at the temperature dependence of the surface flux in Fick's first law equation (26). Since surface diffusion is an activated process D_S has the form given in equation (10). In the Henry's Law range the concentration on the surface for a fixed gas-phase concentration is also exponential with temperature with the form

$$C_S = C_S e^{-\overline{\Delta H}/RT} \tag{64}$$

where $\overline{\Delta H}$ is the heat of adsorption. The temperature dependence of J_S in the Henry's Law region is therefore

$$J_S \propto e^{-\frac{(\Delta E^* + \overline{\Delta H})}{RT}} \tag{66}$$

Since $\overline{\Delta H}$ is negative and usually has a larger absolute magnitude than ΔE^*, the overall effect is for J_S to increase with lowering of the temperature . When the adsorption moves out of the Henry's Law region the concentration no longer depends exponentially on temperature and there comes a point when the exponential effect of the diffusion coefficient outweighs the effect of temperature on the surface concentration. Hence J_S falls with decreasing temperature. This is a simplified treatment since we have discussed the temperature effect of C_S and not dC_S/dx which is a more difficult problem. It does, however, indicate the effects present.

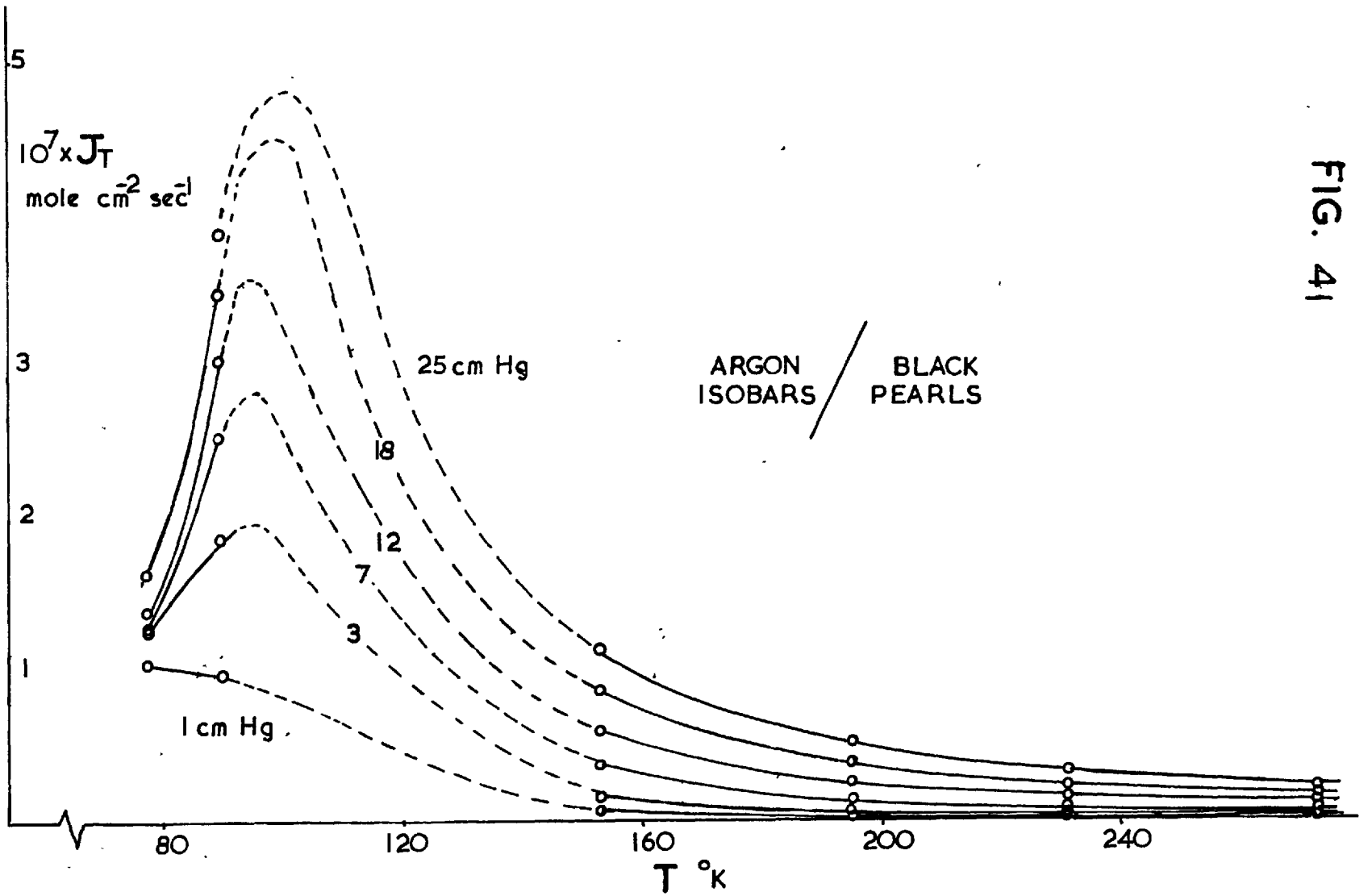
5
3
2
1
$10^7 \times J_T$
mole cm^{-2} sec^{-1}
25 cm Hg
18
12
7
3
1 cm Hg
ARGON ISOBARS
BLACK PEARLS
80
120
160
200
240
T °K

FIG. 41

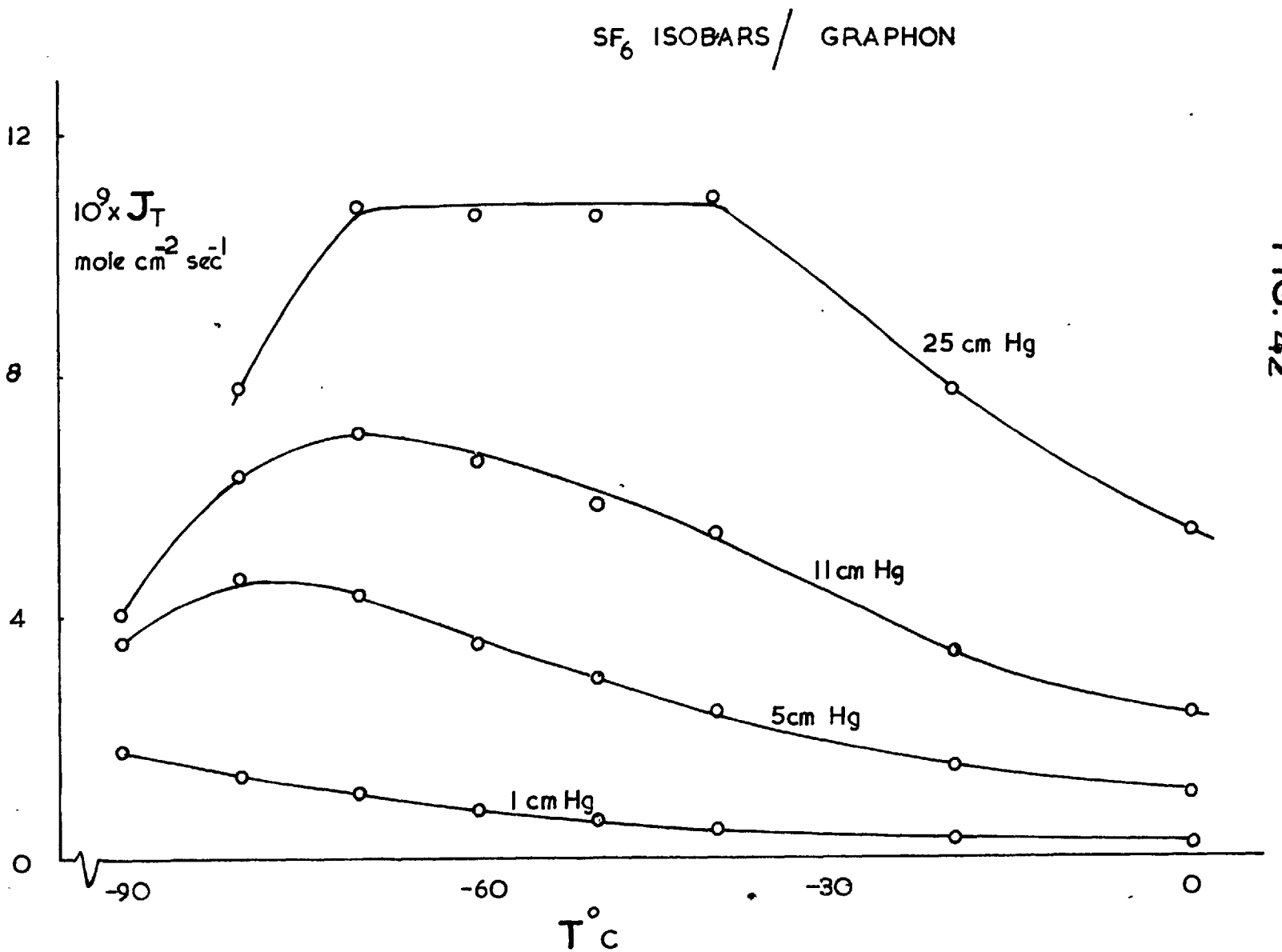
SF6 ISOBARS / GRAPHON
12
8
4
0
10^9 x J_T
mole cm^-2 sec^-1
25 cm Hg
11 cm Hg
5cm Hg
1 cm Hg
-90
-60
-30
0
T°C

FIG. 42

2. Pressure dependence of L and K

That the time lag becomes pressure dependent before the permeability on progressively lowering the temperature has been observed several times in the past as well as in the present work. The reasons for this behaviour have not been clearly apparent before. By using equation (44) we are now able to explain this behaviour simply.

From equation (44) we see that K will be independent of pressure (or C'_g/RT) so long as

$$\left(\frac{dJ_T}{dC'^{0}_g}\right) = \left(\frac{J_T^{*}}{\ell}\right)\left(\frac{dC'_g}{dx}\right)^{-1} \qquad (44)$$

$$= \text{a const}$$

This means that even though the experiments may be outside the Henry's Law range so long as the gas-phase concentration gradient, dC'_g/dx, is a constant, then K will not be pressure dependent.

For L to be independent of pressure it is necessary that the denominator in the Frisch equation (53) varies in the same way as the numerator. The numerator contains the term C the total concentration, whilst the denominator is

$$\int_0^{C^{0*}} D\,dc = J_T \cdot \ell = KC'^{0*}_g .$$

Hence L will be a constant so long as K or dC'_g/dx is a constant and the medium is also in the Henry's Law range. Thus there are generally two conditions for constancy of L whilst for K to be independent of C'^{0}_g only dC'_g/dx must be a constant. In general therefore L will become pressure dependent before K on progressively lowering the temperature.

3. Effect of surface character on the rate of surface diffusion

The Fick's law equation (26) can be rearranged to the form

$$\frac{J_S}{A} = - D_S \cdot \frac{dC_s'}{dx} \qquad (67)$$

If we consider a section of cross-sectional area 1 sq cm and Δx thick, then the total surface area contained in this slice is

$$\frac{\Delta x}{1} \cdot A$$

but if Δx is made very small indeed then the area contained in the slice is also equal to $\gamma \cdot \Delta x$ where γ is the length of the periphery of the pores per sq cm of an x plane. Hence $J_S/\gamma = J_S/A$ = flux crossing per sec across a line 1 cm in length drawn normal to x. The gradient across this line will be dC_s'/dx.

The surface diffusion coefficient of a gas on a series of substances is therefore a measure of the surface flow across a line 1 cm in length drawn normal to x in each surface when there is the unit surface concentration gradient across the surface. In Table 7 are collected a series of results for argon at approximately 300 ^{0}K on different substances. The results of different authors on the same substance vary widely depending on the porosity and other factors but even allowing for this and the slightly different temperatures of the experiments it can be seen that the magnitudes of the values of D_S are in the order (highest to lowest) graphon, black pearls, carbolac, alumina-silica cracking catalyst and Vycor porous glass. The surface diffusion coefficients of graphon and black pearls in particular are very much larger than any of the others.

These results are almost certainly due as was suggested by Barrer and Gabor (1960) to the relative roughnesses of the surfaces. Graphon, and to a slightly lesser extent, blackpearls, are known to have an extremely smooth crystalline nature on which long diffusion paths of the adsorbed molecules would be possible

before they are forced to become completely desorbed. Carbolac has a much more broken surface and hence the average lengths of the surface diffusion paths would tend to be much shorter. Alumina-silica cracking catalyst has an even more broken surface and here the lengths of the surface paths would be very short. The reason for the low value of D_S for Vycor porous glass is probably not due to the roughness of the surface but more to the nature of the pore structure. It has been suggested by Barrer and Gabor from the diffusion results, and by Voigt and Tomlinson (1955) from the adsorption results, that Vycor glass consists of large blind pores connected by small through channels. Hence the amount of the surface being used for surface flow in the steady state is probably much smaller than the value given in table 7, which is obtained from a B.E.T. plot. This will lead to a low D_S value.

More evidence that it is surface roughness resulting in shorter surface diffusion paths of the adsorbed molecules which causes the different values of D_S in Table 7 is obtained when we examine the ratio $\Delta E^*/\Delta E$. ΔE^* is the energy of activation given by equation (10) and ΔE is the energy of adsorption. For argon on graphon and black pearls the ratio is 0.54 and 0.56 respectively whilst for Carbolac it is 0.65 (Ash, Barrer and Clint), for cracking catalyst the ratio $\Delta E^*/\Delta E$ has not been determined for argon, but for methane, ethane and propane the very high value of between 0.8 and 1.05 has been obtained (Barrer and Gabor 1959). Hence as the surface diffusion coefficient decreases the energy of activation approaches the energy needed for complete desorption. This result would be expected the more often the surface diffusion paths are interrupted by the need to evaporate in order to cross surface cracks, blind pores, etc. That is, the distance between the point when the molecule first becomes adsorbed and the point when it finally becomes completely desorbed is decreasing due to increasing roughness of the surface, while the proportion of evaporation barriers is increasing.

REF.		A m^2/g	ε cm^3/cm^3	Temp ^oK	$cm \times 10^7$ k_s	$cm^2 sec^{-1} \times 10^3$ K_T	K_g	K_s	10^5 D_s
Barrer & Barrie 1952	Vycor glass	140	0.27	292	4.9	039	0.39	0	0
Barrer & Gabor 1960	Cracking catalyst	500	0.40	303	1.75	0.98	0.82	0.16	17
Ash Barrer & Clint	Carbolac	940	0.48	308	4.0_7	0.82	0.30	0.51	12
Aylmore & Barrer 1966	"	730	0.50	273	8.3_2	1.21	0.44	0.77	10
Barrer & Strachan 1955	"	839	037	298	6.6	2.01	0.86	1.15	16
" " "	"	901	0.64	298	5.0	7.7	5.6	2.1	54
Ash Barrer & Pope 1963	"	370	0.50	273	4.0_7	3.57	1.46	2.11	120
Author	Black Pearls	194	0.43	303	2.9	4.7	1.8	2.9	560
"	Graphon	76	0.42	303	3.6	7.9	4.8	3.1	980

4. Time-lag discussion

The use of equation (45) and (53) to calculate L has already been discussed in the theoretical section. Since this allows much more accurate and simple determinations of L than previous methods of calculation it was used for as many experimental results as were obtainable from the literature.

The results appear to fall into two main categories. Firstly, one may consider the results obtained when there are very large surface flows. In this category the agreement between L_{expt} and L_{calc} using equation (53) is generally good to very good. These results include the results of Ash, Barrer and Pope (1963) on Carbolac using SO_2 (fig. 43 and 44) and the very low temperature results using N_2 and Ar (fig. 45 and 46) and also the results of the author with Ar on graphon and black pearls (fig. 47). The second category comprises results obtained when an appreciable quantity of the flow was in the gas phase. This category includes the results of Ash, Barrer and Clint (see Table 8) and also the results of Ash, Barrer and Pope for CO_2 and their results for Ar and N_2 at $-77.8\,^{0}C$ (fig. 48). The results of the author for helium and some of the SF_6 results as well as all the results of Aylmore and Barrer (1966) Table 9, and also the results of Ash, Barrer and Logan fall in this class of results (fig. 49). In this second category the low surface flow results, the agreement is not as good as in the first category and generally the calculated result using equation (53) is larger than the experimental.

Let us consider the Frisch method and see how it applies to porous media. Frisch defines a quantity q(t) (the amount of diffusant leaving the medium per second at time t) hence

$$q(t) = + \left[D \frac{dc}{dx} \right]_{\ell} \qquad (68)$$

Then starting from Fick's second law

TABLE 8

Ash, Barrer and Clint on Carbolac plug C

	Temp °K		L_{expt} min	L_{calc} min
He	320		15.1	22.1
	333		14.5	21.8
	353		14.1	21.2
	378		13.4	20.5
Ne	308		39.7	55.5
	320		38.7	54.6
	333		37.0	52.8
	353		35.0	51.3
	378		32.6	48.3
Xe	308		45.1 hr	49.4 hr
	378		21.1	31.4
H_2	308		17.7 min	24.5 min
	320		16.8	23.3
	333		16.2	22.1
	353		15.0	21.2
	378		13.5	19.5
Kr	308	plug D	15.0 hr	22.6 hr
	378		6.1	7.2
He	308		18.8 min	23.7 min
	320		18.4	23.4
	333		17.4	23.0
	353		17.4	23.2
	378		16.3	21.6
CH_4	308		6.6 hr	7.6 hr
Ar	308		3.3	4.2

TABLE 9

Aylmore and Barrer on Carbolac

	Temp ^{0}K	L_{expt} min	L_{calc} min
He	273	8.0	9.3
Ar	273	140	157
Ne	273	125	143
	298	92	107
	323	64	85
Kr	273	720	716
	298	430	445
	323	285	298

TABLE 10

Author's results on black pearls

	Temp ^{0}K	L_{expt} sec	L_{calc} sec
He	323	111	158
Ar	323	422	353
	303	453	435
	273	572	538
	231	893	766
SF_6	523	11.5 min	12.8 min
	473	17.0	14.4
	423	24.0	17.7

TABLE 11

Author's results on graphon

	Temp °K	L_{expt} sec	L_{calc} sec
He	323	37	47
Ar	323	128	136
	303	138	140
	273	167	161
	241	215	188
	195	305	454
SF_6	473	237	238
	423	303	291
	373	429	419
	333	675	571
	303	972	809

FIG. 43

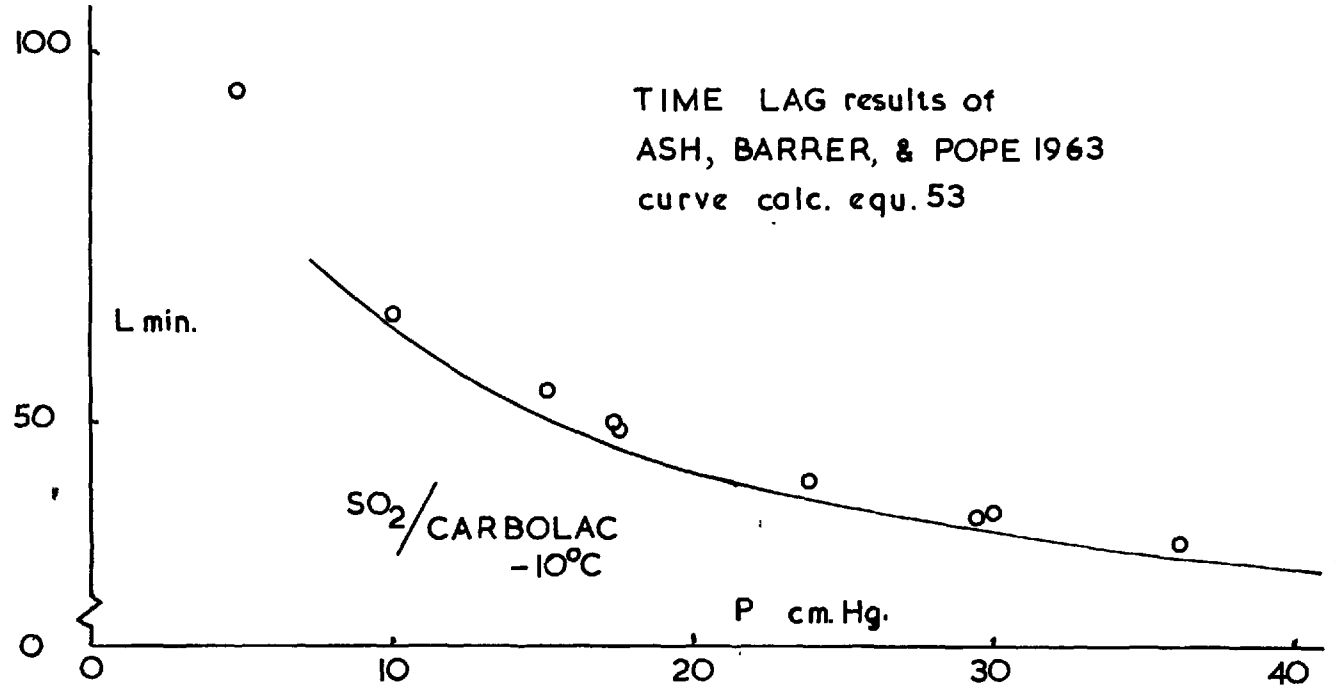
100
50
0
L min.
TIME LAG results of
ASH, BARRER, & POPE 1963
curve calc. equ. 53
SO2/CARBOLAC
-10°C
P cm. Hg.
0
10
20
30
40

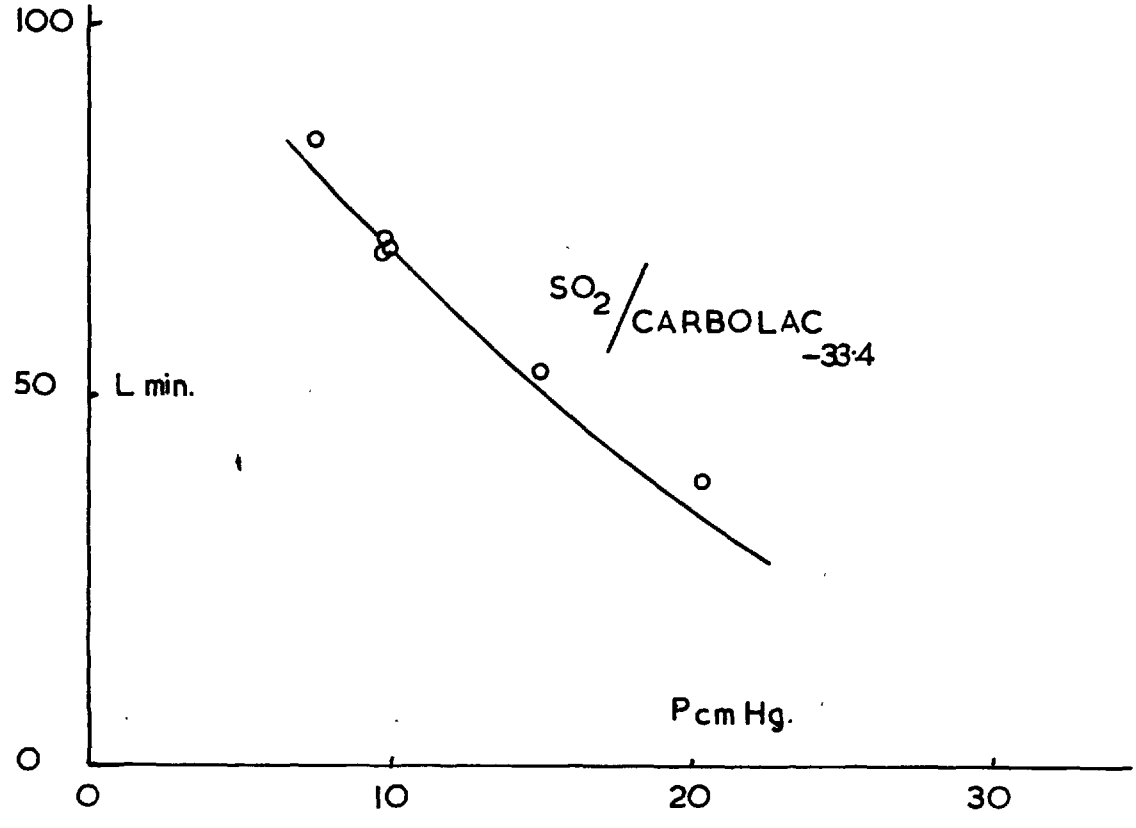
100
50
0
L min.
SO2/CARBOLAC
-33·4
Pcm Hg.
0
10
20
30

FIG. 44.

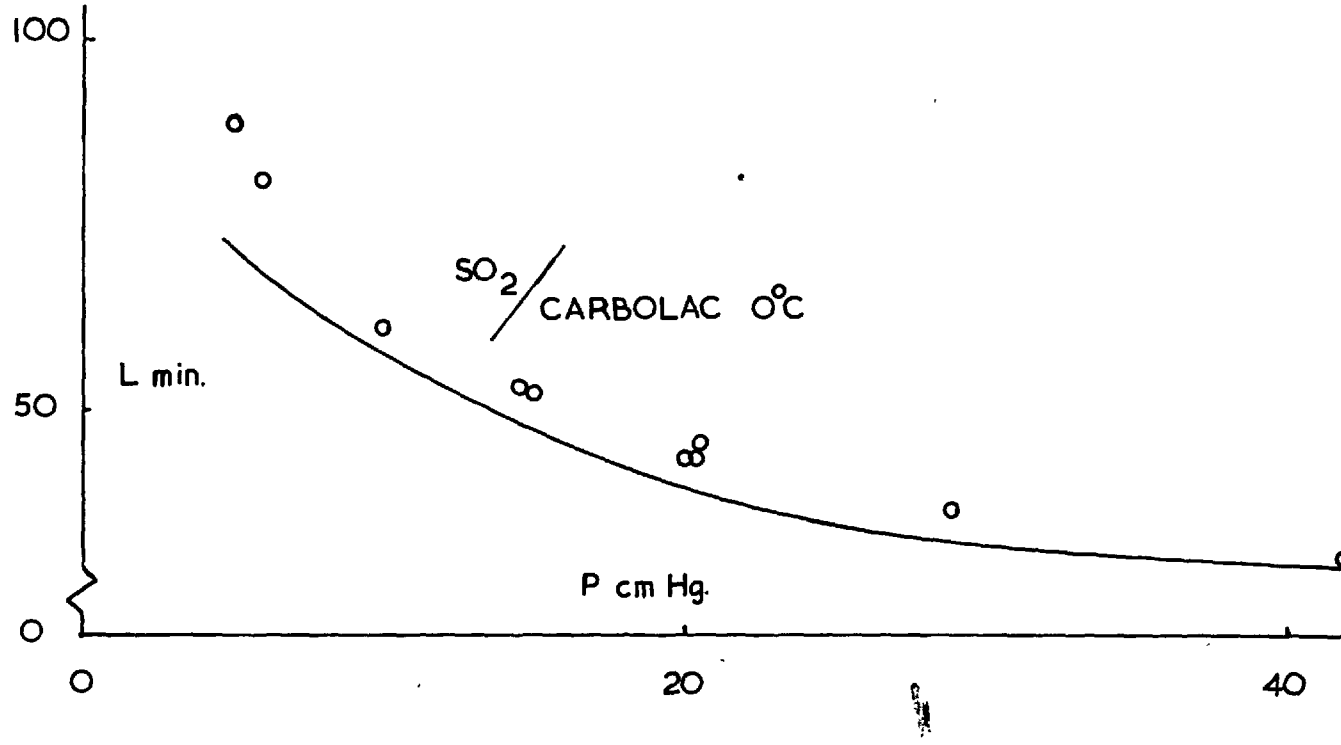
100
50
0
L min.
SO_2 / CARBOLAC 0°C
P cm Hg.
0
20
40

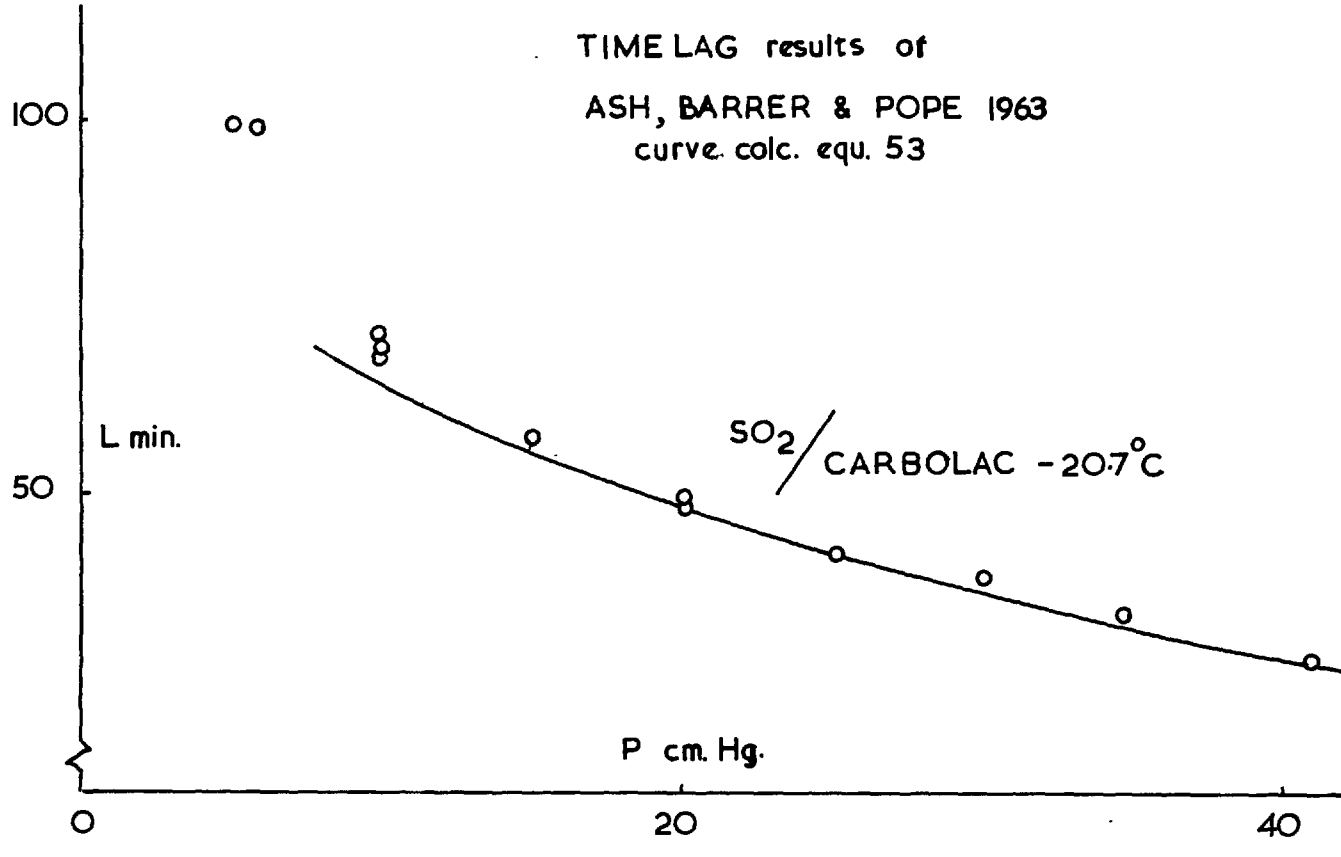
TIME LAG results of
ASH, BARRER & POPE 1963
curve. calc. equ. 53
100
50
L min.
SO_2 / CARBOLAC -20·7°C
P cm. Hg.
0
20
40

FIG. 45.

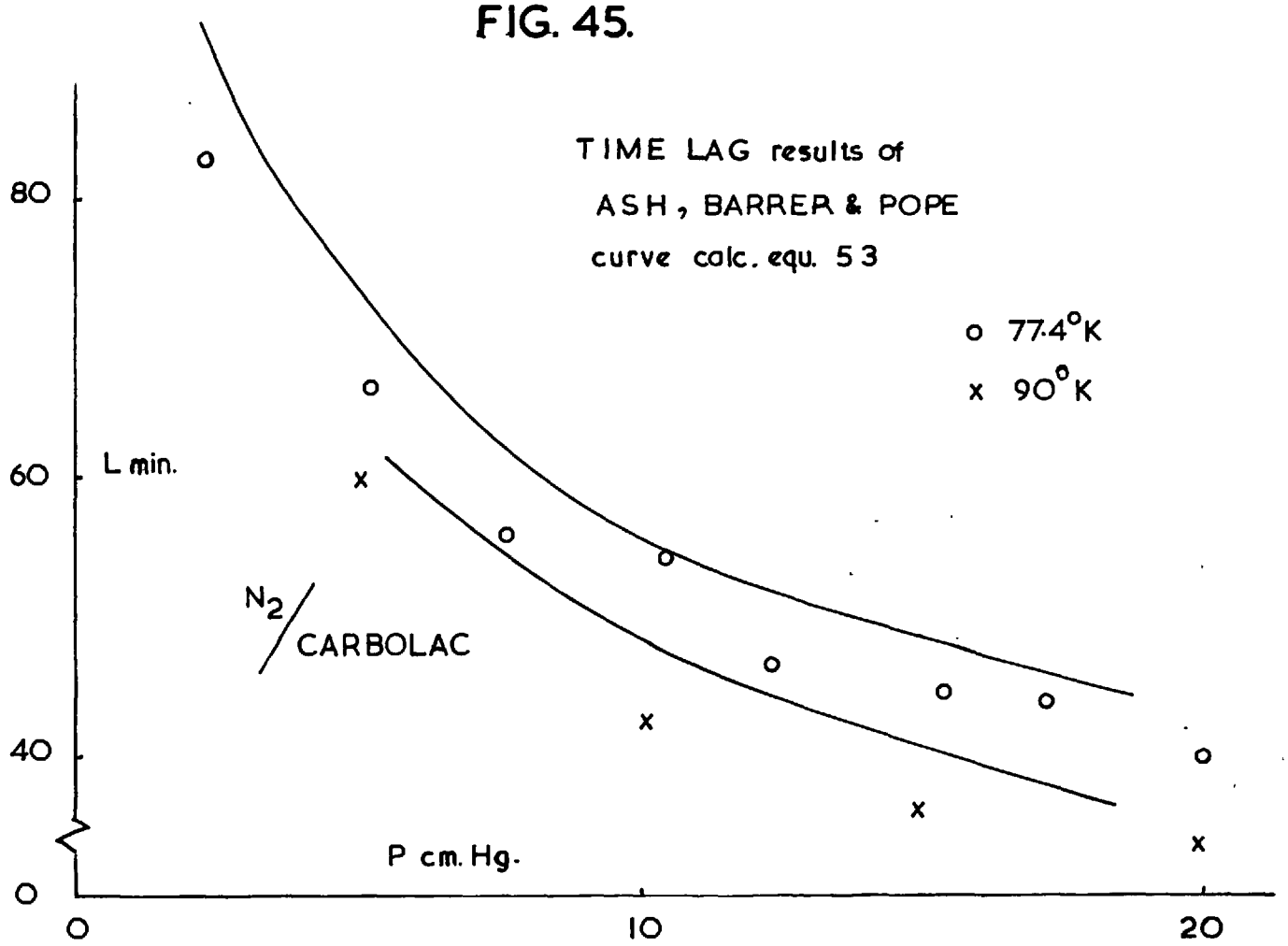
TIME LAG results of
ASH, BARRER & POPE
curve calc. equ. 53
o 77.4°K
x 90°K
L min.
80
60
40
0
N_2 / CARBOLAC
P cm. Hg.
0
10
20

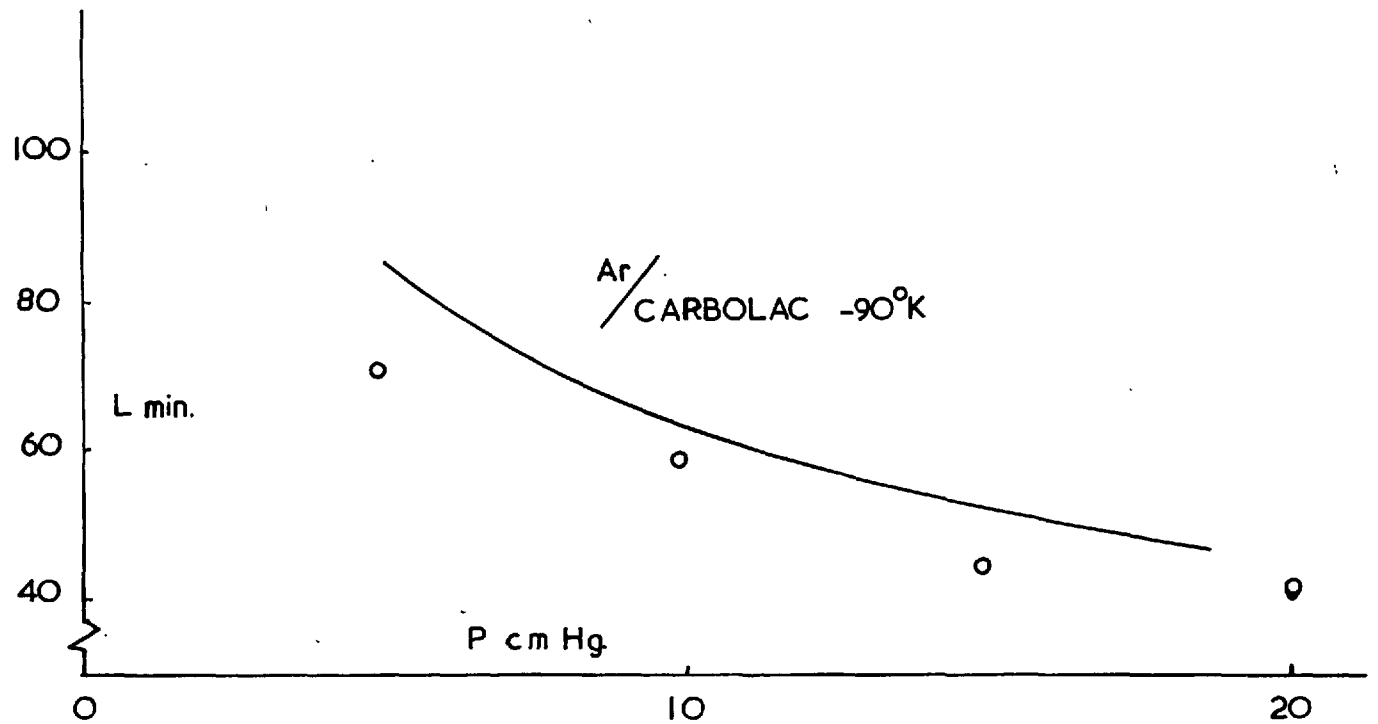
100
80
60
40
L min.
Ar / CARBOLAC -90°K
P cm Hg.
0
10
20

FIG. 46

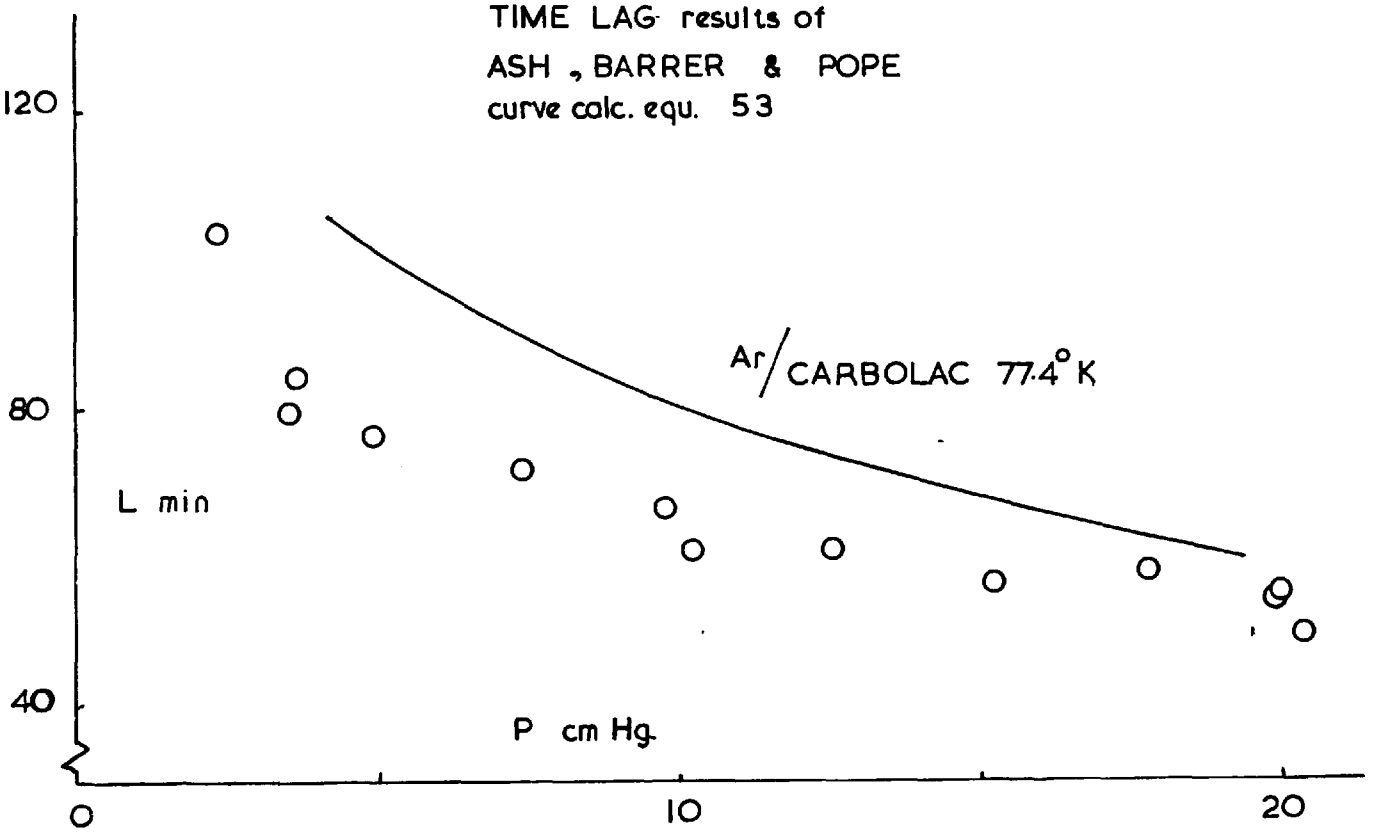
TIME LAG results of
ASH , BARRER & POPE
curve calc. equ. 53
120
80
40
L min
Ar/CARBOLAC 77.4° K
P cm Hg.
0
10
20

FIG. 47

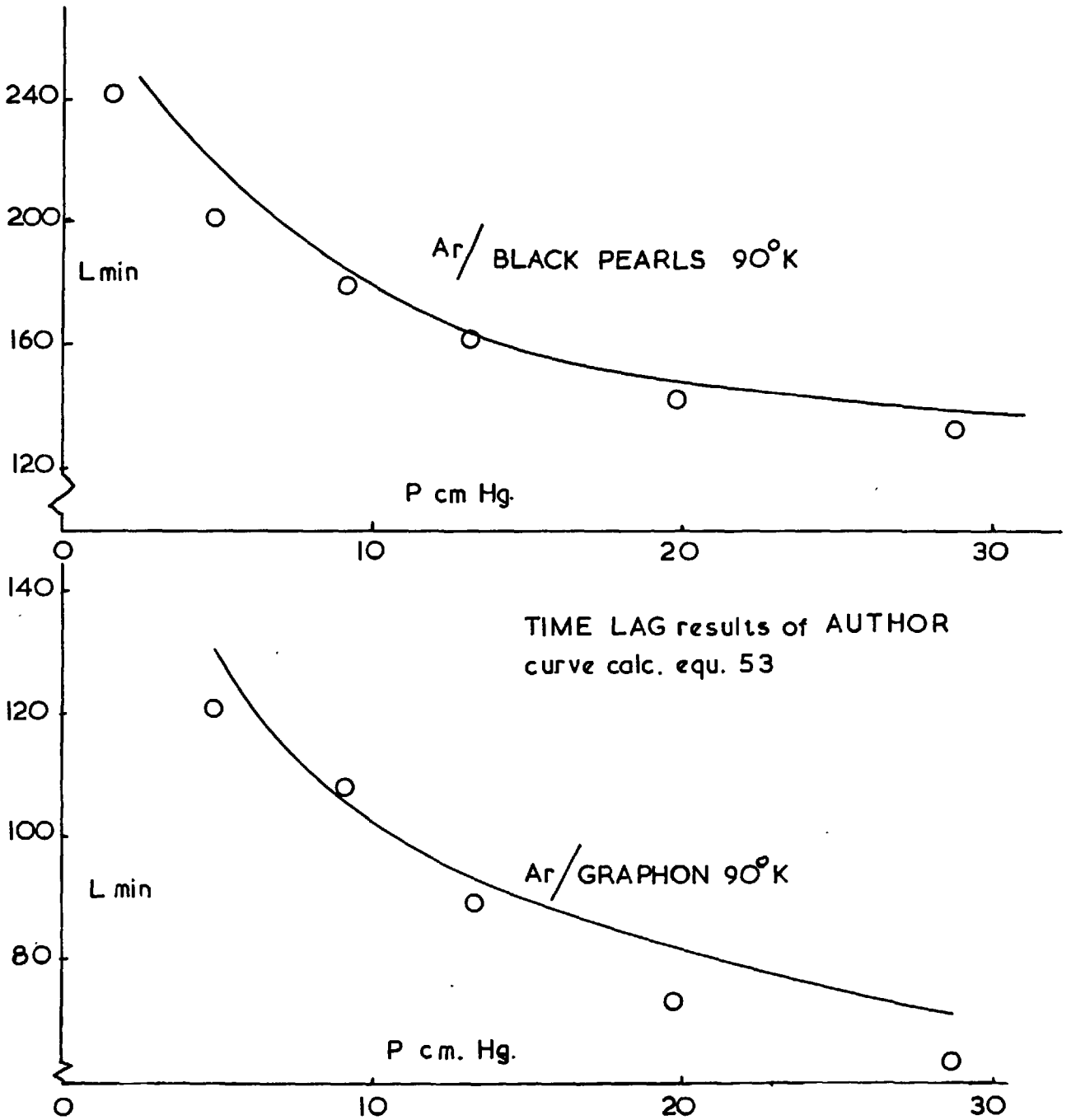
240
200
160
120
L min
Ar/ BLACK PEARLS 90°K
P cm Hg.
0
10
20
30
140
120
100
80
L min
TIME LAG results of AUTHOR
curve calc. equ. 53
Ar/GRAPHON 90°K
P cm. Hg.
0
10
20
30

FIG. 48

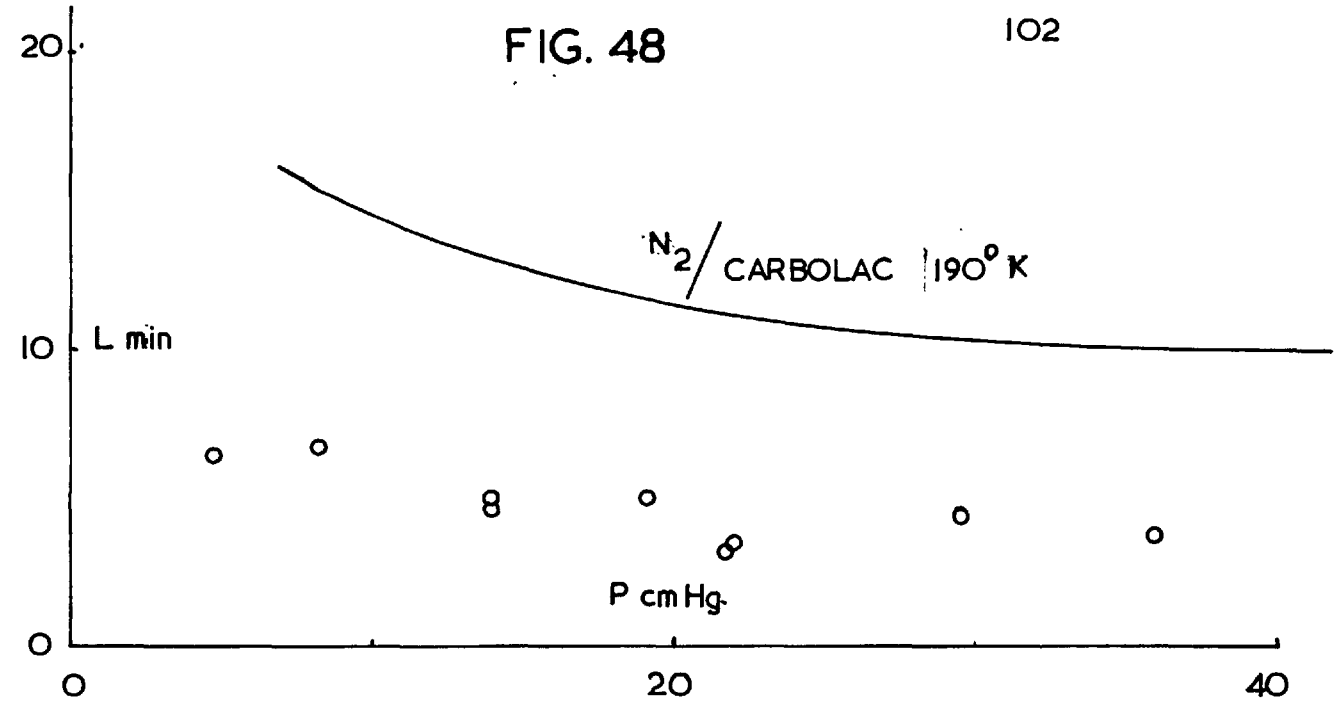
20
10
0
L min
N_2 / CARBOLAC 190° K
8
8
P cm Hg.
0
20
40

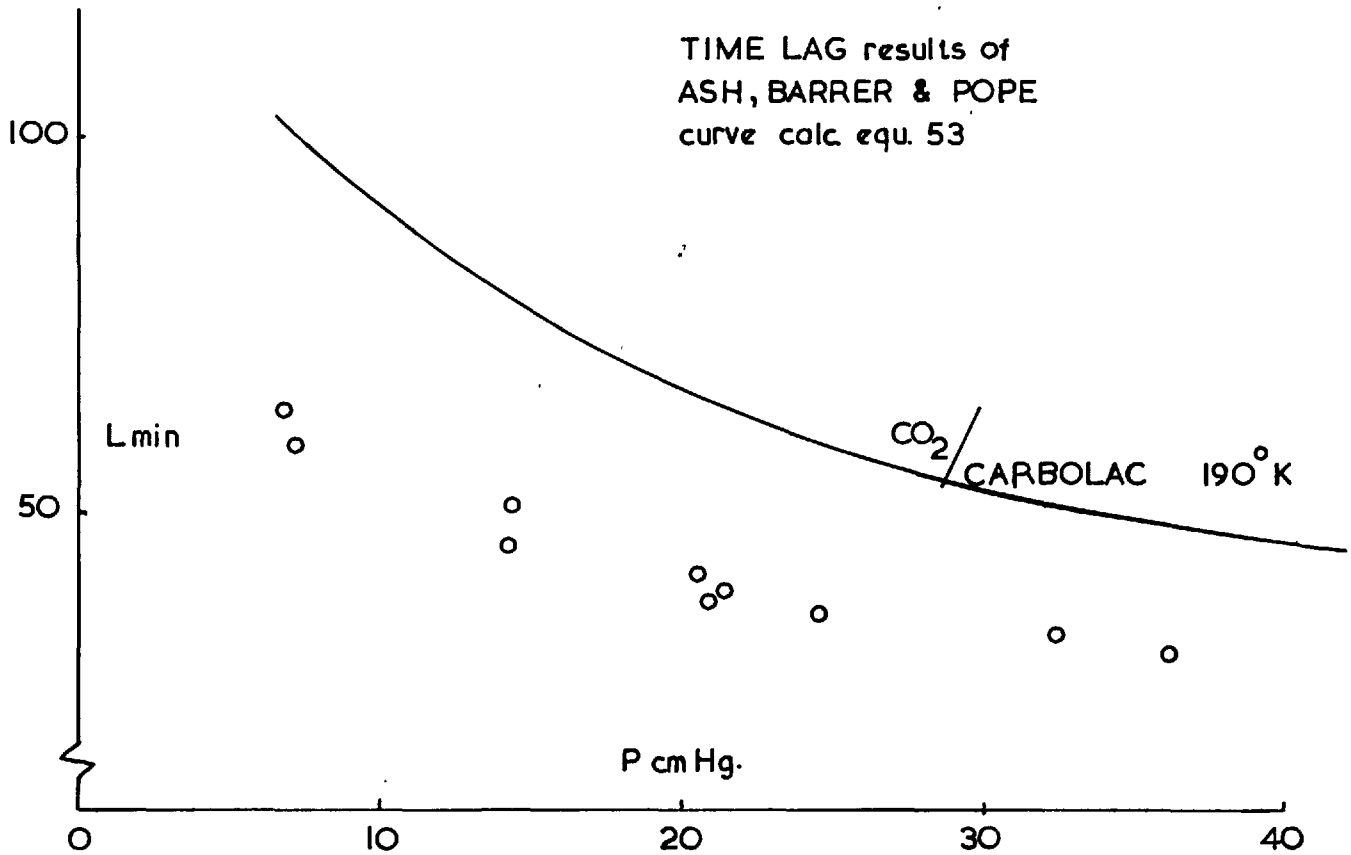
TIME LAG results of
ASH, BARRER & POPE
curve calc. equ. 53
100
50
L min
CO_2 / CARBOLAC 190° K
P cm Hg.
0
10
20
30
40

FIG. 49

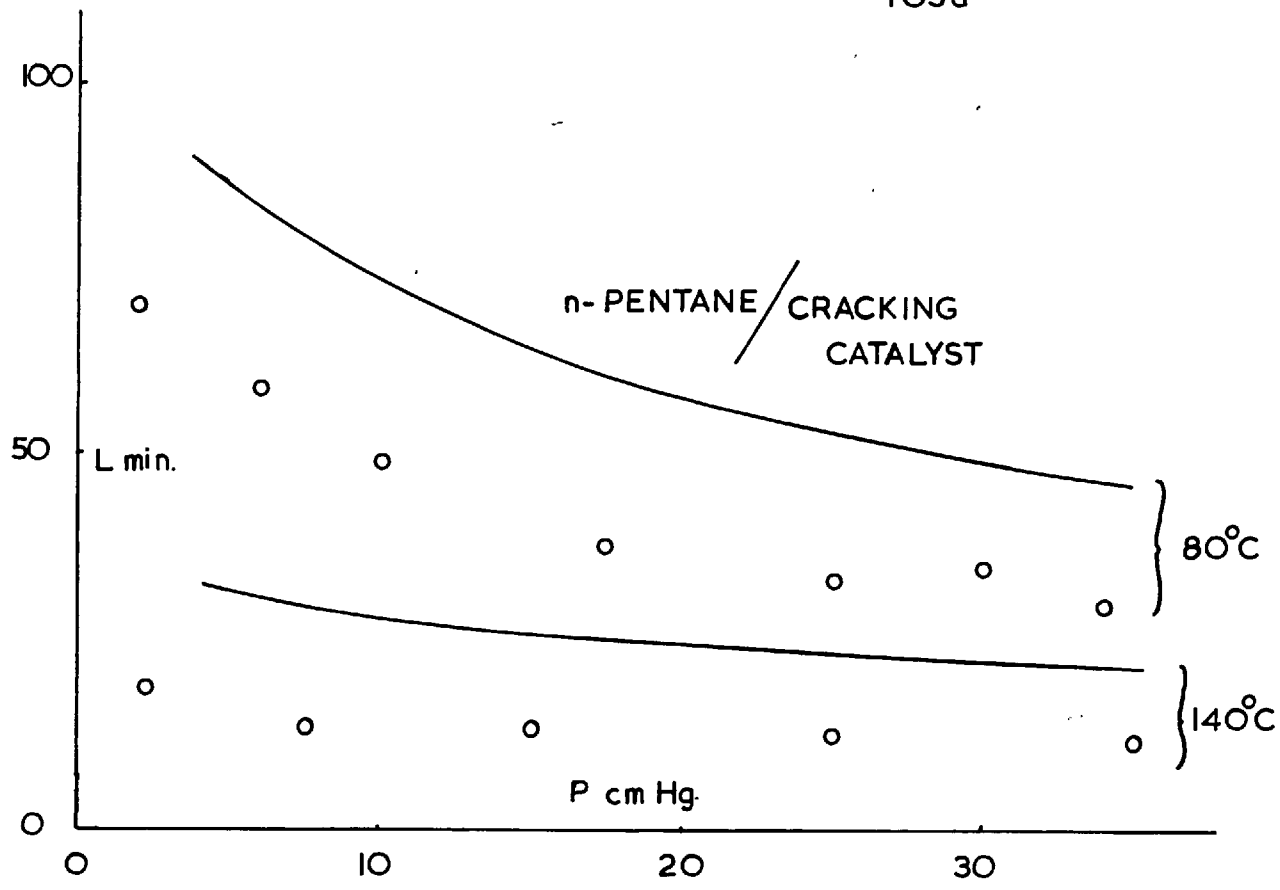
100
50
0
L min.
n-PENTANE / CRACKING CATALYST
80°C
140°C
P cm Hg.
0
10
20
30

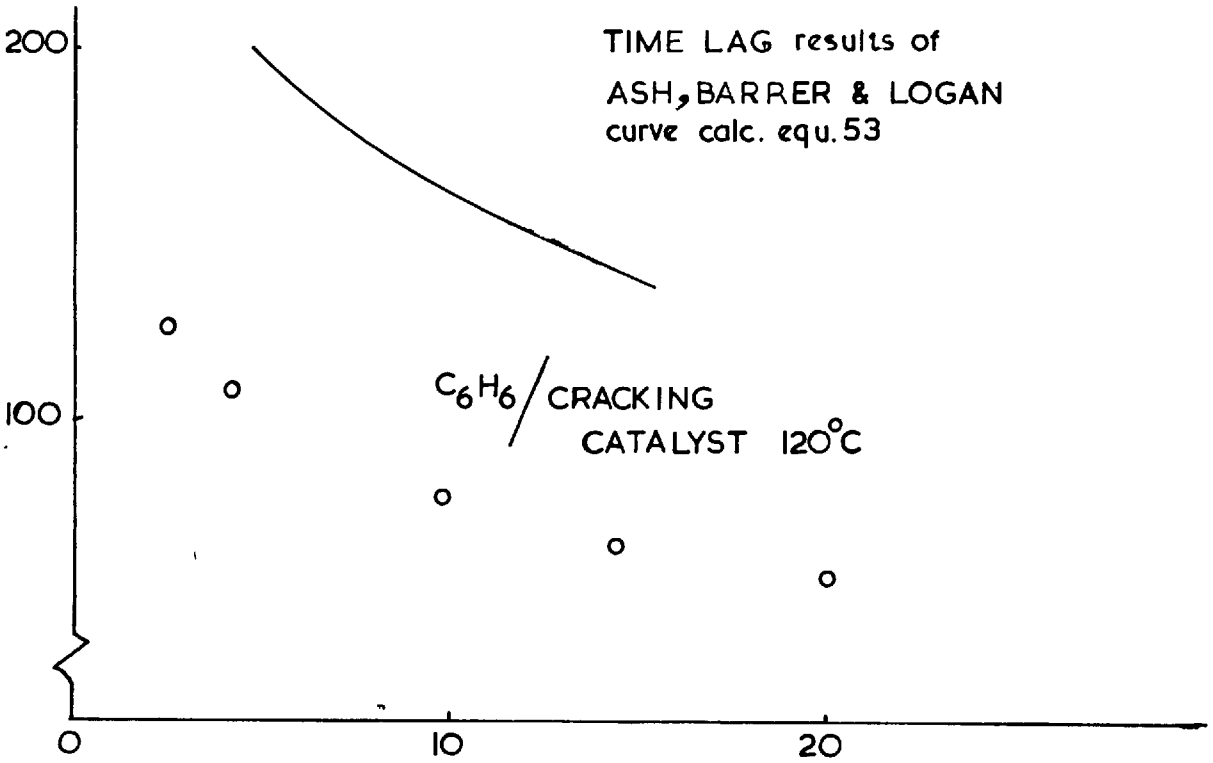
200
100
TIME LAG results of
ASH, BARRER & LOGAN
curve calc. equ. 53
C6H6 / CRACKING
CATALYST 120°C
0
10
20

$$\frac{\partial C}{\partial t} = \frac{\partial}{\partial x}\left[D \frac{\partial C}{\partial x}\right] \qquad - (3)$$

on integration from ℓ to x we arrive at the equation

$$\int_x^{\ell} \frac{\partial C}{\partial t}\, dx - q(t) + D \frac{dC}{dx} = 0 \qquad (69)$$

On integration from ℓ to 0 we then obtain

$$\int_0^{\ell}\int_x^{\ell} \frac{\partial C}{\partial t}\, dxdx - \ell q(t) + \int_0^{\ell} D \frac{dC}{dx}\, dx = 0 \qquad (70)$$

which leads to

$$\int_0^{\ell}\int_x^{\ell} \frac{\partial C}{\partial t}\, dxdx - \ell q(t) - \int_0^{C^{0*}} DdC = 0 \qquad (71)$$

If D is a function of concentration only this leads to equation (53) if D is a function of time asymtotically approaching a steady-state value, D_t, as in some polymers, we may write

$$\int_0^{\ell}\int_x^{\ell} \frac{\partial C}{\partial t}\, dxdx - \ell q(t) - \int_0^{C^{0*}} \left[\partial(Ct) - D_t\right] dC - \int_0^{C^{0*}} D_t\, dC = 0 \qquad (72)$$

which leads to equation (55) (Frisch 1962).

These equations are perfectly applicable to a homogeneous polymer membrane where the gas is dissolved at the ingoing face and transmitted uniformly through the medium to the outgoing face. In this form of medium there are no radial concentration gradients even transiently and surfaces of equal concentration are always normal to the x axis. In a porous medium or in a polymer which is not uniform but consists of two or more phases, this is not the situation. In these cases there are volumes in which there is a concentration gradient and a flow present all the time, and there are also volumes in which there is a flow and a concentration gradient present only in the transient state. These latter volumes are the blind pores.

There have been several treatments of the time lag in porous media, one of the best known of which is that given by Goodnight and Fatt and their co-workers (1960, 1963). Goodnight and Fatt represented a typical section of porous medium, as shown. Hence on this model, per unit cross-section of the porous medium

$$\Delta J_T \cdot \Delta t = - \Delta x . \Delta C \quad ,$$

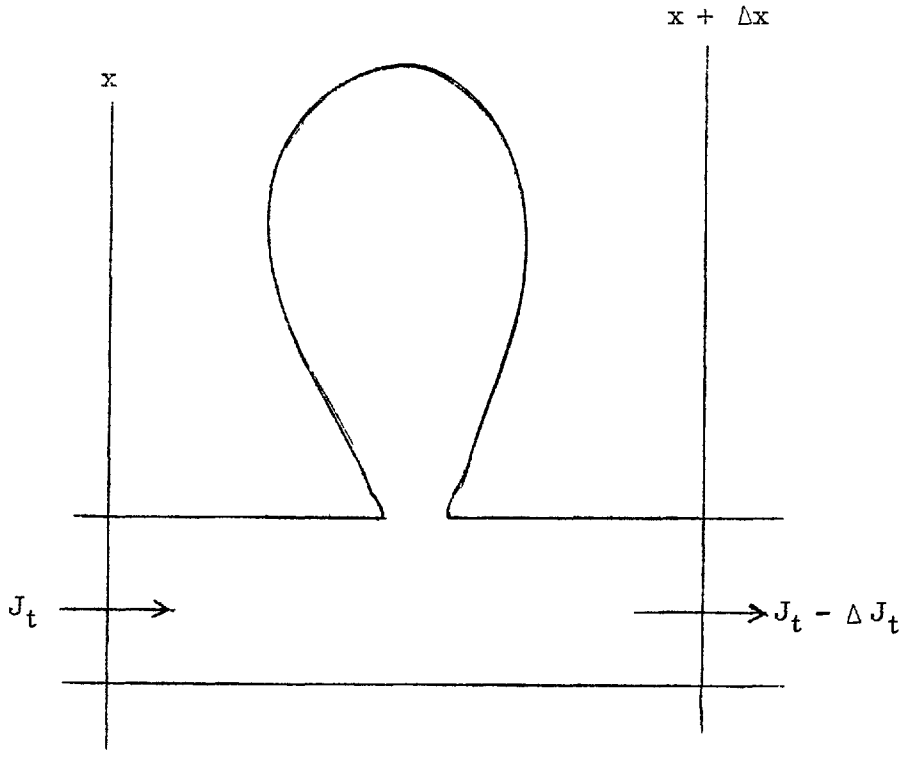

and in the limiting case we arrive at the equation

$$\frac{\partial C}{\partial t} = - \frac{\partial J_T}{\partial x} = \frac{\partial}{\partial x}\left[D_t \frac{\partial C}{\partial x}\right]$$

where D_t is the steady-state diffusion coefficient. This equation leads directly to the simple Frisch equation (53). Goodnight and Fatt broke the term $\partial C/\partial t$, the overall rate of build up of concentration, into two parts:

$\frac{\partial C_t}{\partial t}$ which is the rate of build up of concentration in the through pores,

and

$\frac{\partial C_B}{\partial t}$ which is the rate of build up of concentration in the blind pores and is represented by a sink function.

Whatever the form of $\partial C_B / \partial t$ the time lag will always be the same but the time taken for the medium to reach the steady state will be effected. This was the reason given by Goodnight and Fatt to explain why the experimental results were not always in agreement with the calculated values given by equation (53). They suggested that the form of $\partial C_B / \partial t$ in these cases was such that the medium had not reached the steady state by the end of the experiment.

The fallacy of the Goodnight and Fatt approach is that the section they used is not representative of a porous medium. In the planes x and $x+\Delta x$ there are no blind pore components. The medium made up of these sections would be discontinuous.

Another approach was that of Barrer and Gabor (1959, 1960). They suggested that there might be a time dependence in the overall diffusion coefficientdue to the paths of diffusion not being the same in the transient state as in the steady state. They linked the diffusion coefficients for gas and surface flow in the steady and the transient states by means of constants. The treatment was complicated but they were able to derive the effect of a time dependence in the diffusion coefficient for the case of Henry's Law adsorption and D_g and D_S independent of concentration.

We shall now derive a general equation for the time-lag for gas-phase flow and will later extend it to the case of very large surface flows.

Consider a unit cross section of the x plane of a porous medium. The flow through this plane will be broken up by the pore structure into a great many local flows j_i. The sum of these flows will be the total flux in and through the cross section. The local flows j_i may have x, y and z components. Some of each of the local flows may be regarded as being due to the blind pore character of the pore and some will be due to the through pore character of the pore. The proportion of each will depend on the form of the particular pore. Each of the local flows in the pores can thus be divided into two fractions:

$$\left.\begin{aligned} j_1 &= j_{1t} + j_{1B} \\ j_2 &= j_{2t} + j_{2B} \end{aligned}\right\} \tag{73}$$

and the sums of these two fractions can be put:

$$\left.\begin{aligned} \Sigma j_{it} &= J_t \\ \Sigma j_{iB} &= J_B \end{aligned}\right\} \tag{74}$$

The y and z components of the small flows will sum to zero since there is only an overall concentration gradient in the x direction. Hence

$$J_t = -D_t \frac{\partial C}{\partial x} \tag{75}$$

and

$$J_B = -D_B \frac{\partial C}{\partial x} \tag{76}$$

$$J_T = J_t + J_B \tag{76a}$$

where D_t is the steady-state diffusion coefficient and D_B is some function of time and concentration which will decay to zero in the steady state. That is, for the steady state

$$J_T = J_t = -D_t \frac{\partial C}{\partial x}$$

From (76) we may write

$$\frac{\partial C}{\partial t} = -\frac{\partial}{\partial x}\left[J_T\right] \tag{78}$$

$$= \frac{\partial}{\partial x}\left[(D_B + D_t)\frac{\partial C}{\partial x}\right] \tag{79}$$

This can be treated by the method of Frisch. On integration from ℓ to x we obtain

$$\int_{x}^{\ell} \frac{\partial C}{\partial t} dx - q(t) + D_B \frac{\partial C}{\partial x} + D_t \frac{\partial C}{\partial x} = 0$$

Integrating from ℓ to 0 and then from 0 to t_∞ where t_∞ is a finite time large enough for the diffusion to be considered in the steady state, we obtain

$$\int_0^{t_\infty} \int_0^{\ell} \int_x^{\ell} \frac{\partial C}{\partial t} dx.dx.dt - \int_0^{t_\infty} q(t).\ell.dt + \int_0^{t_\infty} \int_0^{\ell} (D_B + D_t) \frac{dC}{dx} dx.dx = 0 \qquad (80')$$

which re-arranges to

$$\int_0^{t_\infty} \int_0^{\ell} \int_x^{\ell} \frac{\partial C}{\partial t} dx dx dt + \ell.Q(t) - t_\infty \int_0^{C^{0*}} D_t.dC + \int_0^{t_\infty} \int_0^{\ell} D_B \frac{\partial C}{\partial x} dx.dt = 0 \qquad (81)$$

Q(t) is the total quantity of diffusant that has left the plane ℓ in the time 0 to t_∞. That is

$$Q(t) = \frac{t_\infty - L}{\ell} \int_0^{C^{0*}} D_t.dC \qquad (82)$$

On substitution in equation (81) we obtain

$$\int_0^{\ell} \int_x^{\ell} C(x) dx dx + \frac{\ell(t_\infty - L)}{\ell} \int_0^{C^{0*}} D_t dC - t_\infty \int_0^{C^{0*}} D_t d_C + \int_0^{t_\infty} \int_0^{\ell} D_B \frac{\partial C}{\partial x} dx dt = 0 \qquad (83)$$

which re-arranges to give

$$L = \frac{\int_0^{\ell} \int_x^{\ell} C(x) dx dx + \int_0^{t_\infty} \int_0^{\ell} D_B \frac{\partial C}{\partial x} dx dt}{\int_0^{C^{0*}} D_t.dC} \qquad (84)$$

On comparison with equation (53) we see that there is an extra term $\int_0^{t\infty}\int_0^{l} D_B \frac{dC}{dx}\,dxdt$ in the numerator. This term will be negative since $\partial C/\partial x$ is negative and D_B is positive. We may therefore write equation (84) in the form

$$L_{expt} = L_{calc} - \Delta L^* \tag{85}$$

where L_{expt} is the experimental time lag and L_{calc} is the time lag derived from equation (53) and ΔL^* is given by the equation

$$\Delta L^* = \frac{-\int_0^{t\infty}\int_0^{l} D_B \frac{\partial C}{\partial x}\,dxdt}{\int_0^{C^{0*}} D_t.dC} \tag{86}$$

We see that this now explains why for the low surface coverage results where an appreciable fraction of the flux is carried by the gas phase the calculated time lag is generally larger than the experimental time lag because of the ΔL^* term which is not accounted for in the simple Frisch treatment (equation 53).

The qualitative picture is similar to the ideas of Barrer and Gabor. If the medium is homogeneous as in a uniform polymer then the flow lines are always the same, in the transient and in the steady state, and the expression for the time lag is given by equation (53). In a porous medium the flow lines are present throughout the system in the transient state but in the steady state they will only be present in the through pores. The extra time-dependent term in equation (84) is due to this .

Let us now examine the second category of results, those obtained in the very high surface flow experiments. Here there will not be the virtual dead space or blind pore component we obtained for gas-phase flow. The reason for this is best illustrated by means of a diagram (see fig. overleaf).

The shaded volume will for gas-phase flow have blind pore character. For surface flow, however, the flow pattern will be essentially the same in the transient state as in the steady state.

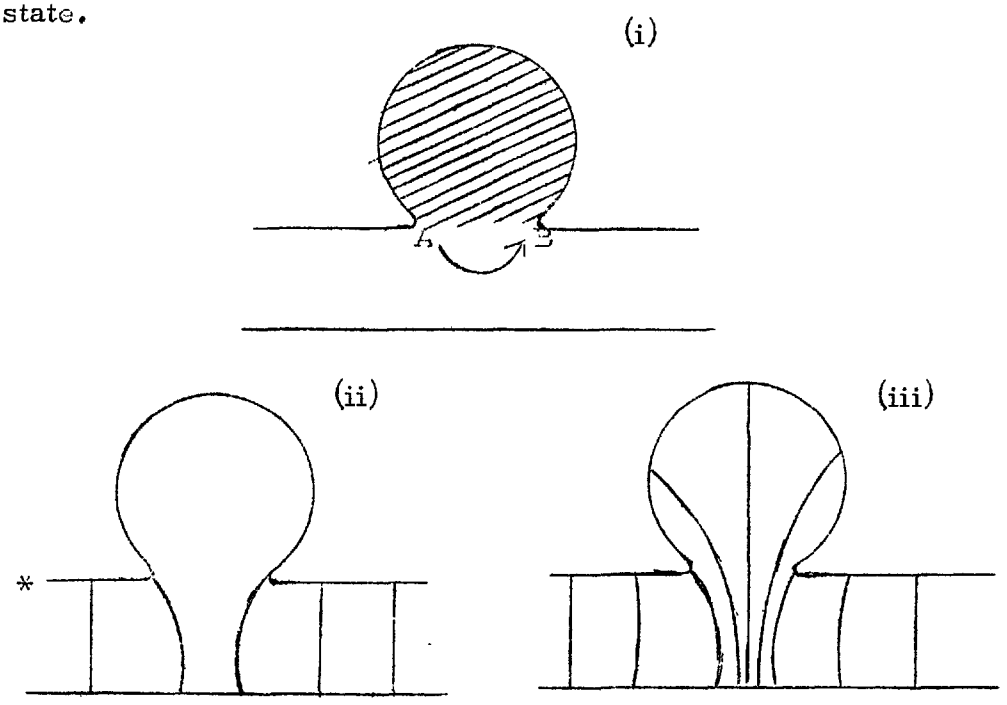

* The lines connect points of equal gas-phase concentration.

If the shaded area in fig. (i) is to have complete blind pore character there must be no concentration gradient in the gas phase or in the surface phase inside the pore. This means that the surface phase must become desorbed at the point A and become adsorbed at the point B. However, by this very act of desorption the gas-phase concentration gradient inside the pore is changed as shown in fig. (ii) and (iii). There will now be a concentration gradient inside the pore.

Since the amount of diffusant flowing in the gas phase is a small fraction of that flowing on the surface it requires only a small fraction of the surface flow to become desorbed to completely

change the gas-phase concentration profile inside the pore. This means that the flow will move mainly on the surface in both the transient and in the steady state, and hence the overall diffusion coefficient will not change markedly with time. This means that in a pore where there is a very large surface flow $j_i \sim j_t$ at all times. Hence $J_B = -D_B \frac{\partial C}{\partial x}$ is small, which in turn means that ΔL^* in equation (85) is also small. For a very thin crack or a very bottle shaped pore this treatment would not be valid. In a normal microporous medium made up of reasonably regular particles this form of pore will probably be unimportant compared with the total volume of the blind pores. We may therefore use equation (53) to calculate L_{expt} since ΔL^* is small. We should expect the equation to give reasonably good agreement with the experimental results. This is the case and the treatment is therefore supported by experiment.

This treatment leading to equation (84) also has useful applications to two-phase polymer systems. Barrer and Chio (1965) treated a non-uniform polymer system in a similar manner to Barrer and Gabor by the use of structure factors. Barrer and Chio determined the diffusion coefficients D_L and D_t. D_L is the diffusion coefficient determined from the time lag using the equation

$$L_{expt} = \frac{\ell^2}{6D_L} \qquad (87)$$

and will become average diffusion coefficient over the period of the transient state. D_t is the steady-state diffusion coefficient. When the medium was above the crystallisation temperature, that is the temperature above which the medium became uniform, and when they were dealing with samples which contained only a small amount of a filler as a second phase, Barrer and Chio found that D_t and D_L were approximately equal. Below the crystallisation temperature or when the medium contained a high proportion of filler they found that the ratio D_t/D_L changed from approximately one to as little as 0.5. From equation (85) we can immediately

explain this. We may write

$$L_{calc} = \frac{\ell^2}{6D_t} \tag{88}$$

for Henry's Law adsorption, and D_t independent of concentration. Hence from (88) and (87) we may write

$$\frac{L_{expt}}{L_{calc}} = \frac{D_t}{D_L} \tag{89}$$

but since for a non-uniform two-phase medium $L_{expt} < L_{calc}$ from equation (85) then the ratio D_t/D_L will be less than one as observed. This effect may be a partial explanation of the apparent time dependence observed in many polymer systems which has in the past been thought to be entirely due to the relaxation effects, though relaxation effects would normally mean $D_t/D_L > 1$.

5. Diffusion results

We may re-arrange the diffusion equation (4) to the form

$$J_T = -D_T \frac{dC}{dC'_g} \frac{dC'_g}{dx} \tag{90}$$

but from the definition of C, i.e.

$$C = AC'_s + \varepsilon C'_g$$

we see that when AC'_s is very much larger than $\varepsilon C'_g$, which is true for even moderate adsorptions, then

$$\frac{dC}{dC'_g} = \frac{AdC'_s}{dC'_g} \tag{91}$$

where AdC'_s/dC'_g is the slope of the adsorption isotherm. Substituting in equation (90) we obtain

$$J_T = -D_T \frac{dC'_g}{dx} A.\frac{dC'_s}{dC'_g} \tag{92}$$

For a particular experiment we can use the expression given in equation (44) and substitute in equation (92) and hence obtain on re-arranging the expression

$$D_T = \frac{\ell}{A} \frac{dC'_g}{dC'_s} \frac{dJ_T}{dC'^0_g} \tag{93}$$

since for a particular experiment

$$J_T = [J]^{C_g^{0*}}$$

Equation (93) is an extremely interesting result since it is an experimental observation that (dJ_T/dC'^0_g) is always far less concentration dependent than dC'_g/dC'_s. This is immediately apparent on inspection of a plot of J_T against C'^0_g and comparison with the adsorption isotherm. In effect the major contribution to the concentration dependence of D_T or D_S when surface flow is dominant comes from the adsorption isotherm andif we assume that dJ_T/dC'^0_g is relatively constant in comparison with dC'_g/dC'_s then we may write approximately

$$D_T \propto \frac{dC'_g}{dC'_s} \tag{94}$$

This result allows us to predict the approximate shape of the curve of the diffusion coefficient against surface conc entration directly from the adsorption isotherm, and is a marked improvement on the treatment of Carman and Haul. The applicability of this proportionality is seen on examining several different forms of concentration dependence of D_T.

Case (i): Ash, Barrer and Pope's results for SO_2 on Carbolac

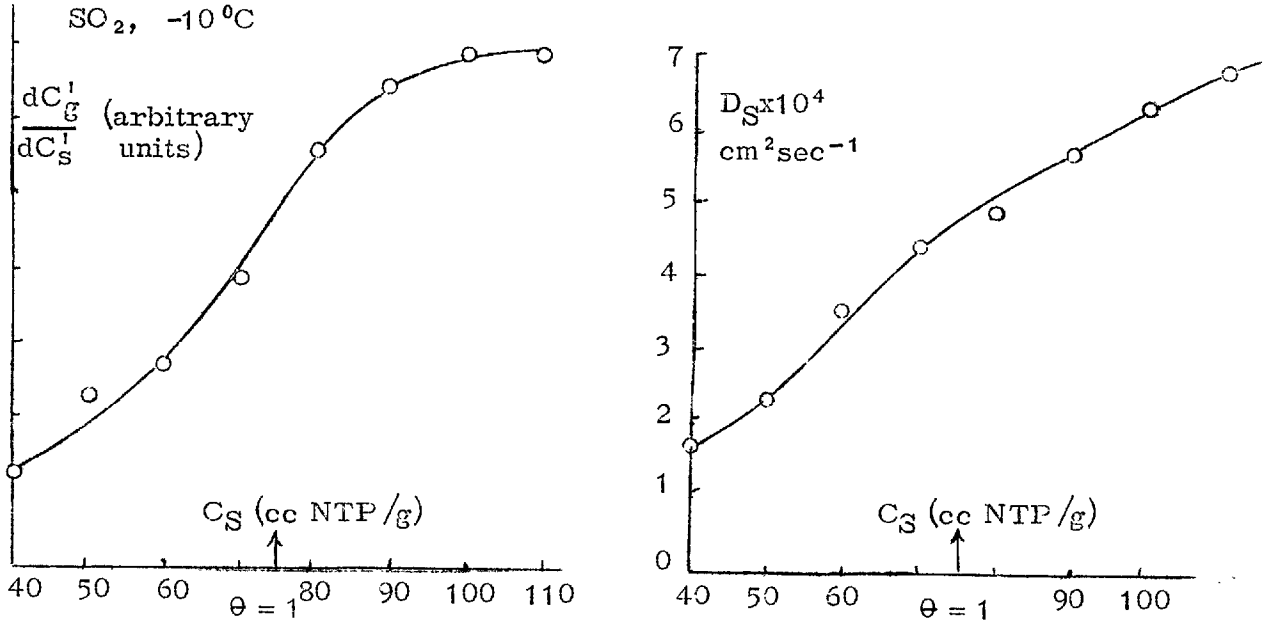

Case (ii): The results of the author for argon on graphon and black pearls.

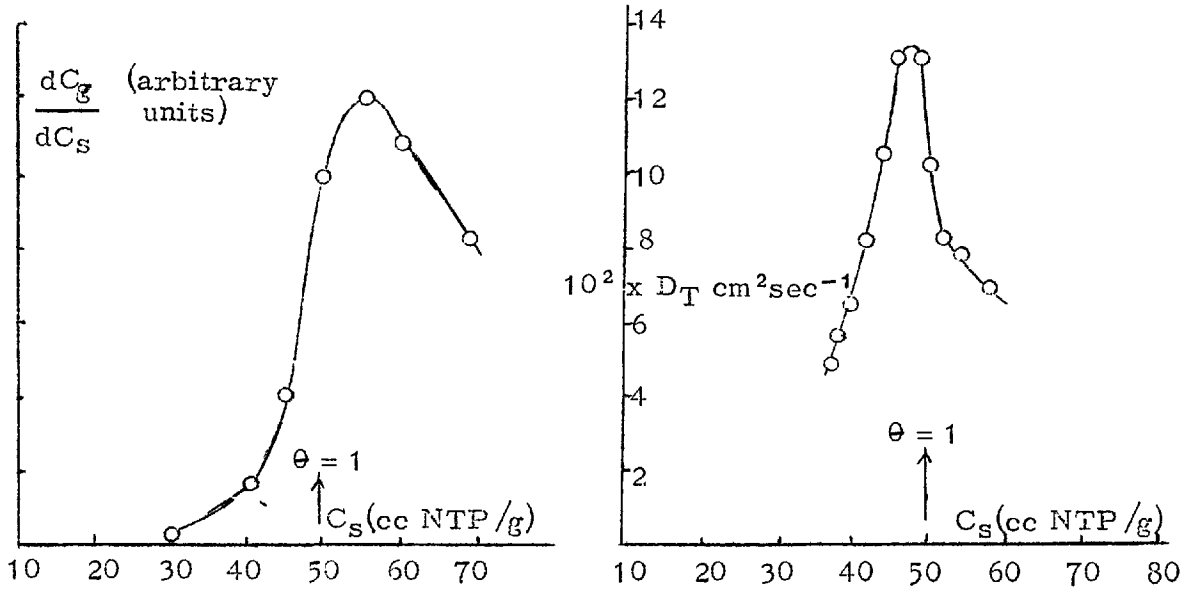

Haul's results for nitrogen on graphon are similar to this except that he observed a second small peak in D_T at a coverage of approximately two monolayers. This is now seen to be due to the adsorption isotherm having the step at this coverage which is characteristic of a homogeneous surface.

Case (iii): Perhaps the most interesting case is that found by the author for SF_6 on graphon and black pearls. Previous theories would have great difficulty in explaining the initial fall of D_T with amount sorbed but from equation (94) it can be seen as an immediate result of isotherms of types III or IV.

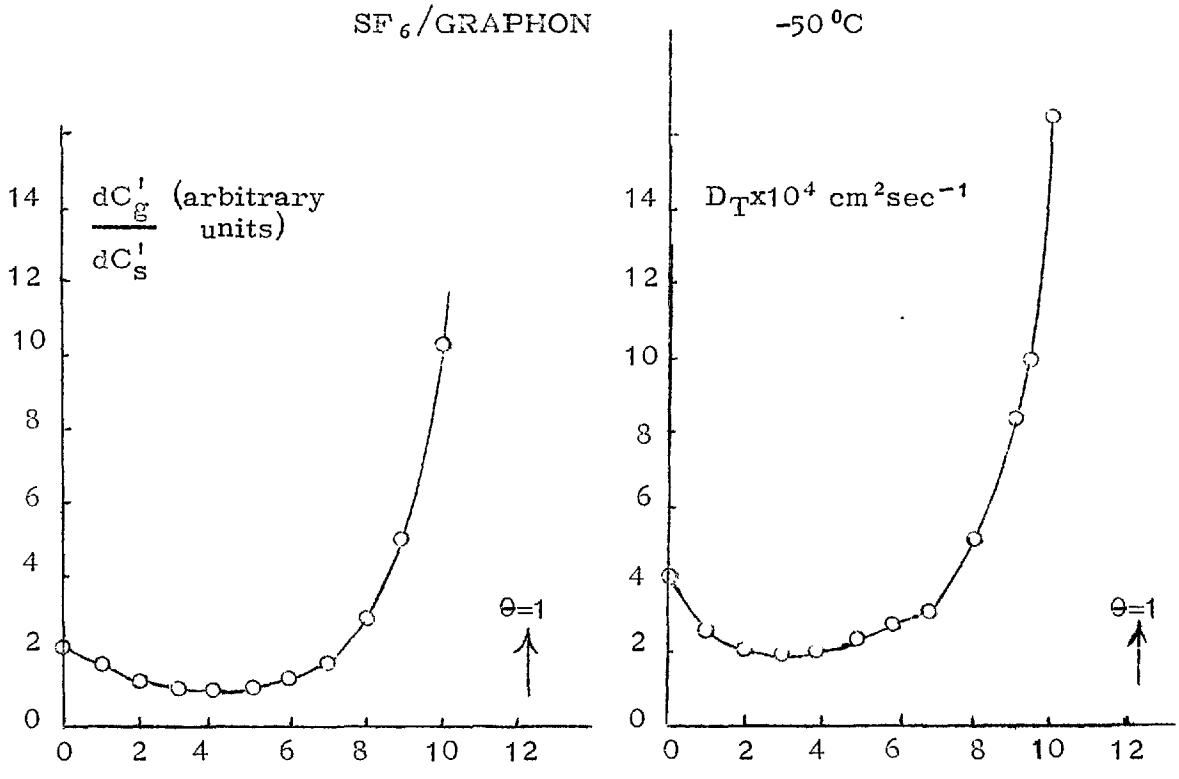

We are thus able to predict the form of the diffusion coefficient curve in terms of the proportionality in equation (94) with reasonable accuracy. However, on examination of equation (93) we see

that it is made up of two parts:

(i) $\frac{dC'_g}{A\,dC'_s}$ which is characteristic of the adsorption isotherm, and

(ii) $\ell.\frac{dJ_T}{dC'^{\,0}_g}$ which is characteristic of the experimental flow results.

By assuming that the variation in $\ell.\frac{dJ_T}{dC'_g}_0$ with $C'^{\,0}_g$ to be so small compared with that of $\frac{dC'_g}{A.dC'_s}$ that $\ell.\frac{dJ_T}{dC'_g}_{,0}$ can be regarded as a constant, which is experimentally reasonable, we have been able to arrive at the approximate form of the diffusion coefficient when plotted against surface coverage. This treatment will not enable us to obtain any information about $\frac{dJ_T}{A.dC_g}_{,0}$ since we have already assumed that it is virtually a constant in deriving equation (94). To obtain information about this quantity we need another approach.

A possible method of obtaining information about J_T in terms of $C'^{\,0}_g$ is given by equation (44), from which we see that if it were possible to predict the form of the concentration profile in the gas phase inside the plug we should be able to predict J_T in terms of $C'^{\,0}_g$. We shall limit ourselves in the following to the Knudsen region in which most of the results we shall discuss have been obtained. There will be several factors affecting the gas-phase concentration profile, but one effect we can treat easily, if only in a qualitative manner, arises from the physical presence of the adsorbed molecules. When there is a sorbed phase present then obviously the diameter of the pore available for gas-phase flow is reduced and the amount by which it is reduced will depend on the surface concentration. For a cylindrical capillary the connection between the pore radius and the flux in the Knudsen region can be put quite clearly, as was shown in the Introduction,

as

$$J_g = -\frac{dC_g'}{dx}\,\frac{4r}{3}\left[\frac{2RT}{\pi M}\right]^{\frac{1}{2}} \qquad (95)$$

In a porous medium this equation cannot of course be strictly applied, but it shows that if the radius of the capillary is reduced then for the same flux to flow in the gas phase the gradient dC_g'/dx must be increased. Hence in the absence of all other effects except the physical presence of the adsorbed molecules dC_g'/dx will increase continuously on going from the plane $x=\ell$; $C_s=0$ to the plane $x=0$; $C_s=C_s^0$.

This then allows us to state from equation (44) that a plot of J_T against $C_g'^0$ must have a decreasing slope. In consequence of this the permeability K as defined by equation (47) will decrease continuously with increasing $C_g'^0$.

For many microporous media and gases, K, when plotted against $C_g'^0$, does decrease continuously with increasing $C_g'^0$. For many other cases it does not and there must therefore be factors other than simple constriction of the pores due to the sorbed phase present. These come under the heading of what has been called flux interconversion (Barrer 1963). By this we mean a net flow of flux from one phase to the other as x increases from 0 to ℓ. If there is this net movement of flux from one phase to the other then it must obviously have an effect on the gas-phase concentration profile, since the flux in the gas phase is a product of the diffusion coefficient (which for a gas in the Knudsen region will depend only on the pore diameter for a particular gas and temperature) and of the concentration gradient.

It might be mentioned here that from the principle of microscopic reversibility, if the system is at equilibrium then the number of molecules being adsorbed and desorbed must on average be equal. Thus if there is flux interconversion the system cannot be considered as being completely in equilibrium and hence equations

(44), (45), etc., are not strictly correct. However, the number of molecules being adsorbed and desorbed from the surface is so large compared to the small net movement of molecules from one phase to the other that this latter effect can be neglected. Whilst C'_s and C'_g are not exactly the same as they would be in a static sorption experiment, they are not noticeably different.

One obvious factor which could cause flux interconversion is partial blockage of capillaries by adsorbed mobile films, an effect which would decrease as x increases. When there is blockage present there will be a tendency for flux to move from the gas phase into the sorbed phase, rather than cause a large concentration gradient in the gas phase. Flux interconversion will therefore tend to counteract the effect of the physical presence of the adsorbed film and would account for the cases when K does not decrease continuously with increasing C'^0_g. However, the actual form of K against C'^0_g plots are extremely varied. It is difficult to see any underlying reason why in some cases flux interconversion should be more important than the physical presence of the adsorbed film and not in others. It is possible that blockage is not the only effect causing flux interconversion and hence affecting the flux behaviour.

Conclusion

We have shown in this thesis that it is possible to obtain the steady-state concentration and the steady-state concentration gradient at any plane in a membrane from a knowledge of the flux through the medium in the steady state for various ingoing concentrations. We have been able to use this knowledge of the concentration at any plane inside the medium to calculate the time lag using the method of Frisch (1957) and we have shown that the simple Frisch equation is inadequate for a porous medium and

an extra term must be introduced for the blind pore character of the medium.

We have confirmed the ideas of Barrer and Gabor (1960) on the effect of surface roughness on the relative efficiencies of the surface to surface flow, and have shown that this effect can have a dramatically large influence on D_S.

Using the equation that gives the surface concentration gradient at any point in the steady state we have been able to split the diffusion coefficient into two factors, one corresponding to the inverse slope of the adsorption isotherm and the other corresponding to the flow data. From this we have been able to predict the approximate nature of the diffusion coefficient when plotted against surface concentration and have explained the unusual form of this plot for argon and SF_6 on graphon and black pearls, carbon blacks which were measured during the course of the investigation. This approximate knowledge of the diffusion coefficient is not precise enough for any information to be obtained about the surface permeabilities and we have been unable to improve on the existing empirical correlations of Kammermeyer (1958) and Gilliland and Baddour and Russell (1958). This aspect of surface diffusion therefore still requires a good deal of work.

REFERENCES

1. Adamson, A.V. and Ling, I. (1961) Advances in Chemistry Series No.33, Am.Chem.Soc.

2. Aitken, A. and Barrer, R.M. (1955) Trans.Far.Soc. 51, 116.

3. Ash, R., Barrer, R.M. and Pope, C.G. (1963) Proc.Roy.Soc. 271A, 1, 19.

4. Ash, R., Barrer, R.M. and Clint, J.H., in preparation.

5. Ash, R., Barrer, R.M. and Logan, A., in preparation.

6. Aylmore, L.A.G. and Barrer, R.M. (1966) Proc.Roy.Soc. 290A, 477.

7. Babbit, J.D. (1950) Canad.J.Res. 29, 426; 28, 449.

8. Barrer, R.M. (1941) "Diffusion in and through solids", Cambridge Univ. Press.

9. Barrer, R.M. and Barrie, J.A., (1952) Proc.Roy.Soc. 213A, 250.

10. Barrer, R.M. and Strachan, E. (1955) Proc.Roy.Soc. 231A, 52.

11. Barrer, R.M. and Gabor, T. (1959) Proc.Roy.Soc. 251A, 353.

12. Barrer, R.M. and Gabor, T. (1960) Proc.Roy.Soc. 256A, 267.

13. Barrer, R.M. and Petropoulos, J.H. (1961) Brit.J.Appl.Phys. 12, 691.

14. Barrer, R.M. (1963) Canad.J.Chem. 41, 1768.

15. Barrer, R.M. and Chio, H.T. (1965) J.Polymer Sci. Part C, No.10, 111.

16. Barrie, J., Levine, J.D., Michaels, A.S. and Wong, P. (1963) Trans.Far.Soc. 59, 869.

17. Beebe, R.A. and Young, D.M. (1954) J.Phys.Chem. 58, 330.

18. Beebe, R.A., Kiselev, A.V., Kovaleva, N.V., Tyson, R.F.S. and Holmes, J.M. (1964) Russ.J.Phys.Chem. 38, No.3, 372.

19. Beebe, R.A., Kiselev, A.V., Kovaleva, N.V., Holmes, J.M. and Camplin, M.E.R. (1964) Russ.J.Phys.Chem. 38, No.4, 506.

20. Brunauer, S., Deming, L.S., Deming, W.E. and Teller, E. (1940) J.Am.Chem.Soc. 62, 1723.

21. Carman, P.C. and Malherbe, P.leR. (1950) Proc.Roy.Soc. 203A, 55, 165.

22. Carman, P.C. (1951) Proc.Roy.Soc. 209A, 69.

23. Carman, P.C. and Raal, F.A. (1951) Proc.Roy.Soc. 209A, 38.

24. Carman, P.C. and Raal, F.A. (1954) Trans.Far.Soc. 50, 842.

25. Champion, W.M. and Halsey, G.P. (1953) J.Phys.Chem. 57, 646.

26. Crank, J. (1956) "The Mathematics of Diffusion", O.U.P.

27. Daynes, H.A. (1920) Proc.Roy.Soc. 97A, 286.

28. Denbigh, K.G. (1951) "Thermodynamics of the Steady State", Methuen and Co.Ltd.

29. Frisch, H.L. (1957) J.Phys.Chem. 61, 93.

30. Frisch, H.L. (1962) J.Chem.Phys. 37, 2408 .

31. Gilliland, E.R., Baddour, R.F. and Russell, J.L. (1958) A.I.Ch.E.J. 4, 90.

32. Goodnight, R.C. and Fatt, I. (1963) J.Phys.Chem. 67, 949.

33. Goodnight, R.C., Klikoff, W.A., Fattes, I. (1960) J.Phys.Chem. 64, 1162.

34. Haul, R.A.W. (1952) Angew.Chem. 62, 10.

35. Haul, R.A.W. (1954) Z.Phys.Chem. NS1, 153.

36. Haul, R.A.W. and Peerbohms, R. (1958) Naturwiss. 45, 109.

37. Hill, T.L. (1946) J.Chem.Phys. 114, 441.

38. Hill, T.L., Emmett, P.H. and Joyner, L.G. (1951) J.Am.Chem.Soc. 73, 5102.

39. Kammermeyer, K. (1958) J.Ind.Eng.Chem. 50, No.4, 697.

40. Kiselev, A.V. (1958) Kolloid Zh. 20, 338.

41. Knudsen, M. (1909) An.Phys.Leipzig 28, 73.

42. Meares, P. (1958) J.Polymer Sci. 27, 391.

43. Meares, P. (1965) J.Polymer Sci. 9, 917.

44. Petropoulos, J.H. (1959) PhD. thesis (Univ. of Manchester).

45. Pollard, W.G. and Present, R.D. (1948) Phys.Rev. 73, 762.

46. Polley, M.H., Schafer, W.D. and Smith, W.R. (1954) J.Phys.Chem. 58, 330.

47. Roger, W.R., Buritz, R.S., Alpert, D. (1954) J.Appl.Phys. 25, 868.

48. Singleton, J.H. and Halsey, G.D. (1954) J.Phys.Chem. 58, 1011.

49. Voigt, E.M. and Tomlinson, R.H. (1955) Canad.J.Res. 33, 215.

50. Weber, S. (1954) Konig. Dansk Vid.Sels.mat.fis.med.64,No.2.

51. Wicke, E. and Kallenback, R. (1941) Kolloidycher 97, 135.

APPENDIX 1

Graphon plug 1

ℓ = 3.376
A_c = 0.290
ε = 0.45

Black pearls plug 1

ℓ = 3.707
A_c = 0.290
ε = 0.46

Helium results 304.8 °K

P cm Hg	L sec	Kx10³ $cm^2 sec^{-1}$	P cm Hg	L sec	Kx10³ $cm^2 sec^{-1}$
4.55	33	25.33	2.31	80	9.66
13.00	42	25.44	5.10	86	9.40
16.75	20	24.79	7.39	80	9.39
18.95	40	25.42	14.35	86	9.44
19.84	52	25.09	18.10	86	9.45
26.10	35	25.55	27.30	82	9.33
14.41	39	25.32	11.65	96	9.17
17.52	38	25.47	14.42	88	9.28

Neon results 304.8 °K

8.94	66	12.34	6.41	204	4.97
15.00	74	12.41	9.98	195	4.92
21.68	75	12.31	14.75	204	5.05
			21.50	198	4.94
			24.51	187	4.92

Argon results 304.8 °K

21.01	120	12.67	30.32	336	6.99
26.91	113	12.81	19.40	336	7.04
27.76	108	12.60	13.08	330	7.09

contd.

Krypton results 304.8 °K

25.33	228	12.14
23.59	210	11.96
10.85	210	10.18
11.29	205	12.61
11.71	206	11.26

2.71	852	7.62
8.33	840	7.67
18.42	840	7.68
18.78	800	7.53
20.44	800	7.56
26.56	780	7.48
10.86	850	6.80
11.32	810	7.32
11.70	805	7.33

Xenon results 304.8 °K

15.28	540	16.39
14.30	540	16.44

	min.	
15.28	26.10	12.98

APPENDIX 2

Graphon plug 2

ℓ = 3.222 cm
A_c = 0.290 cm^2
ϵ = 0.42
Wt = 1.055g

Helium results

Temp.	Run No.	Pressure cm Hg	L sec	$Kx10^3$ cm^2sec^{-1}
50 °C	16	27.60	36	15.60
	17	15.72	38	15.61
	18	4.91	37	15.60
30 °C	1	21.31	39	15.20
	2	20.25	39	15.09
	3	31.88	40	15.06
	4	12.86	37	15.09
	5	2.26	36	15.00
	6	6.47	35	15.30
0 °C	33	23.46	40	14.38
	34	15.10	38	14.40
	54	21.07	37	14.44
	52	22.06	43	14.54
-41.8 °C	44	12.39	49	13.25
-42 °C	45	6.65	49	13.31
-42 °C	46	22.87	41	13.27
194.8 °K	60	13.66	44	13.66
195.0 °K	59	24.50	50	24.50
194.8 °K	61	6.92	41	6.92
151.6 °K	62	14.71	52	10.76
153.2 °K	64	24.83	49	10.93
90 °K	88	6.68	71	9.23
	89	28.11	62	9.00
	90	12.68	67	9.17
77.6 °K	92(A)	6.71	87	8.52
	100	25.09	81	8.78

Argon results

Temp.	Run No.	Pressure	L	$Kx10^3$
50 °C	19	25.32	127	7.72
	20	14.19	128	7.69
	21	7.63	128	7.72
30 °C	7	24.91	137	7.92
	8	5.96	148	7.99
	9	10.16	140	7.94
	10	14.99	-	7.87
	11	14.55	135	-
	12	19.45	134	7.86
	13	27.71	134	7.92
	14	14.47	132	8.14
	15	3.09	141	7.86
	39	8.30	-	7.73
0 °C	22	5.81	164	8.09
	35	29.05	150	8.12
	36	18.77	155	8.09
	37	11.47	159	8.08
	38	4.62	165	8.05
	53	11.58	160	8.13
	67	18.91	142	8.34
	72	13.67	150	7.75
	78	9.19	154	8.23
	85	10.94	148	8.44
	86	19.97	140	8.43
	95	5.90	138	8.54
-42 °C	43	16.01	188	8.44
	47	25.70	189	8.95
	48	12.88	195	8.81
	49	6.26	218	8.99
	50	5.71	204	8.90
	51	13.58	203	9.03

contd.

Temp.	Run No.	Pressure	L	$Kx10^3$
195 °K	58	7.18	301	10.44
	57	17.40	281	10.35
	56	14.35	293	10.43
	55	25.81	278	10.31
155 °K	66	15.08	642	15.31
	69	21.62	432	14.59
	70	8.49	480	15.55
	71	28,59	384	13.43
	73	10.34	456	15.49
	74	16.14	472	15.34
	76	3.38	525	16.67
			min.	
90 °K	79	9.06	108.2	41.26
	80	13.29	89	32.92
	81	28.73	63.5	22.41
	82	19.79	73	26.52
	83	4.91	120.6	50.35
	84	1.5	167	71.53
	87	0.632	-	94.49
	150	0.341	-	152.4
77.6 °K	91	3.60		39.83
	92	15.2		10.97
	93	8.3		18.50
	94	1.479		76.88
	97	3.53		43.21
	98	1.843		68.4
	99	1.015		96.45
	101	19.40		88.49
	147	0.584		159.4
	148	0.165		196.5
	149	0.0903		276.1
	151	0.0572		319.1

SF_6 results

Temp.	Run No.	Pressure cm Hg	t min-sec	$Kx10^3$ cm^2sec^{-1}
200 °C	113	0.905	-	6.19
	117	18.77	3-45	5.96
	115	13.13	3-6	5.94
	108	5.12	1-2	6.04
	129	5.63	-	5.97
	104	11.11	3-57	6.00
	103	29.54	3-58	6.03
150 °C	107	15.87	4-56	6.24
	106	26.60	5-0	6.25
	105	6.94	5-46	6.44
	119	1.456	4-38	6.36
100 °C	120	1.236	6-52	6.98
	111	12.51	7-24	6.88
	110	26.02	7-12	6.89
	109	5.38	7-5	6.81
60 °C	114	4.26	11-9	7.82
	113	27.89	11-6	7.83
	2	14.26	11-28	7.93
31.2 °C	123	17.80	-	9.25
	122	1.083	-	9.35
	121	3.37	16-12	8.90
	124	27.39	-	9.21
0 °C	128	26.60		11.89
	127	1.052		11.82
	125	10.39		11.81
-20 °C	131	20.99	15.70	15.70
	133	1.647		15.38
	132	7.60		15.31
	130	29.35		15.49

contd.

-40 °C	140	1.411	22.84
	139	27.60	19.50
	138	0.803	25.8
	137	13.58	22.28
	136	5.57	23.63
	135	20.93	21.70
	141	1.700	22.58
-50 °C	142	1.036	27.36
	143	26.40	18.87
	144	15.89	22.20
	145	6.61	25.88
	152	0.657	24.03
	170	38.91	15.75
	176	2.44	24.59
-60 °C	153	29.93	16.55
	154	6.87	29.02
	155	19.05	20.73
	156	0.810	30.33
	169	37.33	15.11
	171	12.45	24.24
	175	1.585	32.48
-70 °C	157	0.657	40.99
	158	16.74	21.47
	159	23.03	18.51
	160	9.30	25.44
	168	37.60	13.13
	172	6.35	32.93
	177	3.86	38.44
-80 °C	183	25.31	11.89
	182	17.35	15.87
	161	9.31	24.68
	162	22.71	12.90
	163	4.23	39.26
	164	1.001	55.69
	165	0.384	54.52
	166	1.322	53.93
	167	14.02	10.65
	173	3.79	38.71
	174	5.00	35.12
	181	15.60	17.33
-90 °C	178	2.44	47.33
	179	6.56	21.60
	180	8.07	17.23
	184	0.62	66.40
	185	0.40	62.95
	186	11.49	13.21
	187	4.50	28.28

APPENDIX 3

Black Pearls Plug 2

ℓ = 3.538 cm
A_c = 0.290 cm^2
ϵ = 0.43
Total wt. = 0.9957 g

Helium results

Temp.	Run No.	Pressure cm Hg	L secs	$Kx10^3$ cm^2sec^{-1}
50 °C	16	12.70	111	5.67
	17	22.54	109	5.63
	18	7.40	116	5.67
30 °C	18(A)	22.09	113	5.55
	19	13.03	121	5.51
	20	7.36	126	5.55
0 °C	21	7.18	125	5.26
	22	14.66	122	5.24
	27	21.41	125	5.26
	29	21.48	122	5.20
231 °K	35	25.35	134	4.87
	36	13.33	139	4.88
	37	7.00	136	4.90
194.8 °K	43	26.30	140	4.42
	44	14.93	151	4.52
	45	12.04	144	4.48
	46	27.01	-	4.67
153.6 °K	47	23.68	160	3.95
152.0 °K	48	14.11	165	4.01
90 °K	71	6.67	252	3.58
	72	28.11	235	3.55
	73	12.68	241	3.52
77.6 °K	75(A)	6.71	3.54	2.89
	83	25.09	362	2.89

Argon results

Temp.	Run No.	Pressure	L(sec)	$Kx10^3$
50 °C	11	8.95	428	4.44
	13	13.45	418	4.44
	14	12.61	430	4.48
	15	23.89	410	4.46
30 °C	6	14.90	454	4.67
	7	26.56	-	4.72
	8	25.53	458	4.70
	9	8.21	448	4.65
0 °C	2	10.53	580	5.14
	3	18.73	580	5.15
	4	25.81	564	5.13
	5	15.48	578	5.10
	10	7.81	558	5.07
	12	8.64	572	5.11
	28	11.80	578	5.12
	30	9.42	576	5.11
	55	12.95	588	5.14
	61	9.31	562	5.09
	68	10.98	572	5.32
	78	5.90	614	5.21
231 °K	23	22.46	862	6.16
	24	6.06	858	6.01
	25	9.48	880	6.21
	26	14.11	878	6.21
	31	26.56	853	6.19
	32	14.02	878	6.20
	33	18.08	878	6.24
	34	7.01	886	6.21
194.8 °K	39	12.21	1567	8.21
	40	5.50	1662	8.19
	41	21.67	1490	8.20
	42	15.29	1572	8.20
			min	
153 °K	49	15.02	49.7	14.74
	52	21.57	48.3	14.47
	53	8.49	63.5	15.55
	54	28.59	41.6	13.37
	56	10.35	63.0	15.41
	57	16.08	52.0	14.72
	58	25.19	43.9	14.02
	59	3.39	80.3	15.64

contd.

90 °K	62	9.06	179	55.89
	63	13.29	162	43.05
	64	28.73	134	25.86
	65	19.79	143	33.42
	66	4.90	202.5	83.68
	67	1.5	242	150.9
	70	0.630		194.5
	145	0.341		285.1
77.6 °K	74	3.60		54.66
	75	15.2		14.73
	76	8.3		25.27
	77	1.476		110.09
	80	3.53		56.93
	81	1.843		102.45
	82	1.015		159.1
	84	19.40		12.85
	142	0.584		22.61
	143	0.165		41.90
	144	0.0903		48.70
	146	0.0572		526.7

SF_6 results

Temp.	Run No.	Pressure cm Hg	L min-sec	$Kx10^3$ cm^2sec^{-1}
250 °C	131	1.521		3.22
	129	1.484		3.37
	128	10.65	11-30	3.29
	127	5.63	11-30	3.13
	126	20.62	11-30	3.27
200 °C	134	1.705	17-0	3.93
	133	26.98	-	3.88
	132	5.45	-	3.77
	130	1.541	-	3.73
150 °C	90	15.88	24-5	4.40
	89	25.62	23-12	4.56
	88	6.96	23-42	4.25
	136	1.700	-	4.68
100 °C	94	14.24	38-2	5.44
	93	26.08	36-8	5.49
	92	5.38	40-5	5.46
	101	1.085	-	5.69
60 °C	107	1.052		7.47
	108	5.65		7.00
	104	10.30		7.15
	103	27.89		6.84
	102	17.80		6.76
	121	13.42		7.20
31.2 °C	117	20.93		8.81
	120	13.58		9.06
	119	1.627		9.93
	118	5.57		9.16
	124	27.60		8.88
	123	0.824		9.55
0 °C	114	7.60		12.80
	112	1.623		14.45
	111	29.47		11.60
	110	12.90		12.21
	109	1.256		13.88

contd.

Temp.	Run No.	Pressure cm Hg	$kx10^3$ cm^2sec^{-1}
-20 °C	137	1.036	13.06
	138	26.40	15.58
	140	6.64	16.85
	147	0.657	16.10
	139	15.89	15.97
-40 °C	148	29.97	15.84
	149	6.87	23.11
	150	19.05	18.89
	151	0.810	24.53
-50 °C	152	0.657	38.41
	153	3.36	31.01
	154	16.74	21.09
	155	23.03	18.36
	156	9.30	25.03
-60 °C	157	9.31	27.72
	158	4.23	37.35
	159	1.001	50.41
	183	20.00	18.61
	184	35.00	13.31
-70 °C	160	0.384	65.49
	161	1.423	59.07
	162	11.07	21.64
	172	2.44	52.04
	173	6.56	32.94
	181	35.00	11.42
	182	22.00	15.84
-80 °C	170	2.44	52.16
	171	3.86	41.06
	174	8.07	25.27
	175	17.35	14.67
	176	25.31	9.95
	177	0.62	78.21
	178	0.40	68.98
	179	11.49	19.71
	180	4.50	36.81

APPENDIX 4

Graphon Powder. Argon adsorption results.

Temp.	P cm Hg	ccs. NTP	P cm Hg	ccs. NTP
50 °C	29	0,010	8.6	0.023
	4.7	0.014	13.9	0.035
	7.5	0.019	22.4	0.058
	12.3	0,033	36.8	0,103
	19.4	0.053		
			11.7	0.028
	8.4	0.020	18.8	0.046
	13.5	0.031	30.9	0.076
	21.7	0.050	47.9	0.117
	35.8	0.090		
	21.7	0.051		
	13.5	0.029		
	8.4	0.018		
30 °C	3.4	0.012	6.4	0.020
	5.6	0.021	10.4	0.032
	8.9	0.029	16.5	0.056
	14.6	0.047	26.8	0.085
	22.5	0.071	42.2	0.140
0 °C	3.8	0.019	10.9	0.051
	9.4	0.044	17.4	0.082
	22.3	0.106	27.3	0.130
			43.4	0.208
-41.8 °C	13.8	0.145	7.3	0.077
	21.0	0.222	11.4	0.120
	32.0	0.331	17.3	0.187
			26.3	0.273
			37.0	0.386
-77.8 °C	8.5	0.246	7.0	0.202
	12.3	0.346	10.5	0.296
	17.2	0.480	15.2	0.424
	22.4	0.610	21.4	0.529
			27.7	0.761
	7.2	0.206		
	10.7	0.304	10.8	0.315
	15.5	0.427	16.2	0.456
	21.9	0.590	23.3	0.658
	28.4	0.761	33.0	0.798
			43.0	1.150

contd.

-120 °C	8.77	1.187	2.15	0.337
	11.53	1.562	3.50	0.534
	17.29	2.305	5.66	0.853
	19.44	2.575	8.63	1.205
	21.95	2.930	9,70	1.346
	26.47	3.522	13.28	1.854
	29.66	3.919		
			17.13	2.323
			22.08	2.986
			27.22	3.704
			32.95	4.356
			37.34	4.848
90 °K	0.16	5.3595	38.16	34.297
	0.16	5.415	Desorbing	
	0.23	8.696	35.05	32.725
	0.25	8.735	28.26	28.474
	0.32	11.722	24.99	27.082
	0.33	11.764	18.60	24.918
	0.48	15.088	15.76	24.107
	0.49	15.153	11.17	22.928
	1.09	18.387	9.35	22.464
	1.15	18.528	6.68	21.746
	2.84	20.433		
	3.53	20.814		
	3.97	21.010		
	7.19	21.870		
	10.14	22.677		
	12.12	23.120		
	14.35	23.672		
	20.01	25.228		
	23.13	26.266		
	26.75	27.611		
	28.74	28.438		
	29.97	29.090		
	31.46	29.900		
	33.48	30.907		
	34.60	31.704		
	35.17	32.23		
	37.12	33.402		

contd.

77.6 °K	0.01	4.558	9.64	44.417
	0.02	9.558	9.85	45.037
	0.02	14.017	10.55	47.230
	0.08	18.119	11.34	49.625
	0.62	21.735	11.71	51.091
	2.07	24.070	12.61	53.788
	3.91	25.985	13.29	56.552
	4.13	26.221	13.62	57.987
	5.10	27.587	14.01	59.741
	6.00	29.305	14.43	61.826
	6.30	30.017	14.75	63.285
	6.65	30.700	15.12	65.191
	6.93	31.883	15.41	66.750
			15.67	68.328
	0.01	6.464	15.84	69.326
	0.04	13.635	16.03	70.406
	0.24	20.231	16.29	72.239
	3.53	25.338		
	3.90	25.763		
	5.79	28.753		
	6.17	29.681		
	6.42	30.064		
	6.99	32.298		
	7.38	33.924		
	8.15	37.908		
	8.54	39.812		
	9.23	42.904		

Graphon SF_6 Adsorption results.

Temp.	P cm Hg	ccs. NTP	P cm Hg	ccs. NTP
200 °C	6.51	0.019	5.47	0.019
	10.66	0.032	8.97	0.030
	17.59	0.056	14.81	0.047
	30.34	0.106	25.55	0.087
	48.69	0.176	42.92	0.161
150 °C	4.57	0.028	8.25	0.055
	7.44	0.044	13.39	0.082
	12.05	0.071	21.65	0.135
	20.15	0.122	36.15	0.227
	32.08	0.203		
100 °C	10.57	0.151	8.12	0.118
	16.79	0.236	12.92	0.179
	26.32	0.365	20.26	0.282
	41.86	0.576	32.22	0.444
60 °C	3.79	0.103	31.63	0.844
	5.83	0.160	43.20	1.163
	8.77	0.236	7.24	0.207
	13.00	0.352	11.16	0.315
	17.96	0.476	16.77	0.464
	21.28	0.566	24.93	0.680
			34.38	0.930
31.2 °C	12.71	0.686	8.20	0.438
	18.76	1.008	12.11	0.642
	26.40	1.422	17.09	0.906
	36.06	1.950	23.37	1.243
	45.17	2.439	29.32	1.563
0 °C	5.46	0.666	13.97	1.894
	7.00	0.856	18.50	2.593
	8.54	1.058	23.11	3.305
	9.77	1.2078	27.71	3.991
	11.67	1.474	31.31	4.508
	15.53	2.048	38.40	5.388
	19.32	2.660	47.72	6.367
	22.99	3.236		
	25.82	3.670		
	33.03	4.709		
	42.44	5.857		

contd.

-20 °C	4.85	1.329	5.81	1.639
	7.07	2.095	7.92	2.371
	8.48	2.598	9.15	2.828
	9.63	3.024	12.04	3.882
	10.54	3.375	16.54	5.392
	11.22	3.591	19.85	6.310
	12.61	4.181	21.87	6.717
	15.27	5.053	26.84	7.653
	17.90	5.757	32.85	8.275
	20.56	6.334	38.81	8.776
	22.03	6.779		
	31.14	8.184		
	38.85	8.967		
-40 °C	2.54	1.886	1.61	1.026
	3.21	2.465	2.08	1.374
	6.15	5.328	4.63	3.719
	6.81	5.867	5.59	4.775
	8.09	6.710	9.58	7.593
	11.18	8.022	14.65	8.992
	14.04	8.699	27.35	10.281
	17.54	9.220		
	22.04	9.504		
	26.19	9.980		
	28.26	10.115		
	38.11	10.625		
	47.30	11.077		
-50 °C	0.94	0.991	2.56	3.424
	1.81	2.144	2.81	3.999
	2.06	2.548	4.28	6.283
	2.63	3.578	4.55	6.813
	296	4.188	5.90	8.098
	4.41	6.807	7.49	8.898
	5.50	7.813	8.89	9.311
	8.40	9.012	11.94	9.920
	12.39	10.006	22.34	10.960
	17.61	10.581	25.40	11.161
	25.41	11.185	30.97	11.480
	32.46	11.765		
	40.71	12.145		
	Desorbing			
	25.43	11.176		
	13.70	10.173		
	10.28	9.639		
	7.33	8.711		

contd.

-60 °C	1.53	9.621	4.23	9.136
	5.20	9.613	9.84	10.522
	10.38	10.605	13.22	10.954
	15.42	11.122	17.63	11.303
	20.45	11.554	22.32	11.710
	26.12	12.000	26.13	12.051
	30.58	12.406	28.43	12.245
	0.82	2.372	35.02	12.946
	1.41	4.402	39.89	13.561
	1.52	4.731		
	32.0	8.420		
	3.54	8.699		
-70 °C	0.42	1.638	Desorbing	
	0.66	3.159	26.61	14.337
	0.78	4.036	21.13	13.139
	1.05	6.128	16.06	12.239
	1.29	7.401	9.53	11.606
	1.71	8.629		
	3.82	10.398	0.73	3.666
	5.22	10.816	1.04	5.790
	6.26	11.014	1.41	7.751
	10.22	11.621	2.47	9.740
	19.65	12.960	20.58	13.183
	29.57	14.856	28.06	14.898
	34.43	17.341	31.69	16.290
			34.18	17.385
			35.33	18.096
-80 °C	0.21	1.551	11.64	13.602
	0.40	5.074	13.90	14.425
	0.43	5.169	16.79	16.113
	0.66	8.063	18.13	17.168
	2.27	10.748	20.36	20.021
	5.83	11.802	21.48	21.379
	7.42	12.129		
	9.48	12.778	0.08	0.595
	10.11	12.964	0.35	3.531
	12.01	13.625	0.37	4.086
	15.27	15.058	0.45	5.543
	17.03	16.193	0.51	6.973
	18.38	17.243	0.72	8.320
	19.64	18.870	1.04	9.433
	20.53	20.161	1.49	10.440
	21.53	21.777	1.74	10.618
	22.32	23.194	14.87	15.228
			20.03	20.653
	0.28	2.334	21.71	23.911
	0.40	5.169	23.12	26.573
	0.66	8.479	24.83	29.224

contd.

-30 °C (contd.)

	1.14	10.062
	1.30	10.205
	4.60	11.693
	5.88	11.945
	6.94	12.204
	8.42	12.592
-90 °C	0.15	3.040
	0.23	5.697
	1.56	11.316
	2.72	12.143
	4.05	12.721
	6.71	14.054
	7.52	14.617
	8.49	15.557
	9.04	16.300
	9.40	16.884
	Desorbing	
	7.34	15.232
	6.22	14.055
	0.41	9.700
	7.29	14.549
	10.05	18.769
	11.39	25.295
	Desorbing	
	10.98	22.802
	10.46	20.418
	9.80	18.194
	8.68	16.252
	7.44	14.601
	5.57	13.410
	3.77	12.630
	2.63	12.246
	Desorbing	
	22.555	24.179
	20.38	19.893
	16.46	15.988
	11.60	13.552
	7.08	12.139
	4.00	11.409
	0.13	2.887
	0.19	5.985
	0.29	8.417
	3.23	12.514
	4.22	12.888
	7.10	14.376
	8.33	15.460
	8.80	15.992
	9.38	16.907
	9.70	17.860
	10.16	19.117
	10.63	20.474
	11.12	23.000
	0.245	7.084
	5.563	13.452
	7.565	14.625
	8.900	16.183
	9.918	18.160
	10.742	21.419
	11.640	23.821

APPENDIX 5

Black Pearls Powder. Argon adsorption results.

Temp.	P cm Hg	ccsNTP/g	P cm Hg	ccsNTP/g
50 °C	3.9	0.017	9.9	0.025
	9.8	0.035	15.6	0.031
	25.6	0.156	24.8	0.083
	32.8	0.201	40.7	0.151
			65.5	0.272
30 °C	8.5	0.033	4.9	0.050
	13.3	0.102	7.7	0.038
	21.1	0.127	12.3	0.082
	34.3	0.216	19.9	0.140
	54.3	0.365	31.7	0.223
0 °C	8.7	0.126	17.8	0.211
	21.3	0.268	25.7	0.339
			44.6	0.544
	7.3	0.081		
	11.3	0.125		
-42 °C	22.6	0.675	21.2	5.639
	34.7	1.030	32.6	7.794
	53.6	1.484		
	24.3	0.721		
	37.6	1.075		
	58.5	1.601		
-120 °C	3.96	2.017	11.69	4.008
	4.83	2.249	21.59	6.777
	6.60	2.819	34.35	9.969
	8.73	3.480	38.39	11.549
	11.14	4.195	51.40	18.771
	13.18	4.863		
	19.62	6.683	14.12	4.845
	25.77	8.046	26.66	7.926
	31.62	9.471	33.89	10.278
			41.10	12.083

contd.

90 °K	0.089	9.041	0.224	17.605
	0.182	15.921	0.316	24.495
	0.308	23.692	0.673	36.053
	0.391	28.631	1.800	43.622
	0.910	39.208	3.706	47.449
	2.099	44.705	4.383	48.319
	2.869	46.318	6.048	50.112
	6.042	50.323	8.593	52.439
	8.734	52.759	12.755	55.733
	10.910	54.489	15.900	58.313
	13.615	56.692	20.104	61.887
	18.458	60.681	23.571	65.233
			26.312	67.997
			28.182	70.043
			30.960	73.351
			33.822	75.547
77.6 °K	0.045	34.949	0.045	27.151
	3.214	64.237	0.149	45.250
	3.616	65.951	1.584	56.877
	3.810	66.797	1.866	58.137
	5.084	72.908	4.188	67.648
	5.605	75.677	4.705	69.879
	5.841	77.009	4.938	70.978
	6.872	84.080	6.020	76.657
	7.559	89.681	6.518	80.078
	9.017	104.848	6.750	81.501
	9.725	112.451	7.511	87.327
	10.975	122.777	7.989	91.670
	11.981	131.743	8.171	93.455
	0.014	3.852	16.674	193.240
	0.042	7.612	17.545	209.369
	0.371	48.678	17.705	223.974
	7.297	84.701	18.176	238.799
	11.094	121.302	18.692	253.792
	13.749	147.64	18.990	275.755
	14.311	155.48		
	14.728	158.891		
	16.102	179.961		

Black Pearls Plug 2

Temp.	P cm Hg	cc NTP/g	P cm Hg	cc NTP/g
90 °K	0.132	12.142	0.707	36.491
	0.354	27.133	0.617	37.300
	0.732	36.483		
	0.656	37.316		
	4.595	51.512		
	6.585	53.814		
	8.179	55.250		
	12.812	59.301		
	15.189	61.554		
	17.218	63.336		
	19.030	64.792		
	0.093	9.821	13.122	59.176
	0.095	9.933	15.355	62.373
	0.159	15.795	20.464	65.855
	0.170	15.966	24.568	70.633
	0.399	24.711	27.133	73.289
	0.302	25.093		
	0.313	25.181		
	0.658	37.313		
	0.656	37.837		
	0.658	38.054		
	1.858	44.704		
	2.147	45.982		
	2.331	46.554		
	8.655	54.995		

Black Pearls Powder. SF_6 adsorption

Temp.	P cm Hg	cc NTP	P cm Hg	cc NTP
150 °C	8.9	0.148	3.6	0.074
	13.9	0.205	14.4	0.195
	22.0	0.342	22.5	0.372
	35.7	0.568	35.7	0.569
	57.4	0.913	58.3	0.927
100 °C	13.2	0.432	4.8	0.145
	20.2	0.667	7.4	0.249
	31.6	1.040	11.6	0.375
	50.1	1.613	18.3	0.594
			28.1	0.910
60 °C	12.9	1.006	12.8	0.966
	19.6	1.429	19.5	1.398
	29.8	2.081	29.5	2.045
	45.2	3.023	44.7	2.964
	65.1	4.210	64.7	4.164
30 °C	6.06	0.075	46.79	6.055
	8.88	1.346	63.40	7.938
	12.88	1.864		
	18.28	2.551		
	24.27	3.316		
	32.84	4.379		
0 °C	2.27	0.854	3.70	0.992
	4.14	1.455	10.59	3.467
	6.33	2.179	16.91	5.476
	9.20	3.057	21.66	6.929
	16.83	5.473	26.03	8.245
	25.80	8.204	29.14	9.127
	32.55	10.083	35.41	10.802
	39.84	11.869		
-20 °C	3.38	2.693	2.00	1.460
	6.81	5.000	4.01	2.816
	9.26	6.662	6.61	4.572
	14.41	10.069	10.21	7.030
	19.21	12.854	13.23	9.060
	21.92	14.144	16.19	10.904
	29.80	16.945	19.29	12.634
	41.16	19.414	22.10	13.964
	58.14	21.600	24.27	14.850
			28.76	16.382

contd.

-40 °C	0.58	1.151	1.28	2.233
	0.86	1.587	1.86	3.210
	1.94	3.384	4.09	6.747
	2.47	4.312	5.85	10.235
	2.82	4.867	8.01	13.862
	3.28	5.455	11.50	17.139
	4.59	7.993	15.38	19.341
	6.22	10.745		
	9.61	15.393	0.42	0.861
	11.15	16.781	1.19	2.055
	14.21	18.781	3.08	5.295
	18.35	20.453	4.46	7.653
	30.20	23.082	8.00	13.380
	37.39	24.143	14.83	18.989
	49.30	25.672	29.80	22.927
-50 °C	5.34	15.287	1.10	3.237
	6.00	16.769	1.38	4.109
	6.78	17.865	1.65	4.947
	7.99	19.161	1.90	5.699
	11.37	21.365	2.43	7.339
	15.14	23.006	2.85	8.603
	20.48	24.391	3.07	9.269
	27.59	25.768	3.79	11.630
	34.92	27.136	4.95	14.619
	39.835	27.857	6.37	17.231
	50.281	29.915	12.20	21.629
			20.51	24.089
			25.69	25.122
-60 °C	2.84	15.669	0.26	1.452
	3.62	17.921	0.57	2.995
	8.26	23.095	1.41	7.415
	10.64	24.522	1.61	8.562
	14.28	25.543	2.40	12.973
	22.30	27.846	2.79	14.916
	25.33	28.766	5.29	21.416
	34.91	31.723	10.98	24.915
	45.17	35.948	16.44	26.660
	54.16	40.656	28.57	30.002
			34.04	31.736
			43.88	35.211
			Desorbing	
			29.55	30.310
			22.04	28.206
			15.87	26.500

contd.

-70 °C	3.92	22.886	0.26	2.427
	7.74	25.549	0.58	5.761
	10.08	26.826	0.88	9.174
	13.52	28.183	1.21	12.848
	16.94	29.991	1.51	15.886
	20.32	31.716	1.68	17.119
	22.82	33.180	2.10	19.202
	25.68	34.622	2.62	20.874
	31.53	39.968	8.15	25.578
	37.30	45.044	18.83	30.644
	39.16	50.809	27.65	36.458
	43.59	53.016	32.63	41.006
			35.54	44.225
			40.61	52.035
			Desorbing	
			35.418	44.194
			24.981	33.750
			9.865	25.882
			4.191	22.477
-80 °C	0.39	9.510	0.24	5.184
	0.61	14.737	0.70	15.677
	0.85	18.461	2.18	24.921
	2.09	24.249	6.42	29.063
	3.28	25.810	8.03	30.299
	5.59	27.818	11.59	33.580
	8.01	30.138	14.07	36.457
	9.77	31.812	16.39	39.950
	11.64	33.195	18.08	43.118
	13.81	35.957	19.85	47.249
	15.60	38.492	21.75	52.995
	17.48	41.957	24.26	62.995
	20.19	47.938		
	22.03	53.954	0.32	7.303
	23.19	58.664	0.61	13.856
	24.32	64.129	1.45	22.216
	25.36	71.244		

APPENDIX 6

Graphon / SF_6 diffusion coefficients

	$10^4 \times D_S$ $cm^2 sec^{-1}$	T °C
SF_6	53.1	200
	39.5	150
	25.0	100
	18.5	60
	13.1	31.2

Temp.	$10^4 \times D_T$ $cm^2 sec^{-1}$	cc NTP/g
0 °C	12.6	0.0
	10.4	0.5
	9.4	1.0
	7.6	2.0
	7.0	3.0
-20 °C	6.95	0
	6.25	1
	5.96	2
	6.00	3
	6.00	4
	6.14	5
	6.56	6
	9.21	7
	16.99	8
-40 °C	5.43	0
	3.73	1
	3.222	2
	3.22	3
	3.57	4
	4.16	5
-50 °C	4.07	0
	2.67	1
	2.11	2
	2.05	3
	2.20	4
	2.43	5
	2.83	6

$10^4 \times D_T$ $cm^2 sec^{-1}$	cc NTP/g
4.70	6
5.51	7
6.74	8
15.07	9
32.51	10
3.07	7
4.56	8
8.21	9
10.18	9.5
16.64	10
24.95	10.5
24.31	11
21.55	11.5
15.05	12

contd.

-60 °C	1.80	0		
	1.58	1	9.57	10
	1.34	2	16.93	10.5
	1.29	3	22.05	10.7
	1.34	4	23.70	11.0
	1.86	5	18.96	11.5
	2.46	6	14.37	12.0
	3.18	7	12.99	12.5
	4.10	8		
	5.82	9		
	7.05	9.5		
-70 °C	6.73	10.5	24.31	12.5
	9.20	11	9.57	13
	12.81	11.5	6.79	14
	18.96	12.0		
-80 °C	0.49	6	9.03	12
			5.18	13
	6.18	10	1.84	15
	12.64	11	0.49	19
-90 °C	1.04	9	1.74	13
	2.45	10	0.58	15
	10.90	11	0.17	17.25
	7.48	11.5		
	2.63	12		

Graphon diffusion coefficients - Argon

$10^4 \times D_S$ $cm^2 sec^{-1}$	T °C
102	50
99	30
86	0
62	-42
37	-78
18	-120

Temp.	$D_T \times 10$ $cm^2 sec^{-1}$	cc NTP/g	$D_T \times 10$ $cm^2 sec^{-1}$	cc NTP/g
90 °K	0.14	10	1.82	24
	0.23	14	1.31	26
	0.34	16	1.16	28
	0.79	18		
	1.94	20		
	3.44	21.5		
	3.44	22		
77.6 °K	0.4	10		
	1.0	16		
	2.4	18		
	5.2	19		
	5.9	20		
	8.2	21		
	6.6	22		
	5.8	23		
	5.1	24		
	3.8	25		
	3.5	26		
	0.1	30		
	0.07	40		

Diffusion coefficients Black Pearls

SF%	$10^4 \times D_S$ $cm^2 sec^{-1}$	T °K
	18.8	423
	13.7	373
	11.3	333
	8.25	304.2
	5.78	273

Temp.	$10^4 \times D_{T_1}$ $cm^2 sec^{-1}$	cc NTP/g	$10^4 \times D_{T_1}$ $cm^2 sec^{-1}$	cc NTP/g
-20 °C	3.39	0-10		
	4.45	12		
	7.83	15		
-40 °C	2.13	0-10		
	3.66	16		
	5.52	20		
	7.68	22		
-50 °C	2.02	0-2	1.92	16
	1.77	4	2.41	18
	1.68	6	3.66	20
	1.51	8		
	1.51	10		
	1.60	12		
	1.80	14		
-60 °C	1.81	0	1.76	18
	1.73	2	2.71	20
	1.49	4	4.47	22
	1.16	6	5.37	24
	1.02	8	5.31	26
	0.96	10	4.74	28
	1.06	12	3.93	30
	1.20	14		
	1.38	16		
-70 °C	1.32	0	4.11	24
	1.20	2	4.24	25
	0.99	4	4.78	26
	0.81	6-12	3.57	28
	0.93	14	2.33	30
	1.14	16	1.70	32
	1.43	18	1.31	34
	2.07	20	0.90	36
	3.16	22	0.72	38
			0.57	40
			0.52	42

contd.

-80 °C	0.63	10-12	2.92	28
	0.77	14	1.98	30
	1.02	16	1.36	32
	1.16	18	1.03	34
	1.49	20	0.69	36
	1.95	22	0.45	38
	2.39	24	0.23	40
	2.80	26		

Black Pearls diffusion coefficients Argon

$10^4 \times D_S$ $cm^2 sec^{-1}$	T °C
83	50
53	30
38	0
25	-42
21	-77.8
8.9	-120

Temp.	$D_T \times 10$ $cm^2 sec^{-1}$	cc NTP/g	$D_T \times 10$ $cm^2 sec^{-1}$	cc NTP/g
90 °K	0.48	36	0.64	60
	0.55	38	0.49	62
	0.62	40	0.42	64
	0.81	42	0.36	66-70
	1.05	44		
	1.131	46-49		
	1.06	50		
	0.84	52		
	0.79	55		
	0.69	58		
77.6 °K	0.042	30		
	0.116	40		
	0.543	43-53		
	0.133	60		
	0.028	70		